UNIVERSITY OF OKLAHOMA

GRADUATE COLLEGE

FLASH DROUGHTS: A LOCAL TO GLOBAL ANALYSIS OF RAPID DROUGHT INTENSIFICATION AND THEIR ASSOCIATED IMPACTS

A DISSERTATION

SUBMITTED TO THE GRADUATE FACULTY

in partial fulfillment of the requirements for the

Degree of

Doctor of Philosophy

By

JORDAN ISAAC CHRISTIAN
Norman, Oklahoma
2020

FLASH DROUGHTS: A LOCAL TO GLOBAL ANALYSIS OF RAPID DROUGHT INTENSIFICATION AND THEIR ASSOCIATED IMPACTS

A DISSERTATION APPROVED FOR THE
SCHOOL OF METEOROLOGY

BY THE COMMITTEE CONSISTING OF

Dr. Jeffrey Basara, Chair

Dr. Jason Furtado

Dr. Michael Richman

Dr. Jason Otkin

Dr. Xiangming Xiao

Acknowledgements

This dissertation was completed with the incredible support of several people in my life. First and foremost, I want to thank my wonderful wife Katy Christian for all of the support she has given me during my PhD. She has always pushed me to pursue my dreams and always encouraged me to keep pressing forward, even during the most challenging times in academics. While I spend a majority of this dissertation quantifying flash drought, I'll never be able to fully quantify my endless appreciation and love for her. I also want to give all of my thanks, appreciation, and love to my family, especially my dad, mom, and sister, who have always supported me and encouraged me to pursue what I love. I would also like to give immeasurable thanks to my advisor, mentor, and friend Dr. Jeff Basara. During my time in undergrad and graduate school, Jeff has made me a better writer, researcher, teacher, mentor, leader, and person. I will be forever grateful for all of the advice and wisdom I have received from him along this academic journey. I also want to personally thank the entire CHEWE research group and my office mates over the years, including Paul Flanagan, Ryann Wakefield, Nick Balderas, Noah Brauer, and Taylor Grace. I thank them for all of their support and collaboration, and most importantly, being like family to me. I would like to also express my great appreciation for Dr. Jason Otkin and Dr. Eric Hunt, who co-advised me during my PhD. Both Jason and Eric helped me to become a better researcher and writer, and provided incredible input to greatly improve the quality of this dissertation. I also want to thank my committee members, Dr. Jason Furtado, Dr. Michael Richman, and Dr. Xiangming Xiao. All of my committee members have either taught me in a class, been a coauthor on a paper that derived from this dissertation, or both. I greatly appreciate all of their investment and support in my education and the completion of my PhD.

Lastly, and most importantly, I'm grateful for my faith and hope in Jesus Christ that has blessed me with this scientific journey, given me peace and strength to overcome academic challenges and complete my PhD, and provided me the opportunity to explore the beautifully complex interactions between the land surface and atmosphere, even if only a small fragment of all of creation.

Table of Contents

Abstract

Flash drought is characterized by the rapid intensification toward drought conditions and is primarily associated with detrimental impacts to agricultural production. Unlike conventional (slowly developing) drought, flash drought can rapidly desiccate land surface conditions in only the span of a few weeks and place excessive stress on the environment. Flash droughts form from a complex combination of thermal, moisture, and radiative flux variables, and predictability of these events remains a significant challenge due to their occurrence on subseasonal timescales. To address some of the challenges related to flash drought development and their associated impacts, the primary goals of this study were to develop an objective methodology for flash drought identification, explore the role of flash drought in socio-economic impacts, and create a global climatology of flash drought occurrence.

A comprehensive methodology was developed in conjunction with the standardized evaporative stress ratio (SESR; the ratio between evapotranspiration and potential evapotranspiration) for flash drought identification. After evaluation with the satellite-derived evaporative stress index and U.S. Drought Monitor, a climatology of flash drought events and their characteristics were quantified across the United States. In addition, a case study of a flash drought event over southwestern Russia in 2010 was investigated to explore how rapid drought development resulted in cascading hydrometeorological and socioeconomic impacts. Lastly, global hotspots of flash drought occurrence were identified, revealing their frequency, seasonal timing, and spatial coverage trends with time.

Chapter 1: Introduction

Drought is a significant natural hazard that can lead to detrimental impacts on the economy, environment, and society (Wilhite et al. 2007). These wide-ranging impacts include agricultural yield loss, a reduction in surface and groundwater availability, limits on recreation, adverse effects on human health, and an increased risk of wildfires (Basara et al. 2013; Westerling and Swetnam 2003; Krishnan et al. 2006). While drought onset and the resulting impacts are traditionally expected to develop slowly over time (Wilhite et al. 2007), recent scientific literature has shown that drought conditions can develop rapidly on subseasonal timescales. These events have been labeled as "flash droughts". Within the context of the four traditional drought classifications (meteorological, agricultural, hydrological, and socioeconomic; Wilhite and Glantz 1985), flash droughts begin as a meteorological drought before transitioning to agricultural drought.

Flash drought, or the rapid intensification toward drought conditions, was first acknowledged in Svoboda et al. (2002) when it was noticed that rapid drought onset could quickly lead to agricultural and environmental impacts, such as crop deterioration and increased fire potential. It wasn't until a decade later when the first studies examined the temporal and spatial evolution of flash drought (Anderson et al. 2013, Otkin et al. 2013). After these initial studies, interest over flash drought within the scientific community grew rapidly, with several analyses evaluating rapid drought intensification over the United States and their associated impacts on agriculture (Otkin et al. 2014, Hunt et al. 2014, Ford et al. 2015). However, without a formal definition of flash drought in the scientific literature, different approaches were developed and used to identify flash drought events. One method viewed flash drought from the perspective

of "short duration", with flash droughts identified when extreme anomalies occurred during a small window of time (a pentad; e.g., Mo and Lettenmaier 2015, Mo and Lettenmaier 2016). An alternative method identified flash droughts via an intensification component, in which a variable used for flash drought analysis must rapidly change towards drought conditions over time (e.g., Ford and Labosier 2017).

In Otkin et al. (2018), the two approaches for flash drought identification were assessed to determine how rapid drought intensification should be classified. After a thorough review, it was determined that the time period of flash drought development should be associated with longevity and impact, as these were stated to be fundamental characteristics of drought. This formal definition was then followed with guidelines for identifying flash drought events. These guidelines required the inclusion of a rapid intensification component (the "flash" component), a threshold for which drought is reached (the "drought" component), and a length of time associated with flash drought that would lead to notable impacts on the environment (several weeks).

While the general definition of flash drought has been refined in recent years, the extent of impacts linked with rapid drought development has grown over time. The initial response from the land surface in the event of a flash drought is a rapid loss of near-surface and root zone soil moisture (Hunt et al. 2014). As flash drought development continues and soil moisture is depleted, evaporative stress on the environment will also increase (Otkin et al. 2013). Furthermore, several additional impacts can begin to emerge, including the deterioration of vegetative health and increased risk for wildfires. The most commonly mentioned impact associated with flash drought is agriculture (Otkin et al. 2016, Otkin et al. 2018, Basara et al. 2019, Jin et al. 2020). However, excessive evaporative stress during rapid drought development

can also severely impact ecosystems (Anderson et al. 2013, Otkin et al. 2014, McEvoy et al. 2016). In addition to vegetative impacts, desiccation of land surface conditions and increases in the vapor pressure deficit following a flash drought event may also increase the likelihood for wildfire development (Gerken et al. 2018).

At the start of this dissertation, many studies were unraveling new characteristics about flash drought development, but fundamental questions remained. For example, when and where do flash droughts most commonly occur? Do all flash droughts develop under similar environmental conditions, or are there regionally dependent characteristics associated with flash drought? Can flash drought impacts extend beyond agricultural yield loss and vegetative stress? Addressing these questions can refine the detection and monitoring of flash drought, lay the foundation for improved predictability of rapid drought intensification, and increase our understanding of cascading impacts associated with these events. As such, the hypothesis of this dissertation is that rapid drought intensification can be effectively quantified and evaluated if a comprehensive methodology can be developed for flash drought identification, timing, intensity, and impacts. This hypothesis is addressed by pursuing three main goals: 1) develop a quantitative methodology for identifying flash droughts, 2) explore the role of flash drought in socio-economic impacts, and 3) create a global climatology of flash drought occurrence.

The primary goals of this dissertation are addressed in Chapters 2 through 5. In Chapter 2 (Christian et al. 2019a), a flash drought methodology is created using the guidelines proposed in Oktin et al. (2018a). The approach of the methodology is evaluated with other drought metrics and applied to a reanalysis dataset to produce a climatology of flash drought events over the United States. In Chapter 3 (Christian et al. 2019b), the methodology is utilized to quantify the characteristics of flash droughts across the United States to determine if regional differences

exist in the seasonality of flash drought events and moisture conditions prior to and following rapid drought intensification. In Chapter 4 (Christian et al. 2020), a flash drought case study is investigated using the quantitative methodology across southwestern Russia in the summer of 2010 to determine its hydrometeorological relationship to a devastating heatwave and the role of the flash drought in a set of cascading impacts. In Chapter 5, a global climatology of flash drought occurrence is produced based on the methodology using reanalysis datasets, with analysis of spatial hotspots, seasonality of flash drought events, and trends of flash drought spatial coverage with time. An overarching summary and key findings are presented in Chapter 6.

Chapter 2: A Methodology for Flash Drought Identification: Application of Flash Drought Frequency Across the United States

(Christian et al. 2019a)

2.1 Introduction

Drought is one of the most costly natural disasters (Wilhite 2000) with complex impacts that can impose significant economic, environmental, and social stress (Wilhite et al. 2007). While preferred regions exist within the United States for drought development and persistence, drought occurrence is possible anywhere in the country (Diaz 1983). Furthermore, the impacts of drought are extensive, with diverse ramifications specific to different regions across the United States (Basara et al. 2013; Manuel 2008; Griffin and Anchukaitis 2014; Zou et al. 2018). These primary impacts include agriculture, surface and groundwater availability, recreation, human health, wildfires, and ecosystems (Basara et al. 2013; Westerling and Swetnam 2003; Krishnan et al. 2006). In addition to impacts, the drivers of drought are similarly diverse, including shifts in atmospheric patterns, anomalous sea surface temperatures, and land-atmosphere coupling (Chang and Wallace 1987; McCabe et al. 2008; Basara and Christian 2018).

While drought is generally described as slowly developing (Wilhite et al. 2007), recent studies have unveiled a new type of rapidly developing drought: flash drought. Within the context of the four traditional drought classifications (meteorological, agricultural, hydrological, and socioeconomic; Wilhite and Glantz 1985), flash droughts often begin as a meteorological drought that then transitions to agricultural drought as conditions continue to deteriorate. If extreme atmospheric anomalies (i.e., lack of rainfall, higher surface temperatures, strong winds, and clear skies) persist for several weeks, the onset and development of drought can occur

rapidly. Flash drought is critically important to understand as rapid drought intensification can occur regardless of preceding moisture conditions. For example, even though environmental conditions were near normal at the end of May 2012, the flash drought event across the central United States during the growing season of 2012 was associated with three-, four-, and five-category increases in the U.S. Drought Monitor (USDM; Svoboda et al. 2002; Otkin et al. 2018a). Further, flash droughts induce large impacts on agriculture and can stress short-term water resources through rapid deterioration of vegetation health and rapid depletion of soil moisture. Heat waves may also manifest during flash droughts, which can further lead to significant impact on agricultural yields and loss of life (Mo and Lettenmaier 2015; Thacker et al. 2008).

Rapid drought intensification is also difficult to predict as flash droughts are subseasonal phenomena and the complex drivers are not fully understood (Otkin et al. 2018a). As such, it is critical to understand where flash drought events are most likely to occur to improve predictability and to know where impacts from flash drought are most common. Flash droughts were initially examined in Otkin et al. (2013) using the satellite-based evaporative stress index (ESI; Anderson et al. 2007a,b). The relationship between rapid drought development and changes in ESI was further explored in Otkin et al. (2014) where they showed that the rapid change index (RCI) derived from temporal changes in the ESI can provide early warning of agricultural flash drought. More recently, the evaporative demand drought index (EDDI) has been used as a flash drought indicator (Hobbins et al. 2016). EDDI leverages atmospheric demand to not only detect and track drought, but to provide an early warning indicator of rapid onset drought development (McEvoy et al. 2016). Flash drought events have also been examined by using below-normal soil moisture values. For example, Yuan et al. (2018) used rapid declines

in soil moisture to investigate the spatiotemporal distribution of flash drought over southern Africa while Wang et al. (2016) used temperature, soil moisture, and evapotranspiration anomalies to examine trends in flash droughts across China. Further, Ford and Labosier (2017) investigated the meteorological conditions associated with flash drought in the eastern United States.

With the increasing usage of the term flash drought in the scientific community, a general definition for these features of the climate system was provided by Otkin et al. (2018a) that is based on rate of intensification. While previous studies (e.g., Mo and Lettenmaier 2015, 2016; Zhang et al. 2017) have placed an emphasis on short duration for flash drought identification, Otkin et al. (2018a) argue that identification of flash droughts based on criteria for a short duration deviates from the fundamental drought characteristics of longevity and impact. The general definition of flash drought presented in Otkin et al. (2018a) called for an objective, statistical methodology to identify flash drought events. Therefore, the purpose of this study is twofold: 1) to create a consistent statistical methodology that can be used to identify flash drought cases in any gridded dataset containing evapotranspiration (ET) and potential evapotranspiration (PET), or their constituents, and 2) to apply the methodology to a reanalysis dataset to investigate the climatological characteristics of flash droughts across the United States.

2.2 Flash Drought Identification Methodology

2.2.1 Standardized Evaporative Stress Ratio

The foundation of flash drought identification proposed in this study relies upon the evaporative stress ratio (ESR). ET and PET are used to calculate ESR, such that

$$ESR = \frac{ET}{PET}, \tag{1}$$

where ESR ranges from zero to approximately one. The interpretation of ESR is as follows: as ESR approaches one, the atmospheric demand of ET is met by the available soil moisture and vegetation; as ESR approaches zero, the land surface meets little or none of the atmospheric demand. Thus, the value of ESR is inversely proportional to the amount of evaporative stress on the environment. The satellite-derived ESI (similar to standardized ESR) has been widely used in studies examining drought processes including comparison of ESI with leaf area index and precipitation anomalies, utilizing ESI as an indicator for agricultural drought, and an intercomparison of ESI with soil moisture, ET, and runoff anomalies from reanalysis data (Anderson et al. 2011, 2013, 2015, 2016a,b; Otkin et al. 2013, 2016, 2018b, 2019). As such, ESR was selected for flash drought analysis as it directly incorporates near-surface state variables including air temperature, wind speed, vapor pressure deficit, latent and sensible heat fluxes, as well as soil moisture, precipitation, and shortwave radiation, and follows the guidance of Otkin et al. (2018a).

For flash drought identification, standardized ESR (SESR) values are used to more easily compare the evaporative stress between regions characterized by different climate regimes. Such standardization also allows a more robust comparison of ESR values over multiple years and parts of the growing season for each grid point. Before SESR values are calculated, mean pentad values of ESR are computed. It is highly recommended to use pentad (or longer) time periods when computing SESR due to the volatility that is sometimes present in daily ESR. Computing pentad values smooths out short-term fluctuations in ESR and allows the development of an objective methodology for flash drought identification. As a result, the remaining description of flash drought identification is based on pentad values of ESR. An illustration of the

standardization process is shown in Fig. 2.1. First, pentad SESR values are computed for each grid point,

$$SESR_{ijp} = \frac{ESR_{ijp} - \overline{ESR_{ijp}}}{\sigma_{ESR_{ijp}}}, \quad (2)$$

where $SESR_{ijp}$ (henceforth referred to as SESR) is the z score of ESR for a specific pentad p at a specific grid point (i, j), ESR is the mean ESR for a specific pentad p at a specific grid point (i, j) for all years available in the gridded dataset, and σ_{ESR} is the standard deviation of ESR for a specific pentad p at a specific grid point (i, j) for all years available in the gridded dataset. This standardization is similar to that for ESI (e.g., Anderson et al. 2011; Otkin et al. 2013, 2014) where ESI was standardized for each week at each grid point.

A critical characteristic of flash drought identification involves the "flash" component representing rapid drought intensification. This is derived by calculating the change in SESR values between each pentad. The change in SESR is standardized in the same way as ESR, similar to the standardization of ESI changes in prior studies by Anderson et al. (2013) and Otkin et al. (2013, 2014). In this analysis, the standardized change in SESR is given as

$$\left(\Delta SESR_{ijp}\right)_z = \frac{\Delta SESR_{ijp} - \overline{\Delta SESR_{ijp}}}{\sigma_{\Delta SESR_{ijp}}}, \quad (3)$$

where $\left(\Delta SESR_{ijp}\right)_z$ (henceforth referred to as ΔSESR) is the z score of the change in SESR for a specific pentad p at a specific grid point (i, j), $\overline{\Delta SESR}$ is the mean change in SESR values for a specific pentad p at a specific grid point (i, j) for all years available in the gridded dataset, and $\sigma_{\Delta SESR}$ is the standard deviation of SESR for a specific pentad p at a specific grid point (i, j) for all years available in the gridded dataset. It is important to note that this process is applied to all land grid points in the dataset.

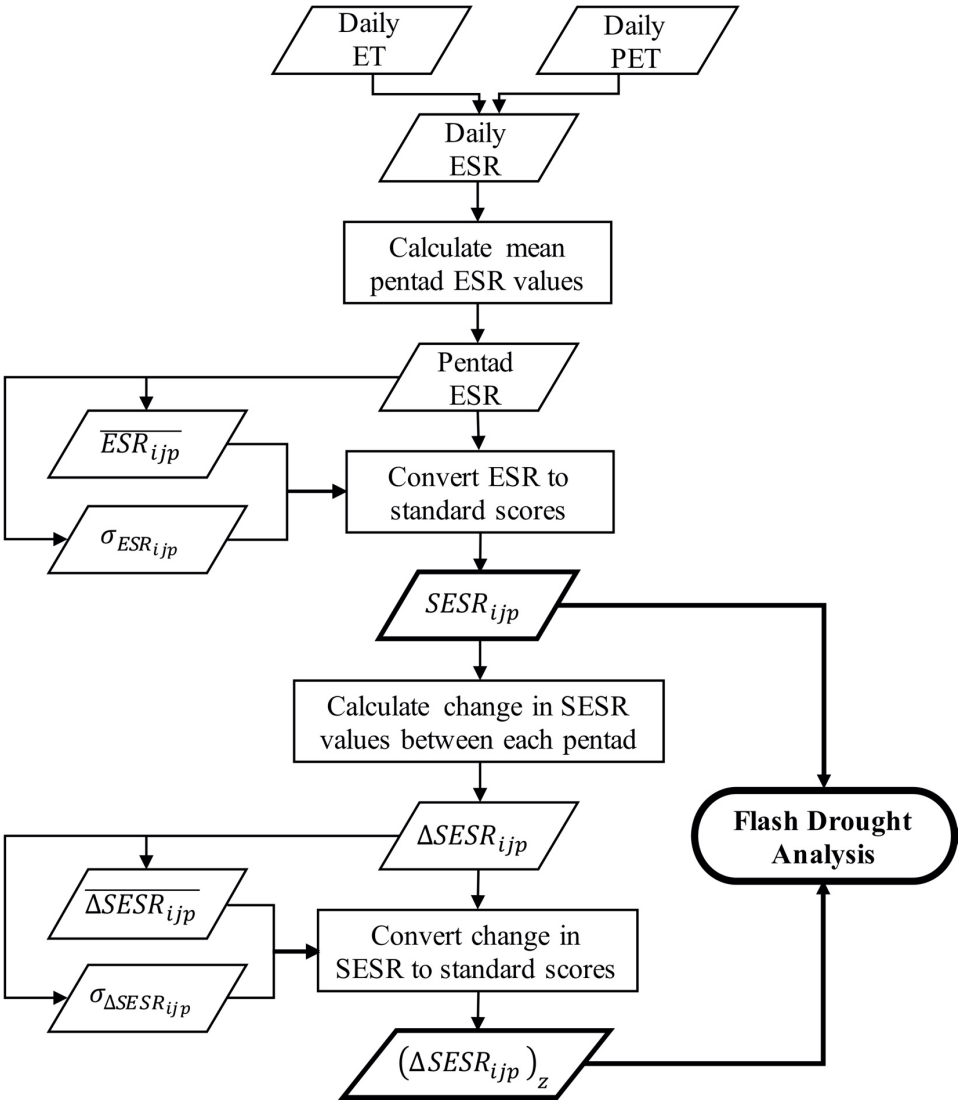

Fig. 2.1. A schematic of the standardization process to obtain $SESR_{ijp}$ (referred to as SESR) and $(\Delta SESR_{ijp})_z$ (referred to as $\Delta SESR$). Subscript indices i and j represent grid point locations, and p represents a specific pentad.

2.2.2 Flash Drought Identification

Four criteria involving SESR are used to identify flash drought events. The first two criteria are used to address the impacts of flash drought on the environment while the latter two criteria emphasize the rapid rate of drought intensification. In this methodology, flash drought

events are required to have 1) a minimum length of five SESR changes (ΔSESR), equivalent to a length of six pentads (30 days), and 2) a final SESR value below the 20th percentile of SESR values. Both of these criteria are founded upon characteristics of flash droughts described in Otkin et al. (2018a). The minimum length of 30 days for criterion 1 was selected based off the previously defined temporal definition of flash droughts provided in Otkin et al. (2018a), and the length of flash droughts depicted in case studies from Otkin et al. (2013). Otkin et al. (2018a) states that the minimum time frame in which flash droughts develop is over the course of "several weeks." Furthermore, each of the flash drought cases examined in Otkin et al. (2013) were a minimum length of 30 days or longer. As such, the combination of this definition and the resulting case studies determined the minimum length of a flash drought defined for criterion 1. The emphasis of criterion 1 is the elimination of short-term dry spells so that the definition captures situations where drought impacts occur (i.e., significant reduction of water resources including soil moisture, stress to the ecosystem, etc.). A rapid change in SESR from one pentad to the next by itself does not necessarily indicate an impact to the ecosystem and environment unless below-average SESR values persist for a longer period of time. Adverse impacts on the environment are most likely to occur when there is continuous rapid development toward drought conditions from one pentad to the next. Regarding criterion 2, Otkin et al. (2018a) states that any variable used to identify flash droughts must fall below the 20th percentile for it to be considered drought. Criterion 2 satisfies the drought component of this definition by requiring that, at a minimum, drought conditions occur by the end of the rapid intensification period.

Regarding the rate of rapid drought intensification, two criteria are used: one that focuses on pentad-to-pentad changes toward drought development (criterion 3) and another that

emphasizes rapid drought development through the entirety of the flash drought event (criterion 4). Criterion 3 contains the following two components:

1) criterion 3a: ΔSESR must be at or below the 40th percentile between individual pentads, and

2) criterion 3b: no more than one ΔSESR above the 40th percentile following a ΔSESR that meets criterion 3a.

If criterion 3b is reached, then the following ΔSESR must meet criterion 3a and have an ending SESR value less than the SESR value preceding the SESR moderation in order for the flash drought to continue. The end of a flash drought is attained at the last pentad for which criterion 3a is satisfied.

The fourth criterion complements the third criterion and is applied to the entire length of the flash drought (beginning from the first pentad where criterion 3a is met and ending at the last pentad in which criterion 3a is met). Specifically, the mean change in SESR during the entire length of the flash drought must be less than the 25th percentile of the climatological changes in SESR for that grid point and time of year. This criterion is used to ensure that features identified as flash droughts have an overall rapid rate of development of drought conditions and are not significantly slowed by temporary moderations of SESR due to the effects of precipitation, lower temperatures, more cloud coverage, or lower surface wind speeds. It is important to note that for all percentile values used in criteria 2 and 3, percentiles were taken from the distribution of SESR and ΔSESR at local grid points and specific pentads for all years available in the dataset. For criterion 4, percentiles were calculated from the distribution of ΔSESR at local grid points for pentads that were encompassed within the flash drought event.

The threshold percentile for individual pentad-to-pentad SESR changes (40th percentile) is more lenient than the threshold percentile for overall SESR change (25th percentile) during the entire length of the flash drought event for two reasons. First, the 40th percentile was used to separate periods of worsening conditions (less than 40th percentile) from those characterized by nearly constant or improving conditions (greater than 40th percentile) during changes between individual pentads. Second, during an extended period of rapid drought intensification, some pentad changes in SESR will exhibit very rapid development (e.g., less than the 10th percentile) while others will experience slower intensification (e.g., 35th percentile). The more lenient 40th percentile threshold for pentad-to-pentad changes accounts for these variations in rapid intensification, while working in tandem with criterion 4 to ensure the average change in SESR throughout the flash drought event is rapid.

To illustrate the four criteria in action for identifying a flash drought event, a time series schematic is presented in Fig. 2.2. In this example, a flash drought event was identified from mid-June to mid-July. The beginning of rapid drought intensification begins on 11 June, with a ΔSESR at the 26th percentile. The subsequent two ΔSESR on 16 and 21 June also remain below the 40th percentile, listed as criterion 3a. On 26 June, ΔSESR is at the 67th percentile. This ΔSESR is identified as a period of moderation and the subsequent ΔSESR is examined to see if it falls below the 40th percentile. The following ΔSESR on 1 July is at the 9th percentile. Furthermore, the SESR value at the end of the ΔSESR (identified as P6 in Fig. 2.2) is less than the SESR value before the period of moderation began (identified as P4). This satisfies criterion 3b, and the flash drought continues. The next ΔSESR on 6 July is at the 27th percentile and satisfies criterion 3a. On 11 July, the ΔSESR is at the 58th percentile, and the following ΔSESR is at the 43rd percentile. Therefore, the end of rapid drought intensification ends on 11 July. The

remaining three criteria are used to complete the identification process. First, the flash drought event illustrated in the schematic is 6 ΔSESR or 7 total pentads long. This satisfies criterion 1 for the minimum length of a flash drought event. Next, the final SESR value of the rapid intensification period is identified as P7 on the time series. An example 20th percentile of SESR is shown to be approximately -0.8, such that criterion 2 is met for the "drought" component of flash drought. Last, the mean ΔSESR for the flash drought event is calculated to verify that any moderation periods within the flash drought did not significantly impede rapid drought intensification. The mean ΔSESR is found to be at the 24th percentile, meeting the requirement outlined in criterion 4. Therefore, this rapid drought intensification period satisfies all of the criteria to be identified as a flash drought event.

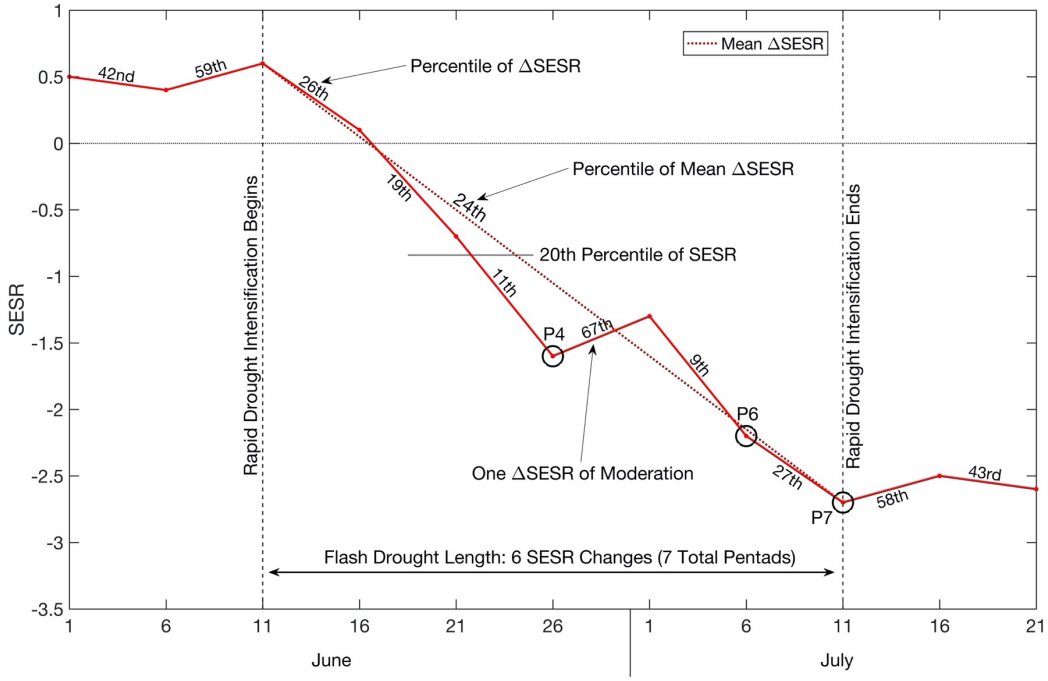

Fig. 2.2. A time series schematic illustrating the four criteria used in the flash drought identification methodology.

A generalized flowchart of the flash drought identification process is shown in Fig. 2.3. Two separate elements are noted in this methodology. The top left side of the schematic represents the rapid rate of intensification toward drought. This is encompassed within criterion 3a of the flash drought methodology. The top right side of the schematic represents an inclusion of moderation within the identification of a flash drought. This is composed within criterion 3b and accounts for brief periods in which a rapid decrease in SESR values (increase in evaporative stress) is limited by precipitation, lower temperatures, and any other set of environmental processes that reduces overall evaporative stress. In the methodology provided here, only one pentad of moderation is permitted because if two or more consecutive pentads of moderation are allowed, it is more likely that conventional droughts (slowly developing) will be erroneously

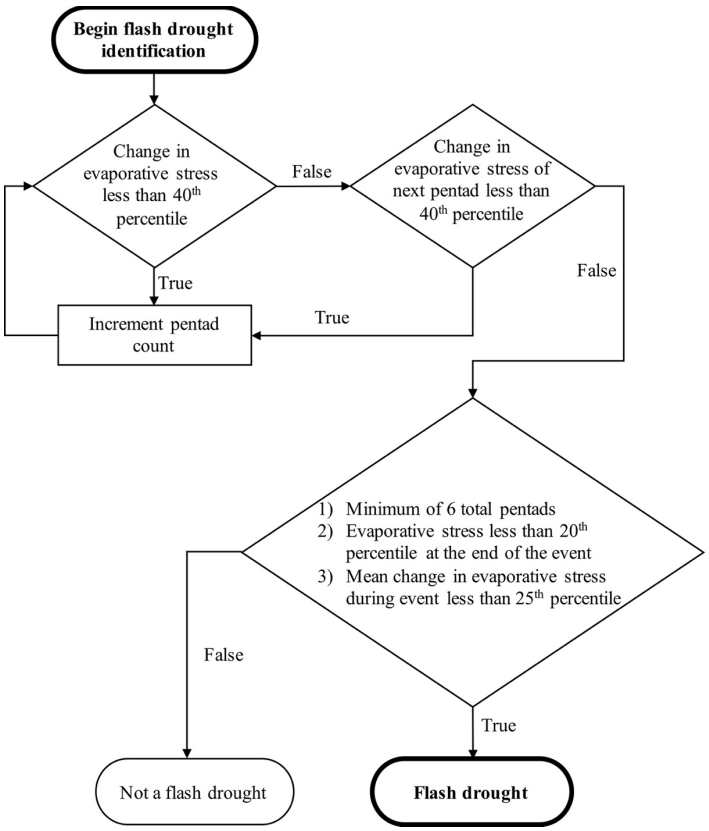

Fig. 2.3. A generalized flow chart of the flash drought identification methodology.

identified as flash droughts. Given that the onset and development of flash drought is on the order of several weeks to a couple of months (Otkin et al. 2018a), inclusion of long periods of moderation is inconsistent with the definition of flash drought.

2.3 Evaluation of the Flash Drought Methodology

2.3.1 Dataset

To demonstrate the methodology, data from the National Centers for Environmental Prediction North American Regional Reanalysis (NCEP NARR; Mesinger et al. 2006) were used. While limited studies exist comparing land surface variables in NARR with observations, NARR has been shown to perform well for precipitation (i.e., have minimal bias; Kennedy et al. 2011). In addition, NARR surface-based variables were found to have comparable accuracy compared to other reanalysis datasets [e.g., the Modern-Era Retrospective Analysis for Research and Applications (MERRA) and the Climate Forecast System Reanalysis (CFSR); Santanello et al. 2015]. Studies have also utilized NARR land-based variables for climatological analysis (e.g., Miguez-Macho et al. 2008; Dominguez and Kumar 2008; Basara and Christian 2018). Because NARR has been shown to be sufficient in representing land-based variables, NARR was selected for application of the flash drought identification methodology and to produce a climatology of flash drought events across the United States.

ET and PET from NARR between 1979 and 2016 were acquired for standardization and analysis following the methodology discussed in section 2.2. The Noah land surface model (LSM) in NARR uses soil evaporation, transpiration from the vegetation canopy, evaporation of dew/frost or canopy-intercepted precipitation, and snow sublimation as input for total surface ET (Mesinger et al. 2006). PET in NARR is calculated with the modified Penman scheme from

Mahrt and Ek (1984). Flash droughts were examined during the approximate growing season (April-October) because rapid development of evaporative stress is less important outside of the growing season. In the winter months, ET is limited due to dormant vegetation and PET is small due to lower temperatures and lower net radiation. The combination of limited ET and PET restricts rapid changes in evaporative stress over an extended period of time, falling outside the definition of flash drought.

2.3.2 Evaluation with the ESI

Four case studies from Otkin et al. (2013) that identified flash droughts using the satellite-derived ESI were compared to the results from the methodology described in this study (Fig. 2.4). The first example assessed the evolution of a flash drought event over eastern Oklahoma and western Arkansas during 2000 (Fig. 2.4a). Evaporative stress values between the 2-week ESI composite from Otkin et al. (2013) and the SESR pentad analysis performed in this study were very similar, both temporally and in magnitude. The 2-week ESI and SESR began approximately at 0.6 and 0.4, respectively, and ended at values near -1.4 and -2.2, respectively. As for the timing, both analyses indicated the start of the flash drought near the end of July, with the conclusion of rapid drought development by the middle of September.

The second flash drought event that was examined occurred over eastern Indiana and western Ohio in 2007 (Fig. 2.4b). The 2-week ESI began to rapidly decrease around 15 April, while SESR started rapidly decreasing after 25 April. The end of the flash drought event (where evaporative stress values no longer rapidly decreased) occurred around 20 May for both ESI and SESR. While the beginning and ending values of ESI and SESR during the flash drought event

were different the overall change in evaporative stress values during the event were very similar (approximately -1.7 for ESI and SESR).

In a flash drought event over southeastern Wisconsin in 2002, SESR produced results that compared poorly with ESI (Fig. 2.4c). Specifically, while SESR had decreased slightly between the end of June and early August, the rate of change of SESR was much smaller than the rate of change in ESI.

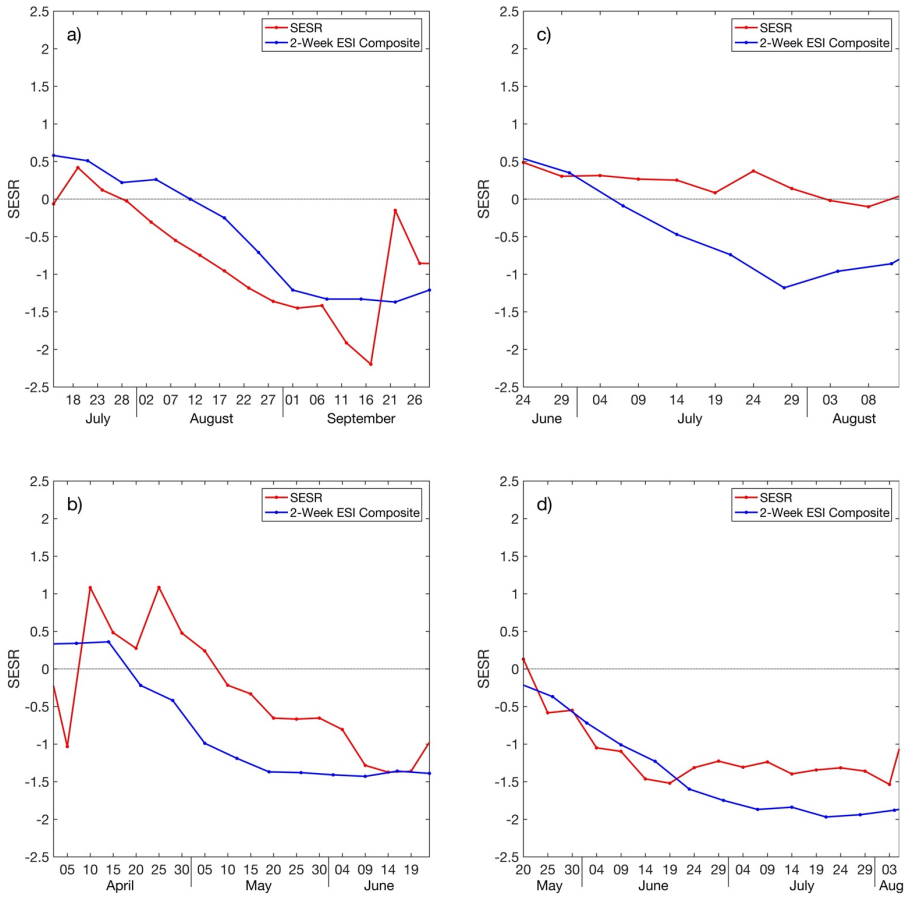

Fig. 2.4. SESR and 2-week ESI composites across (a) eastern Oklahoma and western Arkansas in 2000, (b) eastern Indiana and western Ohio in 2007, (c) southeastern Wisconsin in 2002, and (d) eastern Oklahoma and western Arkansas in 2011. Adapted from Otkin et al. (2013).

In the final case, a flash drought event in May/June of 2011 over a similar spatial domain as the first case was investigated (Fig. 2.4d). The 2-week ESI and SESR were very similar, with beginning values of -0.2 and 0.1, respectively, and ending values of -1.8 and -1.5, respectively. Timing was also comparable, with the beginning of the flash drought in late May for both analyses, and the end of the flash drought in late June/early July from the 2-week ESI and middle to late June from SESR.

While evaporative stress values between ESI and SESR were not identical in the four cases examined, a precise match between these two datasets is not expected as the standardized values of ESI and SESR were taken over different periods of record (2000-2011 for ESI and 1979-2016 for SESR), SESR uses 5-day composites while ESI uses 2-week composites, and SESR is derived from modeled data while ESI is derived from satellite-based remote sensing observations. However, the similar timing and rate of change found between ESI and SESR increase the confidence that the NARR dataset can sufficiently represent evaporative stress and can be utilized for additional flash drought analysis.

2.3.3 Evaluation with the U.S. Drought Monitor

To further evaluate flash drought events identified in the NARR dataset, time series of SESR were compared with the USDM for four flash drought cases. Spatial averages of SESR and the USDM were taken for each of the case study domains (the location and extent of the domains are shown in Fig. 2.5). The first flash drought event over Iowa in 2012 lasted for approximately 30 days between mid-June and mid-July (Fig. 2.6a). Preceding SESR values were slightly below normal (from -0.5 to -1.0) in May and early June before the rapid drought intensification began. The USDM values were initially category 0 before the flash drought event,

but experienced over a two-category increase on average for the domain during the event. The second flash drought event over southeastern Minnesota and west central Wisconsin in 2008 is shown in Fig. 2.6b. Unlike the previous case, SESR values were near normal (approximately 0.3) before the rapid intensification period in late July and early August. This flash drought event also lasted approximately 30 days and underwent close to a two category change in the USDM. The 2016 flash drought over south central Georgia in Fig. 2.6c lasted approximately 35 days from late June to late July. Similar to the Minnesota/Wisconsin flash drought event, near-normal/above-average SESR existed before the rapid intensification period, however a

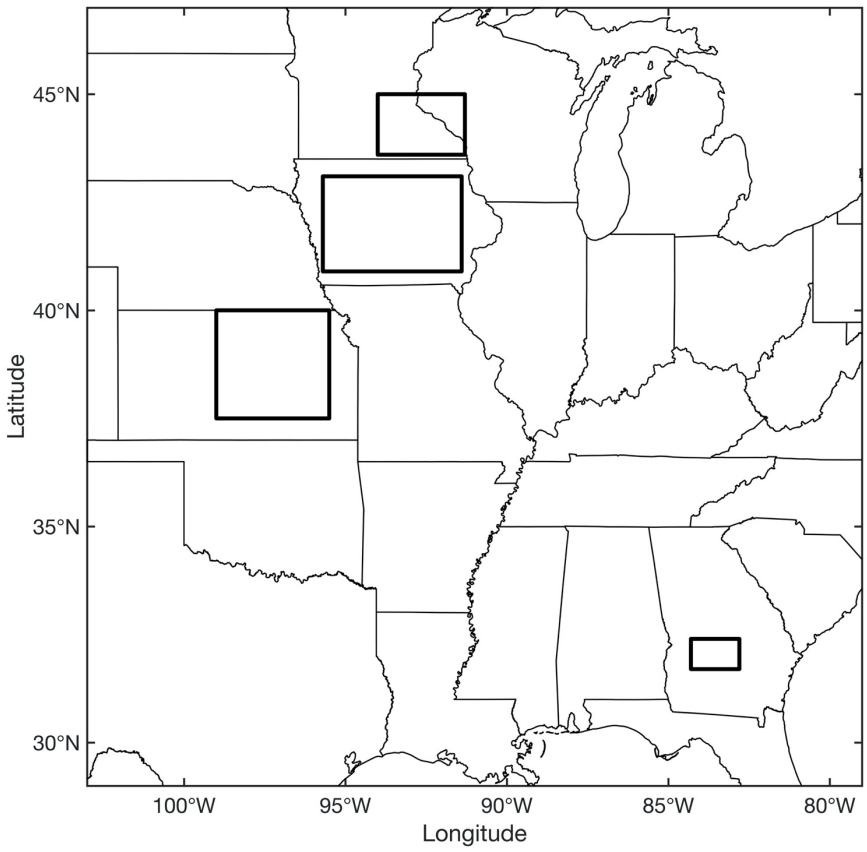

Fig. 2.5. The domains for the four flash drought cases shown in Fig. 2.6.

moderation period was evident toward the end of the flash drought, with one positive ΔSESR in the middle of July. A nearly two-category degradation from the USDM was evident for this region in approximately 30 days. The final flash drought case that was examined occurred across eastern Kansas in 2003 (Fig. 2.6d). The rapid intensification period began in late June and lasted approximately 35 days. This region saw an average three-category degradation from the USDM in a span of only 35 days.

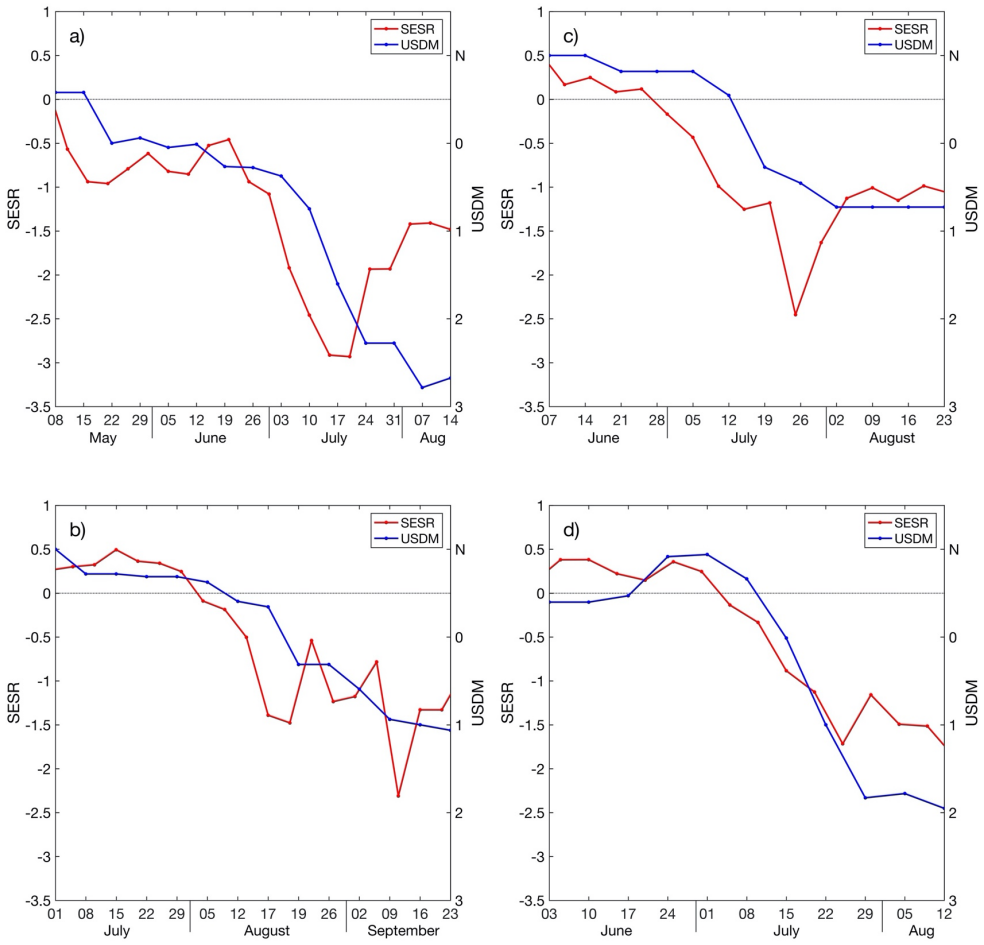

Fig. 2.6. SESR and the USDM for a flash drought event over a) Iowa in 2012, b) southeastern Minnesota and west central Wisconsin in 2008, c) south central Georgia in 2016, and d) eastern Kansas in 2003.

For each of the four cases, SESR rapidly declined 1-2 weeks before a response was evident with the USDM. This is similar to the results found in Otkin et al. (2013), where decreases in ESI preceded the USDM drought depiction by a couple of weeks.

2.4 Application of the Flash Drought Methodology

2.4.1 Flash Drought Frequency

The flash drought methodology was applied to the NARR dataset to quantify the number of years that experienced a flash drought event (expressed as a percentage) across the United States (Fig. 2.7). Immediately apparent is the "hot spot" region of enhanced flash drought frequency over the Great Plains extending into the Corn Belt and western Great Lakes region. In these regions, flash droughts occurred in approximately 40% of the years in the NARR dataset. Local hot spots also exist over the Mississippi Embayment and across the Atlantic coastal plain,

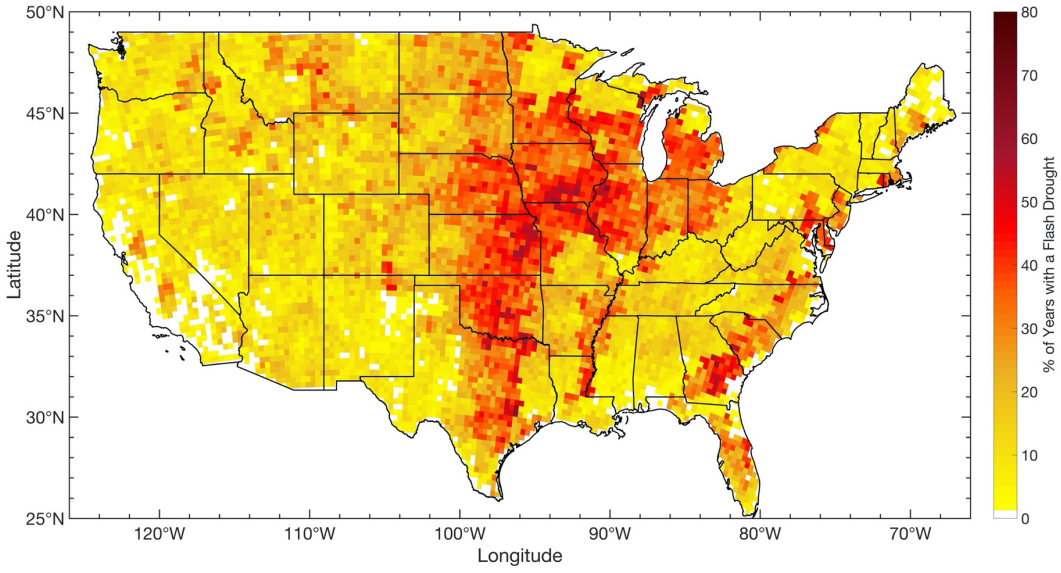

Fig. 2.7. Percent of years in the NARR dataset between 1979-2016 with a flash drought. Flash droughts were identified using the flash drought identification methodology in section 2.2.2.

with approximately 30%-40% of the years containing a flash drought event at these locations. In contrast, regions of less frequent flash drought occurrence were evident across the Northwest, Southwest, Rocky Mountains, Ozarks, and Appalachian Mountains. Flash droughts occurred approximately between 10% and 20% of the total years on record in the NARR dataset in these areas.

2.4.2 Flash Drought Intensity

Flash droughts were categorized by their rate of intensification using the mean SESR change (ΔSESR) during the flash drought. A flash drought intensity index was developed that includes four categories (FD1, FD2, FD3, and FD4) ranging from relatively slower-developing flash droughts (i.e., FD1) to the most rapidly developing flash droughts (i.e., FD4). Although flash droughts are partitioned based on the speed with which they developed, it is critical to note that all flash droughts, regardless of category, are extreme phenomena. The percentile thresholds used for each category are shown in Table 2.1. The percentiles were selected to loosely follow the percentiles used in the USDM, however the percentiles were 5%-10% greater than those used in the USDM (D1-D4). This is due to the fact that the USDM uses percentiles for individual

Table 2.1. Mean change in SESR thresholds for the categorization of flash drought intensity.

Flash Drought Intensity Index	**Flash Drought Intensity**	**Mean Change in SESR**
FD1	Moderate flash drought	20^{th} - 25^{th} Percentile
FD2	Severe flash drought	15^{th} - 20^{th} Percentile
FD3	Extreme flash drought	10^{th} - 15^{th} Percentile
FD4	Exceptional flash drought	< 10^{th} Percentile

moments of time (i.e., drought conditions for a specific week). Requiring a variable (such as SESR) to decline at USDM percentiles (i.e., 20th, 10th, 5th, 2nd) for several consecutive pentads is statistically rare and would likely miss the capture of many rapid intensification periods that produce impacts associated with a flash drought event. The primary focus of the flash drought intensity nomenclature is to categorize the rapid development of flash droughts with limited emphasis on the final severity of the flash drought. While terminating in drought conditions is an essential component of flash droughts, it is the rapid onset and development of drought that separates flash droughts from slowly developing drought conditions.

The frequencies of different flash drought intensities are shown in Fig. 2.8. Beginning with FD1 (moderate flash droughts), flash droughts in this category occur most frequently across

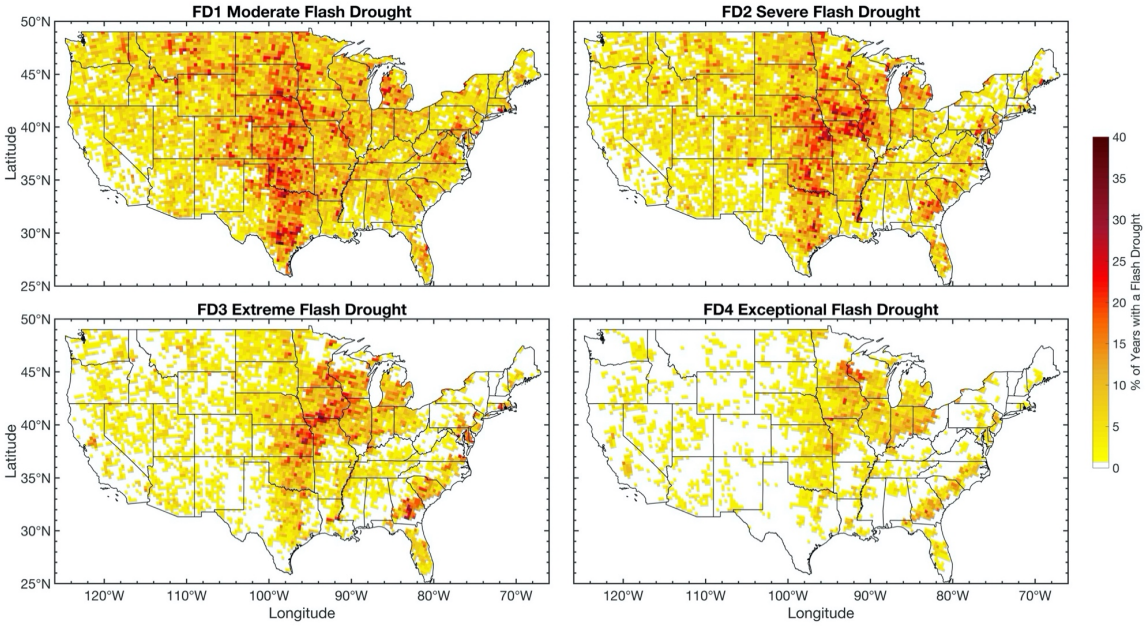

Fig. 2.8. Percent of years in the NARR dataset between 1979 and 2016 with a flash drought categorized by their intensity. Flash droughts were identified using the flash drought identification methodology in section 2.2.2. See Table 2.1 for percentile thresholds of each category.

the entire north-south extent of the Great Plains. A similar signal is evident for FD2 flash droughts (severe flash droughts), with the highest flash drought frequency occurring in the southern and central Great Plains, as well as through the Corn Belt. In addition, portions of the Atlantic coastal plain have hot spots of flash drought frequency in the FD2 category. For extreme flash droughts (FD3), the signal becomes especially refined in the primary flash drought hot spot locations of the central Great Plains and Corn Belt, as well as portions of the Atlantic coastal plain. Last, exceptional flash droughts (FD4) exist almost exclusively across the central Great Plains, Corn Belt, western Great Lakes region, and the Atlantic coastal plain.

2.5 Discussion

The primary purpose of this study was to present an objective methodology to identify flash drought events in gridded datasets using ET-based variables. The methodology provided here is complementary to the general flash drought definition provided by Otkin et al. (2018a). Each component of the flash drought methodology developed during this study, including rapid drought development, drought conditions at the end of the rapid intensification period, and longevity, follows the guidelines presented in Otkin et al. (2018a). While this methodology can be readily applied to gridded datasets, it can also be used in local analyses as well, such as with flux tower/mesonet observations provided that a long enough period of observations is available for standardization and measurements/calculations of ET/PET. Furthermore, while the primary focus of the methodology was for flash drought identification, the methodology could also be leveraged for flash drought monitoring. Similar to how the U.S. Drought Monitor portrays information on drought conditions across the United States, the flash drought methodology

presented here could be used to reveal regions that are currently experiencing or have experienced a flash drought.

SESR values derived from NARR analyses were used to examine individual flash drought examples and to quantify climatological characteristics of flash droughts across the United States. The four SESR time series examples provided in Fig. 2.6 illustrate how flash droughts can develop either with monotonically decreasing SESR (Figs. 2.6a,b,d; based solely on criterion 3a in section 2.2.2) or with the inclusion of a short moderation period in SESR (Fig. 2.6c; utilizing criterion 3b in section 2.2.2). From the analysis of flash drought frequency in section 2.4.1 (Fig. 2.7), partitioning the identified flash droughts into flash droughts that used only criterion 3a and flash droughts that used both criterion 3a and 3b revealed that 24% of all flash drought events were the monotonic decrease case and 76% of all flash drought events included significant but temporary moderation. A more thorough investigation of this partitioning, however, will be a topic of future research.

The results from the climatological frequency of flash droughts revealed a significant "hot spot" of greater flash drought occurrence across the Great Plains, Corn Belt, and western Great Lakes region. Two key characteristics of these regions might be contributing to the maxima in flash drought frequency: agriculture and land-atmosphere coupling. The representation of vegetative differences in NARR is via the NCEP Eta Model. Thirteen vegetative types are prescribed in the Eta model, including a category for cultivations. Agricultural regions may be more susceptible to flash drought due to a shallower root zone and a higher rate of ET (soil moisture depletion) relative to natural grassland. The second factor that may lead to increased flash drought frequency is land-atmosphere coupling. The Great Plains has been identified by several studies as a hot spot for land-atmosphere coupling (Koster et al. 2004;

Dirmeyer 2011; Basara and Christian 2018). Semiarid regions such as the Great Plains show greater sensitivity of surface fluxes and ET to changes in soil moisture (Guo et al. 2006; Dirmeyer 2006; Wei et al. 2016). As soil moisture decreases, ET is reduced, which limits the availability of locally sourced boundary layer moisture. In the absence of significant moisture advection, the atmosphere continues to dry and increases evaporative demand. This results in a positive feedback in which dry soils modify the environment and make it less favorable for convective precipitation (Findell and Eltahir 2003a,b; Pielke 2001). Such positive feedbacks due to land-atmosphere coupling could serve to accelerate decreases in SESR and may be a key contributor to the greater frequency of flash droughts observed in the Great Plains.

Regions with a lower frequency in flash drought occurrence were also identified from the climatological analysis of flash droughts. These regions primarily existed over arid, high-elevation, or forested regions. Three main factors could contribute to a lack of flash drought events in these regions: 1) lack of available water in the soil profile, 2) sparse vegetation, and 3) vegetation type. Even when rainfall occurs in arid locations, limited soil moisture capacity prevents the wetting of the environment toward semiarid or dry subhumid conditions. Furthermore, transitions from limited evaporative stress to strong evaporative stress over an extended period of time in these regions are less likely due to a lack of available water in the soil profile. The second potential contributing factor to minima in flash drought occurrence is sparse vegetation. This mostly includes high-elevation regions (e.g., the Rocky Mountains) or desert locations. With minimal vegetation, transpiration is limited and leads to restricted ET. To obtain a rapid change in SESR for flash drought development, a rapid decrease in ET is required (in conjunction with a rapid increase in PET). Furthermore, regions of sparse vegetation will likely have short periods of declining SESR. For example, the Mojave Desert can receive an abundance

of rain during the monsoon. This will ultimately lead to frequent large spikes in ET followed by a large decrease in ET due to the large evaporative demand. However, this transition from minimal evaporative stress to large evaporative stress would likely happen during a short time period (i.e., one or two pentads). These short transitions from minimal evaporative stress to large evaporative stress would not meet the criteria or definition for an agricultural flash drought. Last, vegetation type can also play a critical role in inhibiting flash drought development. For example, in forested regions, such as the Ozarks and Appalachian Mountains, deeper root zones can access more subsoil moisture, precluding a rapid increase in evaporative stress.

In section 2.4.2, flash droughts were partitioned by their rate of intensification, following a categorization similar to that used by the Drought Monitor (Svoboda et al. 2002). The agricultural regions across the United States (central Great Plains, Corn Belt, and portions of the Atlantic coastal plain) emerged as a significant hot spot for the most rapidly developing flash droughts (FD3/ FD4; Fig. 2.8). This supports the hypothesis previously discussed, where regions with crops act as an accelerant for changes in evaporative stress, and as such, lead to the most intense flash droughts. Furthermore, while moderate and severe flash droughts are possible in any region across the United States, hot spots of flash drought frequency in the FD1 and FD2 categories were still seen across the Great Plains and Corn Belt. This implies that while flash droughts can develop over other vegetation types (grasslands, forests, etc.), agricultural regions tend to contain a higher frequency of flash droughts of any intensity.

The methodology presented in this study provides objective identification of flash drought events. However, it is important to be cognizant of two artifacts resulting from this methodology. First, while the methodology performed well with the individual flash drought cases and the climatological analyses in this study, it is possible that changes in SESR could be

dependent on the LSM used by different reanalysis datasets. Grid point by grid point daily standardization of ESR provided in section 2.2.1 should largely account for these differences as long as the LSM still captures the variability in ET and PET, but variations in the distribution of ΔSESR among different datasets could make the 40th-percentile-based methodology presented in this study (in conjunction with the minimum 25th percentile change in evaporative stress over the entire length of the flash drought) too strict or too loose. However, it was ultimately shown that, through the standardization process in section 2.2.1, SESR values and change values from a reanalysis dataset (NARR) compared well with the ESI, which has been shown in prior studies to accurately capture the evolution of flash droughts as well as the USDM. This provides confidence that the given methodology should be able to account for differences between datasets satisfactorily for application across a diverse set of datasets.

The second limitation is inherent in the development of any objective-based methodology for flash drought identification. That is, identifying features that are not actually flash drought events and not identifying features that are actually flash drought events. From an objective standpoint, this requires an upper bound and a lower bound to identify flash droughts. To illustrate, we allow the upper bound to represent the identification of features that are not flash droughts (i.e., false alarm; too many flash droughts identified) and the lower bound to represent missed identification of features that are flash droughts (i.e., misses; too few flash droughts identified). The methodology presented in this study provides a cap for the upper bound of flash drought identification by placing four criteria to capture flash drought events. The four criteria in section 2.2.2 emphasize the minimum requirements for a flash drought event, pertaining to the rate of intensification and impact of flash droughts [following the guidelines presented in Otkin et al. (2018a)]. However, the lower bound of flash drought identification (missing the

identification of flash drought events) can be partially subjective. For example, in the inclusion of periods of moderation within the methodology, moderation could be adjusted to include up to two or three pentads before continuing the rapid intensification of evaporative stress toward drought. Even so, the authors believe that including a moderation period this large in the objective flash drought methodology could mistakenly identify features that take several months to develop as "flash droughts" when instead they more closely fit the definition of conventional slower developing droughts.

Finally, additional reanalysis datasets exist with varying spatial resolution, for instance, phase 2 of the North American Land Data Assimilation System (NLDAS-2; Xia et al. 2012) and MERRA, version 2 (MERRA-2; Gelaro et al. 2017). Future work will examine the impact of the resolution of the LSM on the variability of the drivers associated with flash drought and flash drought identification. While beyond the scope of this study, scalability of flash drought identification among datasets is critical and will be a topic of future research.

2.6 Conclusions

This study follows upon the proposed flash drought definition provided in Otkin et al. (2018a) in which flash droughts are identified based on their rapid rate of intensification. Two major components were discussed: a methodology for flash drought identification and application of the methodology to a reanalysis dataset. A percentile-based methodology for flash drought identification was developed utilizing standardized anomalies of evaporative stress. The proposed flash drought identification methodology emphasizes vegetative impact and rapid rate of intensification from flash drought. Two criteria in the identification methodology incorporate vegetative impacts by separating dry spells from flash droughts and ensuring that a flash drought

event ends in drought conditions. Two additional criteria emphasize the rapid rate of drought intensification, with one criterion focused on pentad-to-pentad changes in evaporative stress, and the other criterion focused on the rate of change in evaporative stress through the entire length of the flash drought event.

Values of SESR from the NARR were compared with ESI values from satellite-based thermal infrared observations and were found to have comparable timing and rate of change in evaporative stress. A climatological analysis of flash drought events in the NARR dataset from 1979 to 2016 revealed a hot spot of flash drought events over the Great Plains, Corn Belt, and western Great Lakes region. Flash droughts were partitioned by intensity (rate of intensification) and revealed that flash droughts with the largest rate of intensification occurred across the central Great Plains, Corn Belt, and western Great Lakes region.

With the flash drought methodology presented in this study, future work will investigate flash drought climatologies using other reanalysis and observational datasets. Furthermore, the initial climatological results indicate that future work is also needed to examine regional characteristics of flash droughts across the United States.

Chapter 3: Regional Characteristics of Flash Droughts across the United States (Christian et al. 2019b)

3.1 Introduction

Flash droughts are characterized by the rapid onset and development of drought conditions (Otkin et al. 2018). Given the four traditional drought classifications (meteorological, agricultural, hydrological, and socioeconomical; Wilhite and Glantz 1985), flash droughts develop on timescales between meteorological and agricultural drought. When a combination of extreme atmospheric anomalies (such as lack of rainfall, higher surface temperatures, higher surface wind speeds, and higher vapor pressure deficit) persist for several weeks, rapid depletion of soil moisture can occur and lead to increased evaporative stress on the environment. Through this process, flash droughts can lead to large agricultural yield losses and impact the availability of short-term water resources. For example, expansive flash drought occurred across the central Great Plains and Midwest regions of the United States (US) in 2012, which led to significant agricultural losses in excess of $30 billion (Otkin et al. 2018, National Centers for Environmental Information 2019) and disrupted the global food supply (Boyer et al. 2013). More recently, rapid drought intensification occurred in the northern High Plains in 2017 which significantly impacted wheat production and increased the risk for wildfires (Gerken et al. 2018, National Centers for Environmental Information 2019). As such, the rapid and devastating impact of flash drought necessitates a deeper understanding of the fundamental characteristics of flash drought.

Overall, individual case studies have primarily been used to examine the characteristics of rapid onset drought. For example, Otkin et al. (2016) and Basara et al. (2019) explored the temporal and spatial evolution of the 2012 flash drought event across the central US. Hunt et al.

(2014) investigated a flash drought event that occurred in Mead, Nebraska in 2003 by comparing soil water, evapotranspiration, and gross primary productivity to two drought indices and its effect on dryland crop yields. In addition, several flash drought case studies have been examined that reveal differences in flash drought characteristics across different years and geographic regions. For example, Otkin et al. (2013) investigated four flash drought events across the central US during different parts of the growing season and each event had unique rates of rapid intensification toward drought. Ford et al. (2015) examined five flash drought events between 2000 and 2013 across Oklahoma and indicated varying degrees of drought conditions from the US Drought Monitor (USDM; moderate drought, abnormally dry, and no drought) preceding flash drought events. In addition, flash droughts do not necessarily transition to longer term drought (e.g., hydrological) and can undergo a period of rapid recovery from drought conditions (Otkin et al. 2019). Along with these case studies, it is also important to perform more comprehensive climatological studies to determine if characteristics found during individual case studies are representative and to explore geographic differences that may exist in the rapid onset and development of drought. In addition, improved understanding of the characteristics of flash drought events unique to specific climate regions lays the foundation for improved flash drought monitoring, detection, and predictability.

From an observational standpoint, flash drought development can be examined via the use of evaporative stress, evaporative demand, soil moisture, or other related variables. Otkin et al. (2013) initially examined flash droughts via the satellite-derived Evaporative Stress Index (ESI) (Anderson et al. 2007a, 2007b). Subsequently, the Rapid Change Index (RCI) was derived from temporal changes in ESI and used to explore the relationship between rapid drought development and changes in evaporative stress (Otkin et al. 2014, 2015) Similarly, Hobbins et al.

(2016) and McEvoy et al. (2016) leveraged atmospheric demand via the Evaporative Demand Drought Index (EDDI) to monitor the development of flash drought while Ford et al. (2015) examined the utility of soil moisture for monitoring flash drought. Each of these methods provides one to two weeks of lead time with respect to drought impacts on the environment (i.e., significant reduction of soil moisture, stress on vegetation and agriculture, etc.).

Overall, two approaches for flash drought detection have been developed in the scientific literature: by (1) rapid intensification (e.g., Otkin et al. 2013, 2014) or (2) short duration (e.g., Mo and Lettenmaier 2015, 2016). Otkin et al. (2018) performed an assessment of these two definitions, and ultimately argued that flash droughts are defined by rapid intensification with corresponding impacts versus overall short duration. Based on (1) and the criteria and suggestions outlined in Otkin et al. (2018), Chapter 2 shows how a percentile-based methodology for the identification of flash droughts is developed using the standardized form of the Evaporative Stress Ratio (ESR); ESR is the ratio between evapotranspiration and potential evapotranspiration and is inversely proportional to the amount of evaporative stress on the environment such that higher (lower) ratios are indicative of lower (higher) stress. The use of ESR for flash drought identification is advantageous compared to individual variables (e.g., soil moisture) as it incorporates the impacts of changes in air temperature, wind speed, vapor pressure deficit, latent and sensible heat flux, soil moisture, and precipitation. Additionally, four criteria were employed to identify flash droughts using standardized ESR (SESR) with two criteria which emphasized the rapid intensification toward drought and two criteria focused on vegetative impact (further details on the standardization of ESR and development of the percentile-based methodology are available in Chapter 2). As such, this study uses the Otkin et

al. (2018) flash drought definition (rapid rate of intensification toward drought) and the methodology presented in Chapter 2 for the identification of flash droughts.

The purpose of this study is to explore seasonal characteristics of flash droughts and how they vary across the United States. Specifically, this analysis focuses on quantifying (1) the timing of flash droughts (2) the intensity (rate of intensification) of flash droughts, (3) the moisture conditions preceding flash drought events and (4) the likelihood of persistence from flash drought to hydrological drought. Lastly, potential attributions of the regional differences in flash drought characteristics are discussed.

3.2 Data and Methods

The primary dataset used in this study for the identification and evaluation of flash drought characteristics over CONUS is the National Centers for Environmental Prediction North American Regional Reanalysis (NCEP NARR; Mesinger et al. 2006). The NARR was selected as results in Chapter 2 showed that SESR derived from NARR compares well with the satellite-based Evaporative Stress Index (ESI) and to drought depictions from the USDM. The time period used during this study spans 1979 to 2016. The variables used during the analysis include evapotranspiration, potential evapotranspiration, and volumetric soil moisture.

Flash droughts were identified when values of SESR and changes in SESR satisfied four criteria described in Chapter 2, where SESR and change in SESR are defined in equations (2) and (3). SESR and ΔSESR were detrended by removing the linear trend for the time series of SESR and ΔSESR for each pentad and at each grid point between 1979 and 2016. Detrending SESR and ΔSESR accounts for changes in the flash drought identification thresholds that may occur over time. For the first two criteria, a flash drought event had to have a minimum length of

five negative SESR changes, equivalent to a length of six pentads (30 days), and have a final SESR value below the 20th percentile from climatological SESR. These criteria place an emphasis on drought impacts (e.g., depletion of soil moisture, stress on the ecosystem, etc.) and fulfill the drought component of flash drought (Otkin et al. 2018). The final two criteria emphasize the rapid rate of intensification toward drought. One criterion focuses on pentad-to-pentad changes in drought development (the change in SESR must be below the 40th percentile between individual pentads), and the other criterion accounts for rapid drought development through the entire flash drought event (the mean change in SESR during the flash drought event must be less than the 25th percentile). In addition, conditional inclusion of one moderation pentad (pentad-to-pentad change exceeding the 40th percentile) was also incorporated into the flash drought identification. For criteria 2 (final SESR value) and 3 (pentad-to-pentad changes in SESR), percentiles were taken from the distribution of SESR and ΔSESR at local grid points and each individual pentad from 1979 to 2016. For criterion 4 (mean change in SESR), percentiles were taken from the distribution of ΔSESR at local grid points for pentads that were encompassed within the flash drought event.

3.3 Quantifying Flash Drought Characteristics

To quantify the regional characteristics of flash drought events, the analysis was partitioned into nine climate regions across the United States grouped by their climatologically similar characteristics (Karl and Koss 1984). Flash droughts were identified by using the percentile-based methodology described in section 3.2 and with further detail in Chapter 2. From the compiled set of flash drought events identified, the start date of each flash drought event (the first pentad change in SESR below the 40th percentile; i.e., the pentad when the period of rapid

intensification began) was used to partition flash droughts by month. The temporal analysis of flash drought was focused over the growing season from April through October as evapotranspiration and potential evapotranspiration are limited during the winter months, preventing rapid changes in evaporative stress over extended periods of time. However, it is important to note that flash droughts that began in March were included in the analysis as long as the period of rapid intensification ended in the growing season (e.g., April). The end of rapid intensification was marked at the last pentad where the preceding pentad change in SESR was below the 40th percentile. In addition to identifying the timing for peak frequency during the growing season, the average intensity of flash droughts in each month was also calculated. Following upon the work shown in Chapter 2, intensities were categorized on a scale from FD1 (moderate flash drought) to FD4 (exceptional flash drought). FD1 indicates the mean change in SESR during a flash drought event was between the 20th and 25th percentile of SESR changes, while FD2, FD3, and FD4 indicate percentiles between the 15th and 20th, 10th and 15th, and below the 10th, respectively.

While SESR is influenced by thermal, moisture, and radiative flux variables, moisture is an especially critical component of SESR. This is due to contributions from surface storage (soil moisture), the magnitude of vapor transfer from the land surface to the atmosphere (evapotranspiration/latent heat flux), and the atmospheric demand for moisture (e.g., vapor pressure deficit). As such, SESR provides a comprehensive summary of environmental moisture conditions and was used to examine regional differences in these conditions preceding flash droughts. A two-month average of SESR was calculated before each flash drought event to investigate the evaporative stress on the environment before the rapid intensification toward drought began.

The probability of hydrological drought persisting from flash drought was also computed for each climate region. Hydrological drought can be challenging to determine because its impacts (streamflow, reservoir levels, lake levels) can be difficult to quantify from a meteorological perspective (e.g., soil moisture). However, deeper soil moisture will have a slower response to precipitation and evapotranspiration compared to near-surface soil moisture due to groundwater recharge and percolation, and will be more representative of hydrological impacts. As such, 40-100 cm soil moisture was used from the NARR to quantify persistence of flash drought to hydrological drought. Drought is generally classified by its associated impacts (meteorological, agricultural, hydrological; Wilhite 2000), however a common time period of analysis is required to provide a progression of impacts on water resources. Ultimately, the 6 month period following flash drought was selected to examine the persistence of flash drought to longer term drought and to mark a notable progression from flash drought impacts (increased evaporative stress, depleted near-surface soil moisture) to hydrological impacts (reduced streamflow, declining reservoir and lake levels). This time period was also selected as the USDM uses the same threshold for short to long term transitions in drought (National Drought Mitigation Center 2019). A 6-month average of standardized 40-100 cm soil moisture following each flash drought event was calculated. The centered percentile of the 6-month soil moisture average was determined from the distribution of 38 years of 6-month average soil moisture values at the given time of year and associated grid point and categorized into surrogate drought classes based on USDM drought monitor percentiles (Svoboda et al. 2002). Percentiles less than 30th were classified as D0 (abnormally dry), less than 20th were classified as D1 (moderate drought), less than 10th were classified as D2 (severe drought), less than 5th were classified as D3 (extreme drought), and less than 2nd were classified as D4 (exceptional drought). Soil

moisture values greater than the 30th percentile or classified as D0 were identified as no drought, while categories D1 through D4 were identified as drought.

It is critical to note that the use of percentiles in the analysis of drought to flash drought persistence do not necessarily universally represent similar progressions of drought impacts in different climate regions. For example, a humid subtropical region may experience a flash drought and progression to longer term drought, but with little variation in soil moisture within these regions, impacts to the ecosystem and streamflow may be low. In contrast, a desert region with low soil moisture overall may experience a much larger impact to hydrological impacts (such as streamflow) due to a severe depletion of soil moisture, resulting from a persistence of drought following a flash drought event. As such, the primary purpose of this analysis is to investigate the overall progression and evolution of drought impacts within individual climate regions, with a lesser focus on the specific magnitudes of those impacts.

3.4 Results and Discussion

Temporal frequency of flash drought events for each of the nine climate regions across the United States are shown in Fig. 3.1 with regional differences in the timing of peak frequency. In the western United States (Northwest, West, and Southwest climate regions), generally characterized by arid and semi-arid climate regimes as well as mountainous topography, flash droughts occur more often during the early portion of the warm season (May and June). An exception is the Northwest climate region, in which an additional peak of flash drought frequency is seen at the very end of the growing season. Further eastward across the United States in regions with more intensive agricultural production (West North Central, South, East

North Central, and Central), flash drought frequency is greatest in the middle portion of the growing season (June and July).

In addition to the peak frequency, the distribution during the growing season is unique for particular climate regions (Fig. 3.1). A common theme among several climate regions is increased frequency at the beginning of the growing season and a decrease in frequency in the latter portion of the growing season. This was evident in the Southwest, West North Central, South, East North Central, Central and Northeast climate regions. However, three of the climate regions yielded alternate distributions. For the Northwest and West climate regions, monthly flash drought frequency is variable between March and October. In the Southeast region, the flash drought frequency generally increases in the beginning and middle portions of the growing season, with a peak of frequency interspersed during May.

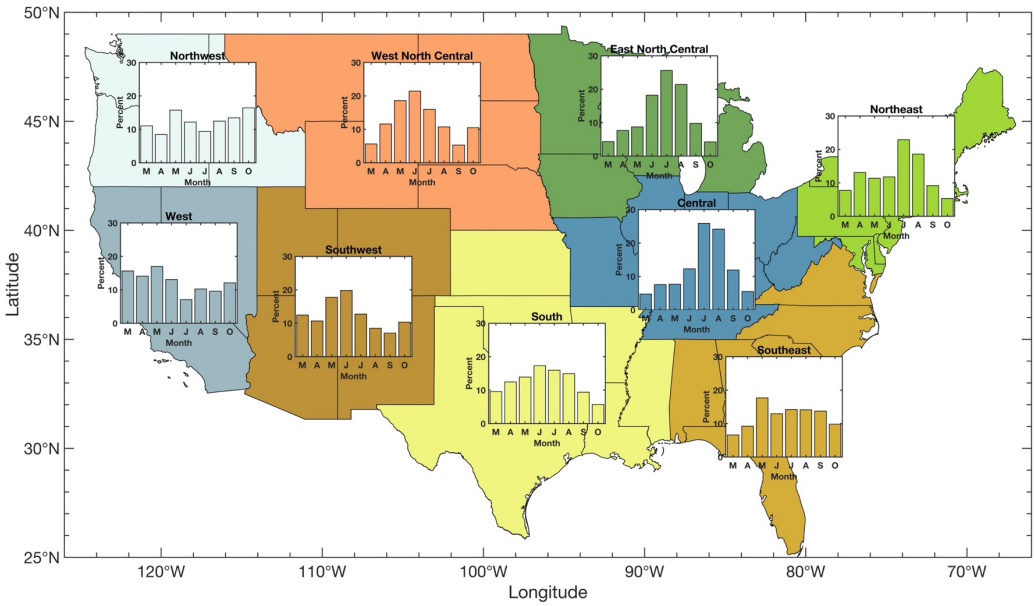

Fig. 3.1. Percentage of flash drought occurrence partitioned by the starting month for flash drought for each of the nine climate regions across the United States between 1979 and 2016.

Regional differences in the timing of flash drought development can possibly be attributed to several meteorological and climatological factors. Beginning with the west coast of the United States, the timing of atmospheric rivers during the growing season may contribute to the development of flash drought. While atmospheric rivers are generally described as cold-season phenomena, they still occur throughout the year along the United States west coast (Mundhenk et al. 2016). Atmospheric rivers have also been shown to contribute to a large fraction of the precipitation (15%-60%) in Washington, Oregon, California, Idaho, and Nevada within the cold season (Rutz et al. 2014). Given the significant moisture transport from these features, a lack of moisture transport and associated precipitation extending from the cold into the warm season may increase the likelihood for flash drought development.

In the Southwest climate region, approximately 50% of the total annual rainfall in Arizona and New Mexico occurs in the months of July, August, and September due to the North American monsoon (Sheppard et al. 2002). The onset of the monsoon is typically in early July, but can begin in the latter portions of June or as late as the end of July (Higgins and Shi 2000). Given the higher flash drought frequency in the months of May and June (Fig. 3.1), a delay in the onset of the monsoon may contribute to the development of flash drought in this region.

The peak of flash drought frequency in the summer months across the central United States (West North Central, South, East North Central, and Central climate regions) is likely due to a combination of factors, including atmospheric demand of evapotranspiration (potential evapotranspiration), agriculture, and land-atmosphere coupling. In Hobbins et al. (2012), enhanced values of potential evapotranspiration were found to exist in July across the Southern Great Plains, extending into the Northern Great Plains and Midwest. As such, increased atmospheric demand of evapotranspiration within this region in the summer may increase the

likelihood of flash drought development due to elevated evaporative stress on the environment. Another contributor to the temporal hotspot in flash drought frequency is agriculture. Vegetation type in the NARR is prescribed by the National Centers for Environmental Prediction Eta Model. Within the thirteen vegetation types is a category for cultivations, which characterize a large portion of the land type across the central US. As crops develop in the growing season, a higher rate of evapotranspiration will occur, which in turn will quickly deplete soil moisture, rapidly increase evaporative stress, and promote the development of flash drought. The last factor that may lead to a higher frequency of central US flash droughts during the summer is land-atmosphere coupling. The Great Plains has previously been identified as a hot spot for land-atmosphere coupling in June, July, and August (Koster et al. 2004, Dirmeyer 2011, Basara and Christian 2018). Dry soils modify the environment such that evapotranspiration is reduced and locally sourced boundary layer moisture is limited, which acts to both inhibit precipitation and increase evaporative demand. This results in a positive feedback that may make flash drought development more favorable in the summer months.

A likely factor contributing to the distribution of flash drought frequency in the growing season for the Southeast and Northeast is persistent upper-level ridging. In the Northeast, a blocking ridge can induce enhanced subsidence and the inhibition of climatological precipitation leading to flash drought development during the warm season. For the Southeast in particular, anomalous subsidence associated with a persistent upper-level ridge can suppress the diurnal convection typical during the warm season. If precipitation inhibition persists for extended periods, evaporative stress can develop leading to flash drought development. In addition, rainfall from tropical cyclones in the Southeast can prevent flash drought or terminate rapid drought development in the latter portions of the warm season (Maxwell et al. 2013, Brun and

Barros 2014). As such, the higher frequency of flash droughts observed in the beginning of the warm season (e.g., May) compared to later in the warm season may be attributed to the timing of tropical cyclones.

The monthly averaged flash drought intensity for the nine climate regions is shown in Fig. 3.2. The relative number of flash drought events that contributed to the average intensity calculation for each month are also shown via flash drought occurrence per grid point. A similar trend seen among each of the climate regions is an increase in the average intensity during the beginning of the growing season and a decrease in the average intensity toward the end of the growing season. However, the timing in peak intensity varies among the climate regions. For example, the West climate region has peak flash drought intensity centered around June, July,

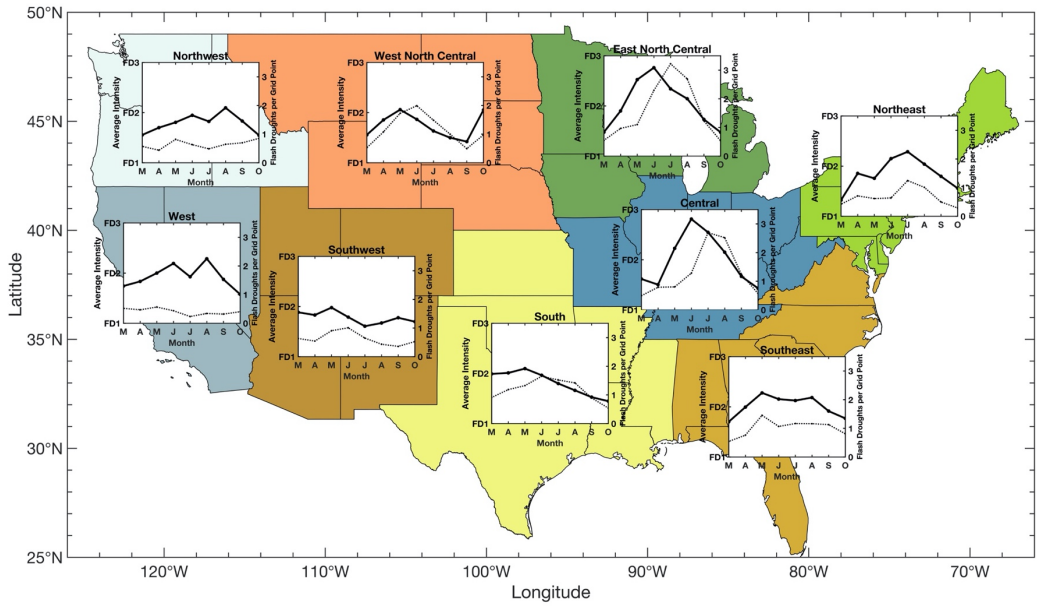

Fig. 3.2. Average flash drought intensity (solid black line) and total flash droughts per grid point (dotted black line) partitioned by month for each of the nine climate regions across the United States between 1979 and 2016.

and August, while the adjacent Southwest climate region has peak intensity in May. For the eastern half of the United States, June and July were the primary months for peak intensity. Further, while most climate regions have an average intensity (i.e., rate of intensification) that remains near or below FD2 throughout most the growing season, the Central and East North Central climate regions had a peak average intensity approaching FD3 in the month of June. Such rapid intensification toward drought in these regions could be attributed to agriculture and ecological features. As previously discussed, crops and vegetation may act as an accelerant for rapid increases in evaporative stress and lead to the most intense flash drought. The resulting influences of cultivations could also possibly be related to the larger overall frequency of flash drought seen across the Midwest in Figs. 3.1 and 2.7.

The overall environmental conditions preceding flash drought development depicted by SESR are shown in Fig. 3.3. First, three of the nine climate regions (West, Southwest, and Southeast) had a distribution in which over 70% of the flash drought events were preceded by a 2-month mean SESR below zero. These results suggest that within these regions, a 'kickstart' of abnormally dry conditions is often needed to prompt the initiation of rapid drought development. In particular, the Southeast climate region had over 77% of flash droughts preceded by below normal SESR. While the Southeast region has some of the largest mean annual temperature values in the US from a climatological perspective, the region also receives large amounts of precipitation annually (>100 cm). Overall, this combination acts to reduce the vapor pressure deficit at the land surface, reducing the evaporative stress. Because evapotranspiration is an important process in the depletion of soil moisture and subsequent increased evaporative stress, it is likely that antecedent drying of soil moisture is needed to promote rapid drought development. The West climate region similarly had a large percentage of flash droughts preceded by below

normal SESR (~75%). Given that the highest frequency of flash droughts is in the beginning of the growing season (Fig. 3.1), drier than normal moisture conditions following the winter months may set environmental conditions favorable for flash drought development as the atmospheric demand for evapotranspiration increases into the growing season. Lastly, the Southwest climate region had approximately 72% of flash droughts preceded by 2-month mean SESR below zero. Via the temporal analysis, the months with the highest flash drought frequency preceded the typical onset period for the North American monsoon. As such, if a delay of the monsoon occurs, drier than normal environmental conditions earlier in the growing season may be more likely to transition to flash drought.

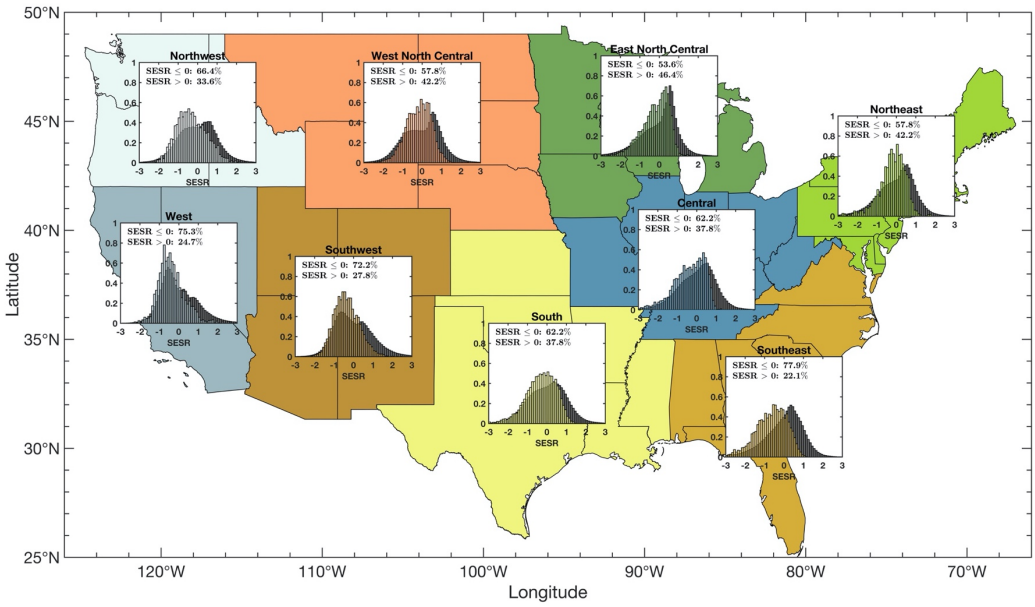

Fig. 3.3. A probability density function of two-month averaged SESR preceding each flash drought event (color) and all SESR values (gray) for each of the nine climate regions across the United States between 1979 and 2016. SESR values greater than zero indicate wetter than normal conditions while SESR values less than zero indicate drier than normal conditions.

Conversely, within the West North Central, South, East North Central, Central, and Northeast regions 37% to 47% of the flash drought events were preceded by above normal SESR. This demonstrates that even when environmental conditions were generally void of evaporative stress drivers during preceding months, rapid acceleration of drought could still occur in later periods regardless of prior conditions. Given the expansive land-use dedicated to agriculture in these regions, such results yield significant challenges related to flash drought predictability focused on antecedent conditions.

Overall, the distribution of SESR values preceding flash drought were shifted to drier moisture conditions compared to the entire SESR distribution for each region. Comparing the two distributions for each climate region with a two-sided Mann-Whitney U-test revealed that the lower medians for SESR values preceding flash drought events were statistically significant at the 99% significance level. As such, while the climate regions have different magnitudes in the shifts of the medians toward the drier side, below normal moisture conditions across the United States increase the likelihood for flash drought development.

Lastly, the percentage of flash droughts that persisted to hydrological drought is shown in Fig. 3.4. A critical result from this analysis is that over 50% of flash droughts did not transition to long term drought in each of the climate regions. However, it is important to note that even in the absence of this continuation, flash drought can lead to detrimental impacts on agriculture, ecosystems, and short-term water resources. In contrast to a lack of drought persistence following flash drought, 5% to 10% of all flash droughts in each climate region transitioned to the highest drought category (D4). In addition, the percentage in each drought category (D1 through D4) for every climate region was higher than the expected frequency (10%, 5%, 3%, and 2% for D1, D2, D3, and D4, respectively). Because the rapid intensification of flash droughts

concludes in a certain level of drought, it is not surprising that a larger frequency compared to the expected frequency exists. However, additional factors may also enhance this signal and aid in the persistence of flash drought to long-term drought such as positive feedbacks associated with land-atmosphere coupling and persistence of upper-level ridging.

Flash drought to long term drought transitions were also partitioned by month (Fig. 3.5). Two of the climate regions (Southwest and Southeast) yielded a decreasing trend in persistence percentages, indicating that long term drought following flash drought was more likely if the flash drought occurred within the beginning of the growing season. In contrast, the West and

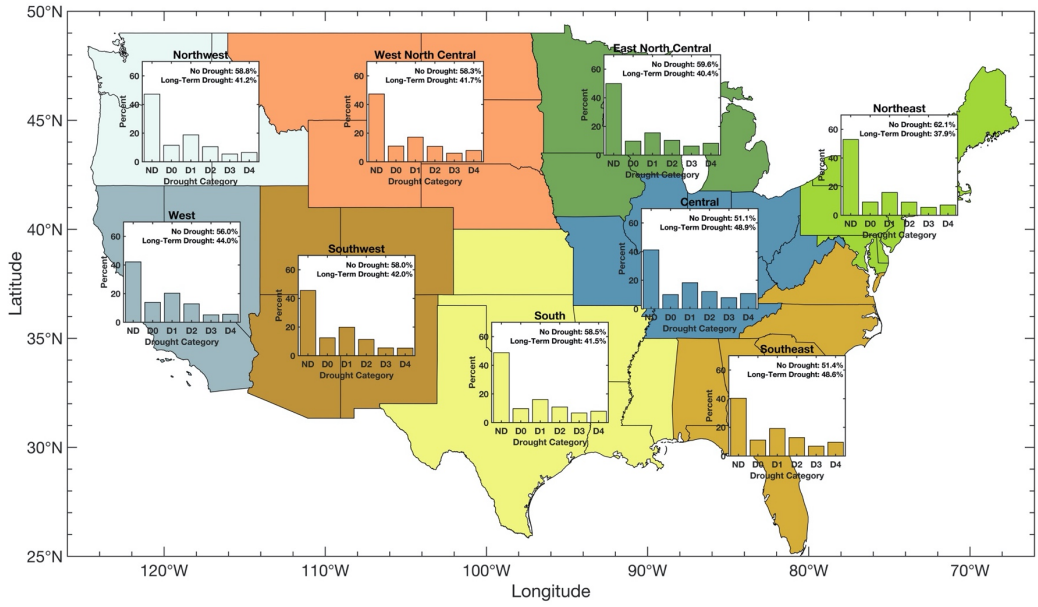

Fig. 3.4. Percentage of flash droughts that transitioned from flash drought to longer term drought (6 months) for each of the nine climate regions across the United States between 1979 and 2016. The drought categories represent the 6-month average of standardized 40–100 cm soil moisture. No drought (ND) and D0 constitute no drought, while the categories of D1 through D4 constitute drought.

Northeast climate regions had an increasing trend in percentages, demonstrating that long term drought is more likely if the onset of flash drought occurs at the end of the growing season. The central United States (West North Central, South, East North Central, and Central climate regions) had the greatest likelihood for long-term drought transition in the month of May. Lastly, the Northwest climate region yielded an increasing trend in the beginning of the growing season and a decreasing trend in the latter portion of the growing season. In addition to the previously mentioned factors for flash drought to long-term drought transitions (land-atmosphere coupling, upper-level ridges, etc.), the magnitude and timing of precipitation, with respect to the monthly climatological distribution of precipitation for each region, may also play a critical role. For example, the monthly climatological peak in precipitation for many of the states in the South

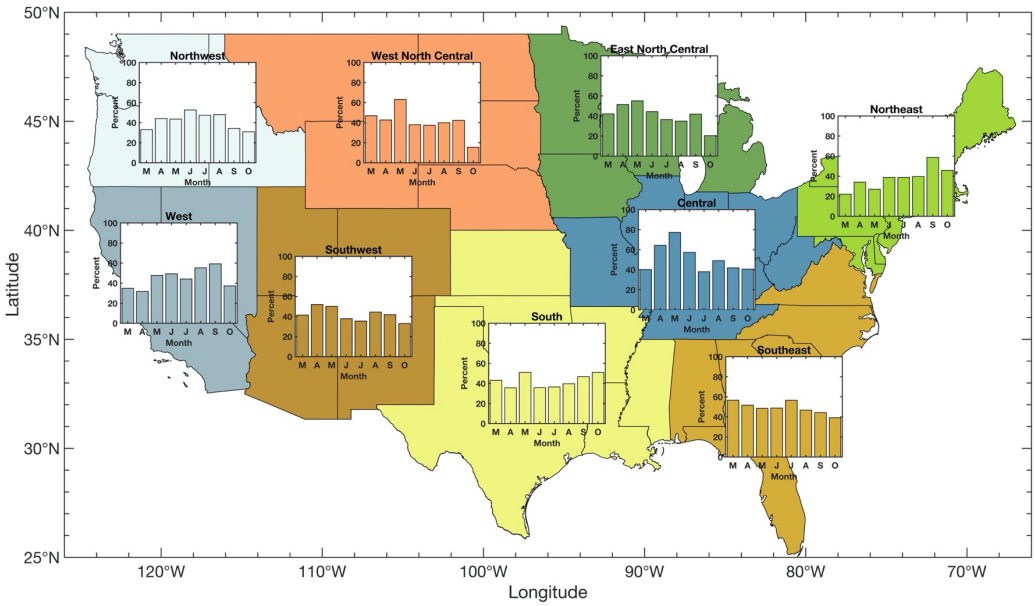

Fig. 3.5. Percentage of flash droughts that transitioned from flash drought to longer term drought (6 months) for each of the nine climate regions across the United States between 1979 and 2016, partitioned by month.

climate region is in May. Similarly, May was found to be the month with the highest percentage of flash drought to long-term drought transitions. As such, it is possible that an absence of precipitation due to a flash drought during a month that is climatologically important for precipitation may increase the likelihood of transitions to long-term drought, especially if subsequent monthly precipitation amounts are climatologically smaller.

3.5 Conclusions

This study presents a regional perspective of flash drought characteristics across the United States using the conceptual framework of Otkin et al. (2018) and the objective methodology developed and detailed in Chapter 2. First, differences exist in the seasonality of flash drought risk across climate regions. This includes key fundamental characteristics focused on the timing and intensity of flash drought events during the growing season. For example, May and June generally had a higher frequency of flash droughts in the western US, while July and August contained the climatological peak in flash drought frequency for a majority of the eastern US. Among all climate regions, flash drought intensity was found to increase in the beginning of the growing season, then decrease in the latter portion of the growing season. In addition, the preceding environmental conditions and potential post flash drought persistence to hydrological drought were quantified for the various climate regions in the United States. In all climate regions, less than half of all flash drought events persisted to hydrological drought. However, for long term droughts that did persist from flash droughts, the percentage of long term droughts in each drought category (D1 through D4) was higher than the expected frequency for each category. Furthermore, antecedent dry conditions increased flash drought risk for all of the climate regions. Even so, in five of the nine climate regions, 37% to 47% of flash drought events

occurred when the ambient environmental conditions in the preceding two months appeared unfavorable for drought development.

The results here provide important insight into the climatological characteristics of flash drought; however, a deeper understanding of these features is needed. As such, future work should examine why these regional differences exist along with critical surface and atmospheric drivers associated with flash drought development. Furthermore, regional characteristics of flash droughts across the globe should be investigated using additional reanalysis datasets, observations, or models. Finally, it should be noted that this analysis produced a climatological directory of flash droughts and its associated characteristics available for future research.

Chapter 4: Flash Drought Development and Cascading Impacts Associated with the 2010 Russian Heatwave

(Christian et al. 2020)

4.1 Introduction

The 2010 heatwave across western Russia was an extreme event that led to profound environmental, economic, and societal impacts. In the agricultural sector, grain yields were severely impacted, as the 'wheat belt' extending across southwestern Russia (the Central and Volga federal districts) experienced grain harvests that were less than half of what they were the previous year (Wegren 2011). As a result, the Russian government imposed an export ban on wheat in August 2010 that significantly increased its price in the global market (Welton 2011). Due to environmental conditions that included anomalously high surface temperatures and vapor pressure deficits, large wildfires were also prevalent. Thousands of people were displaced due to catastrophic loss of property (Bondur 2011) and severe air pollution from the fires significantly increased mortality during the late summer when the spatial extent of the wildfires was at its peak (Shaposhnikov et al. 2014). In all, the resulting impacts associated with the heatwave event led to a total of approximately 11,000 excess deaths (i.e. a near 20% increase in deaths for the given time period; Shaposhnikov et al. 2014).

Placed in historical context, the summer of 2010 was likely one of the warmest for Europe and western Russia in the last half millennium (Barriopedro et al. 2011). Record-high surface temperatures exceeding 32°C were reached for Moscow and the surrounding region by mid- to late July and persisted until the second week of August (Barriopedro et al. 2011, Grumm 2011). Three primary meteorological components have been connected to the development and

propagation of the heatwave event: (1) a quasi-stationary upper-level ridge centered over western Russia during July and August (Barriopedro et al. 2011, Grumm 2011), (2) sensible heat advection (Schumacher et al. 2019), and (3) land-atmosphere temperature coupling via heat storage in nocturnal residual layers (Miralles et al. 2014). The subsidence from the associated upper-level synoptic environment inhibited precipitation throughout most of the summer (Fig. 4.1) while persistent desiccation of the land surface occurred due to high evaporative demand. Sensible heat associated with desiccated soils southeast of the primary heatwave region were

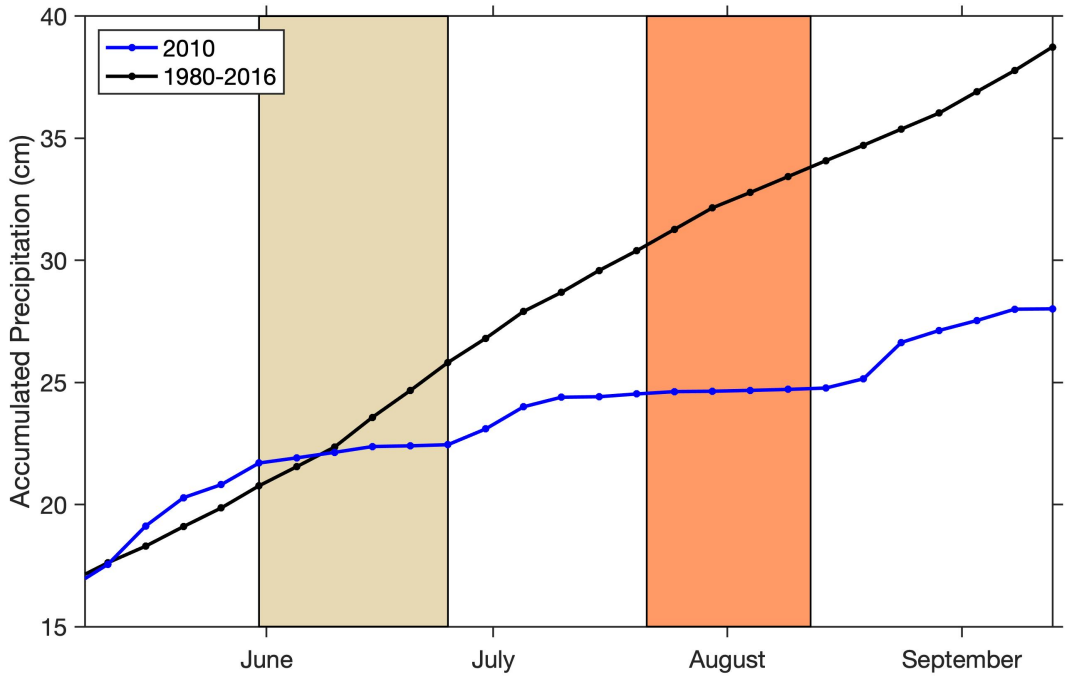

Fig. 4.1. Domain-averaged accumulated precipitation from MERRA-2 for the flash drought domain shown in Fig. 4.2. Accumulated precipitation beginning from 1 January is shown for 2010 in the blue line with the climatological mean for the period between 1980-2016 shown by the black line. The tan color indicates the time period of rapid drought development and the orange color indicates the time period of heatwave conditions.

advected northwestward and augmented the local sensible heat flux (Schumacher et al. 2019). In addition, progressive accumulation of heat in the boundary layer amplified the above-average surface temperatures (Miralles et al. 2014) already set in place by the overlying synoptic environment and land surface conditions.

This study expands upon the knowledge of the 2010 heatwave by linking the desiccated land surface and resulting sensible heat advection associated with the heatwave to a critical precursor subseasonal phenomenon: flash drought. Flash droughts are uniquely defined by their rapid rate of intensification toward drought conditions (Otkin et al. 2018). When a combination of environmental anomalies drive persistent, enhanced evaporative demand for several weeks, rapid depletion of available soil moisture will occur. As evapotranspiration (ET) from the land surface diminishes, the partitioning of surface energy fluxes contributes to a decreased evaporative fraction. Consequently, low values of evaporative fraction correspond with a decreased efficiency to moderate land surface temperatures and the resulting increase in evaporative demand will exacerbate the moisture stress on the environment. This process associated with rapid drought development directly impacts ecosystem health and agriculture productivity, such as was observed during the expansive flash drought across the Great Plains in 2012 that led to $30 billion in agricultural losses (Basara et al. 2019, National Centers for Environmental Information 2019) and the 2017 northern High Plains flash drought that significantly impacted wheat yields and increased the risk for wildfires (Gerken et al. 2018, National Centers for Environmental Information 2019). Heatwaves have also been related to flash droughts, but this has been examined from a short-term anomaly perspective that is different than that employed in this study (Mo and Lettenmaier 2015). The Russia flash drought examined in this study is significant as it presents a flash drought precursor event that (1) yielded

a rapidly desiccated land surface, (2) primed the land-atmosphere interactions necessary for heatwave development and sensible heat advection, and (3) significantly contributed to a sequence of cascading and catastrophic impacts. Following the data and methods section, the results provide a quantitative analysis of land surface conditions associated with the initial rapid intensification toward drought, an assessment of the hydrometeorological response to the flash drought, and the spatial spread of desiccated land surface conditions across southwestern Russia.

4.2 Data and Methods

Data from the Modern-Era Retrospective analysis for Research and Applications, Version 2 (MERRA-2; Gelaro et al. 2017) were used to provide land surface variables for analysis of the flash drought and heatwave event across southwestern Russia with a spatial resolution of 0.5° x 0.625°. Daily values for each of the variables and derived quantities were averaged into pentads, then detrended and standardized using data from 1980-2016. The variables were detrended to evaluate anomalies in surface conditions after accounting for changes in the climate during the 37 years of the MERRA-2 dataset. In addition, variables were standardized to convert values to a statistical metric for domain-averaged calculations and for comparison of anomalies across the analysis window (May through September). The enhanced vegetation index (EVI; Huete et al. 2002) from the Moderate Resolution Imaging Spectroradiometer (MODIS) onboard the NASA Aqua and Terra satellites was also used to leverage vegetative health as a proxy for the spatial propagation of land surface desiccation within the region of rapid drought development and heatwave onset during the summer months. The EVI was used as it reduces atmospheric influences on the canopy background signal (Huete et al. 2002) and is more sensitive to drought than the normalized difference vegetation index (NDVI; Wagle et al. 2014, Bajgain et al. 2015).

Further, EVI can accurately represent drought conditions via vegetative health as long as drought conditions persist for an extended period of time (e.g. greater than one month; Wagle et al. 2014) and the drought events are severe (Bajgain et al. 2015). EVI from Aqua was detrended and standardized with data from 2003–2019, while EVI from Terra was detrended and standardized with data from 2000–2019. The spatial resolution of the EVI used in the analysis was 0.05 degrees.

The spatial extent and temporal evolution of the flash drought event is analyzed using a comprehensive identification methodology in conjunction with the standardized evaporative stress ratio (SESR; Chapter 2, Chapter 3, Basara et al. 2019), which is a reanalysis-based variant of the satellite-derived evaporative stress index (ESI; Anderson et al. 2007a, 2007b) that has also been used extensively in flash drought research (Otkin et al. 2013, 2014, 2016, 2019, Nguyen et al. 2019). To calculate SESR, the ratio of ET and potential ET (PET; derived using the FAO Penman-Monteith equation; Allen et al. 1998) from MERRA-2 were used to calculate daily values of the evaporative stress ratio (ESR). Mean pentad values of ESR were computed and standardized at each grid point using equation (2), while the temporal change in SESR was calculated and standardized using equation (3).

The flash drought identification criteria follow guidelines previously established for classification of rapid drought development with a dual emphasis on longevity and impact (Otkin et al. 2018). Four criteria were used in total, with the first two focusing on the impacts of flash drought and the latter two emphasizing the rapid rate of intensification toward drought. Details of the criteria are provided in Chapter 2. In this study, the threshold percentile (30th percentile) in criterion (4) was slightly loosened compared to the threshold used for the climatological analysis of flash drought across the United States using a different dataset (25th percentile;

Chapter 2). The higher threshold (30th percentile) was used to better reveal locations that underwent flash drought development in this specific case study (especially for grid points with a mean overall change in SESR only slightly above the 25th percentile), while still requiring an overall rapid rate of intensification toward drought.

In addition to flash drought identification, the rate of intensification toward drought was classified into four categories using the mean SESR change (ΔSESR; criterion 4) using percentiles similar to those outlined in Chapter 2: FD1 - between the 25th and 30th percentile, FD2 - between the 20th and 25th percentile, FD3 - between the 15th and 20th percentile, and FD4 - less than the 15th percentile.

4.3 Temporal Evolution and Spatial Extent of Flash Drought

The primary flash drought development in southwestern Russia encompassed a region of approximately 260,000 km2 (Fig. 4.2). Rapid drought development occurred concurrently across the area in the latter portions of May (Fig. 4.2a). This large-scale and simultaneous rapid drought intensification is in contrast to what was observed during the 2012 Great Plains flash drought in the United States whereby flash drought spatially propagated over several months (Basara et al. 2019). However, the timing and location of the 2010 Russian flash drought was likely attributed to the presence of a quasi-stationary upper-level ridge and a different vegetation type across the region. The blocking high that began in June was expansive and covered a large area over much of eastern Europe and western Russia (Barriopedro et al. 2011, Grumm 2011). This blocking feature set the foundational atmospheric conditions for rapid drought development with a lack of rainfall and enhanced evaporative demand (e.g. increased surface temperatures and reduced cloud coverage) at the land surface. However, the specific location of the flash drought event

was likely due to ecosystems dominated by agriculture primarily south of 55°N (Fig. 4.3, Flach et al. 2018). This is attributed to increased ET rates across the region and a more rapid depletion of root zone and near-surface soil moisture as compared to forested areas (Figs. 4.3, 4.4, and 4.5; Chapter 2). This process rapidly lowers the evaporative fraction and limits the moderation of increased surface temperatures (Fig. 4.4). The higher surface temperatures further contribute to increased evaporative demand leading to a positive feedback and further desiccation of the terrestrial surface. As such, land-atmosphere coupling worked in tandem with the overlying synoptic environment to maximize rapid drought transition in this region. Areas north of 55°N in southwestern Russia are forest-dominated ecosystems and were shown to have normal and above-normal gross primary productivity during the summer of 2010 (Fig. 4.3, Flach et al. 2018). Due to the deeper rooting depths of trees, forests can provide locally-sourced

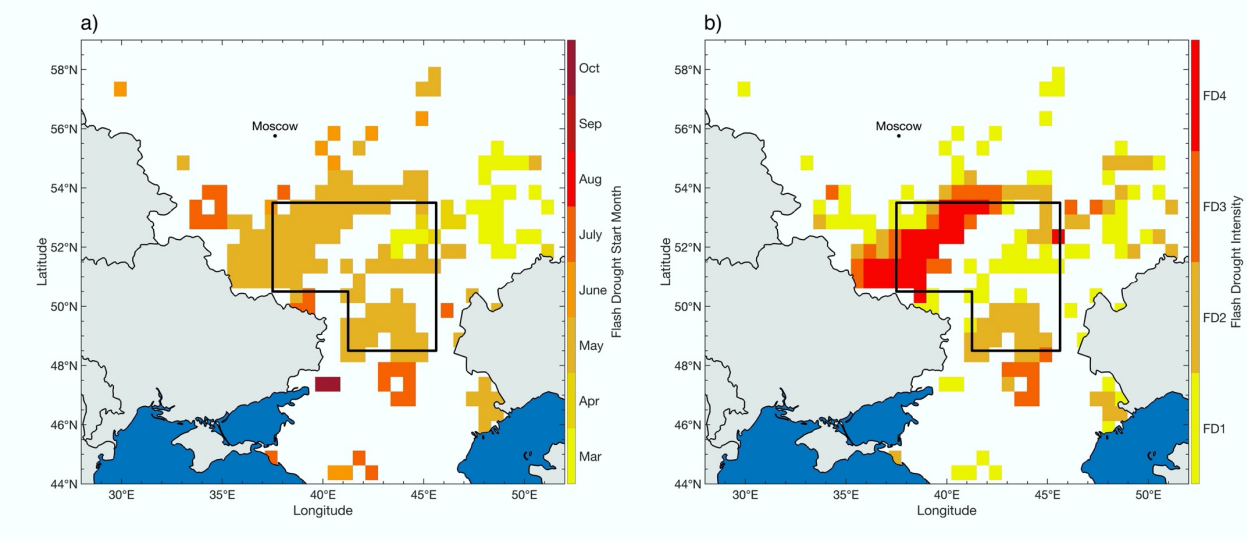

Fig. 4.2. Grid points identified as having flash drought development during 2010 with (a) the month in which flash drought began and (b) the flash drought intensity (rate of intensification toward drought). The domain outlined by the black lines define the boundaries used for the temporal analysis of flash drought development in Figs. 4.1, 4.4, 4.5, 4.8 and 4.9.

boundary layer moisture and moderate rapid drought development compared to an agriculturally dominated ecosystem. As a result, the region north of the primary flash drought area did not experience rapid drought development due to a slower decline of near-surface and root zone soil moisture over a couple of months (Fig. 4.5).

In addition to the very large spatial extent of the flash drought, the rate of intensification towards drought was unusually rapid even by the standards of flash drought. The rate of drought

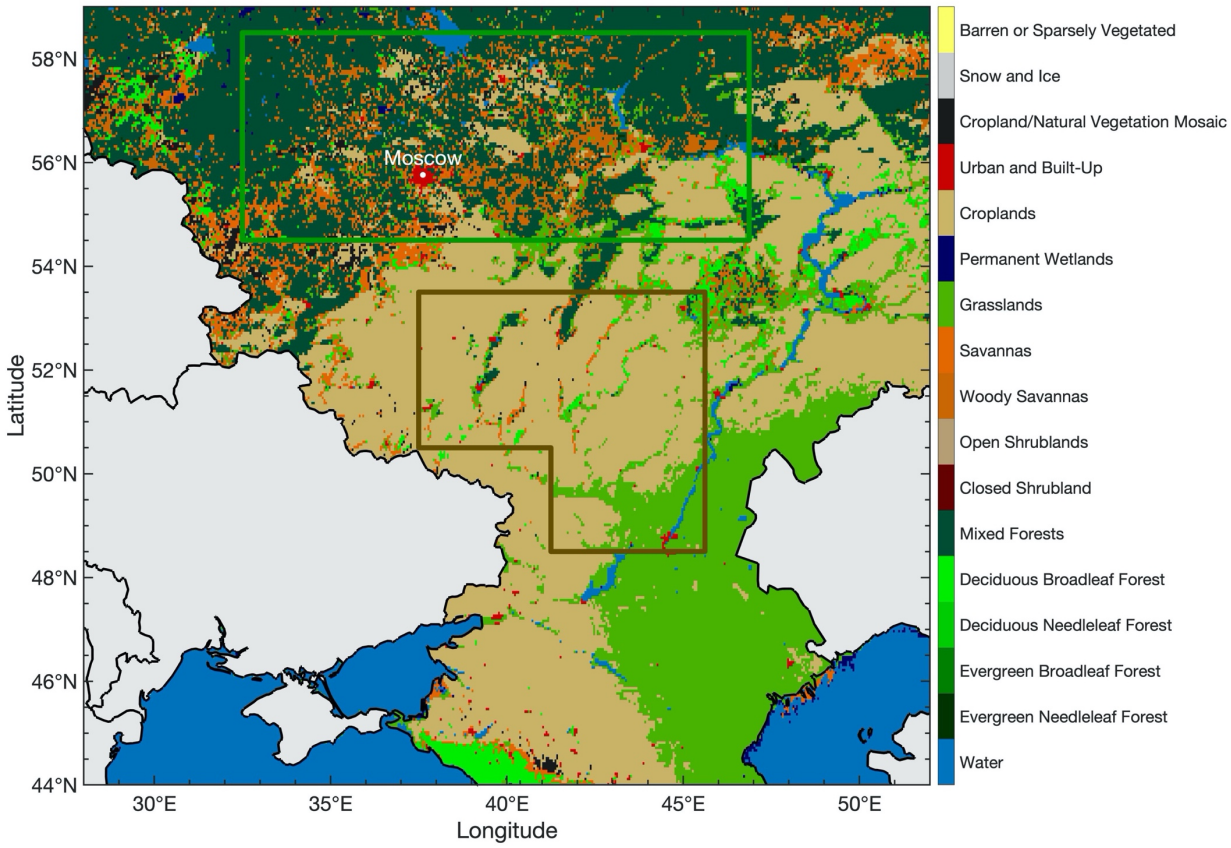

Fig. 4.3. Boundaries for the domains used for flash drought analysis (outlined with brown lines) and for the forest-dominated ecosystem in the region north of flash drought development (outlined with green lines). Land cover type (MCD12C1) is given by MODIS version 6 for 2010 using the International Geosphere-Biosphere Programme classification.

intensification was previously classified in Chapter 2 into four categories using the mean change in SESR at a given grid point during a flash drought: FD1 - moderate flash drought, FD2 - severe flash drought, FD3 - extreme flash drought, and FD4 - exceptional flash drought. While rapid drought development was classified as FD1 for much of the northeast portion of the domain, the southeastern section of the domain experienced flash drought categorized as FD2, and the western part of the study region saw the most rapid drought development, reaching FD4 classification. The southeastern portion of the domain was positioned within a temperature and precipitation gradient during the month of June (Figs. 4.6 and 4.7b), with higher standardized

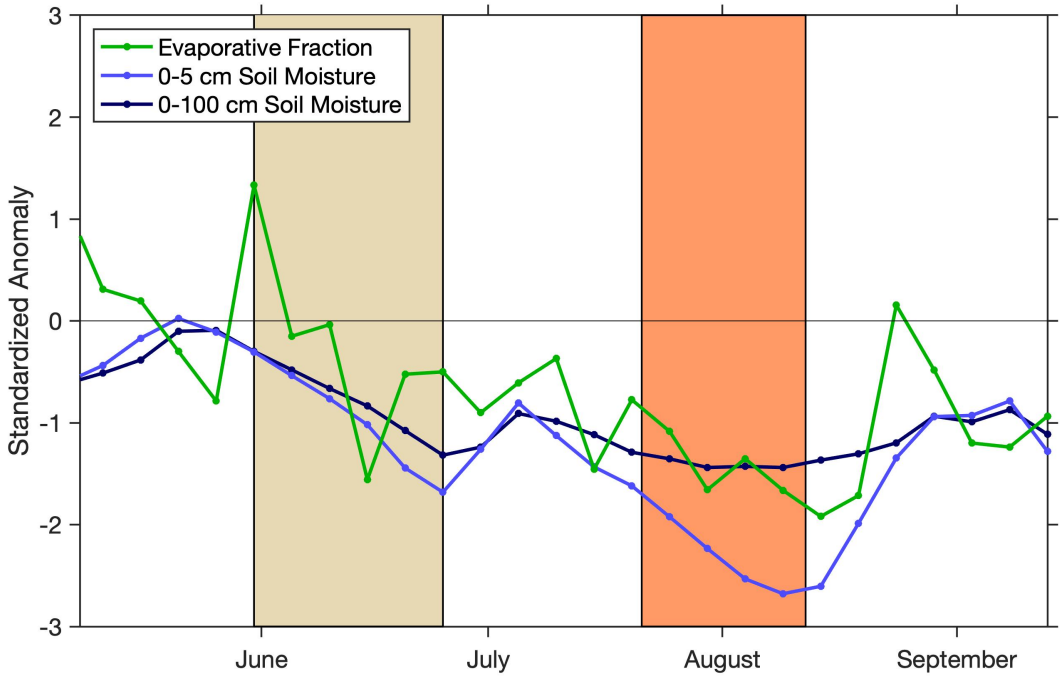

Fig. 4.4. Domain-averaged standardized anomalies of evaporative fraction, near-surface soil moisture (0-5 cm), and root zone soil moisture (0-100 cm) from MERRA-2 for the flash drought domain shown in Fig. 4.2. The tan color indicates the time period of rapid drought development and the orange color indicates the time period of heatwave conditions.

temperature anomalies in the west and lower precipitation amounts in the east (south of 50.5°N). The alignment between these two gradients promoted the very rapid drought intensification within this region, with the eastern part primarily driven by a deficit in precipitation and the western part supplemented by enhanced evaporative demand due to higher overall surface temperatures. For the western area of the study domain, below normal rainfall occurred in May prior to the onset of flash drought (Fig. 4.7a), with a further lack of rainfall during the rapid drought intensification period in June that was also coupled with above average surface

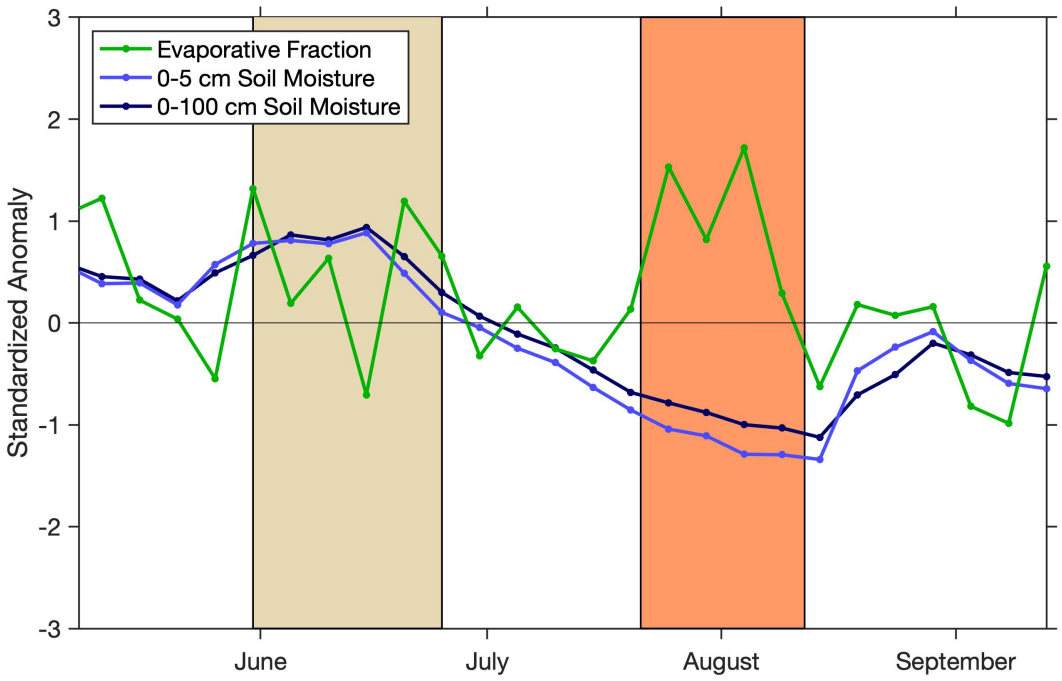

Fig. 4.5. Domain-averaged standardized anomalies of evaporative fraction, near-surface soil moisture (0-5 cm), and root zone soil moisture (0-100 cm) from MERRA-2 for the domain characterized by forest-dominated ecosystems (Fig. 4.3). The tan color indicates the time period of rapid drought development and the orange color indicates the time period of heatwave conditions as identified in the flash drought domain (Fig. 4.2).

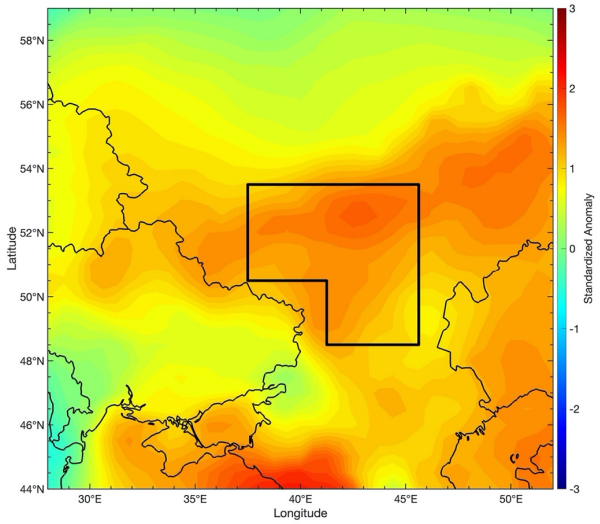

Fig. 4.6. Standardized anomalies of monthly averaged 2-meter temperature for June 2010 from MERRA-2. The domain outlined by the black lines define the boundaries used for the temporal analysis of flash drought development.

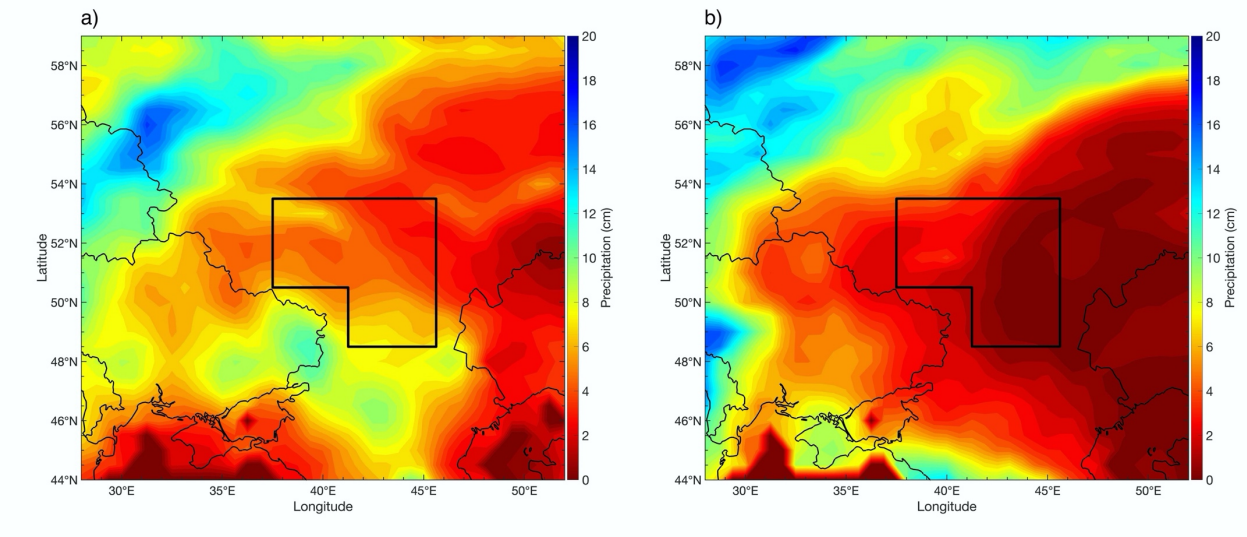

Fig. 4.7. Accumulated precipitation for a) May and b) June of 2010 from MERRA-2. The domain outlined by the black lines define the boundaries used for the temporal analysis of flash drought development.

temperatures (Figs. 4.6 and 4.7b). The coexisting deficit in precipitation and above-normal evaporative demand led to the rapid development of flash drought in this region.

The linkage between the flash drought event and heatwave event can be visualized by examining the temporal evolution of SESR and critical land surface variables that drive evaporative demand (Fig. 4.8). The domain used for analysis was selected to encompass a majority of the grid points that underwent flash drought during a similar period of time (Fig. 4.2a). The median start date of rapid drought intensification determined from identified flash drought grid points in the study domain was 31 May while the median end date of rapid

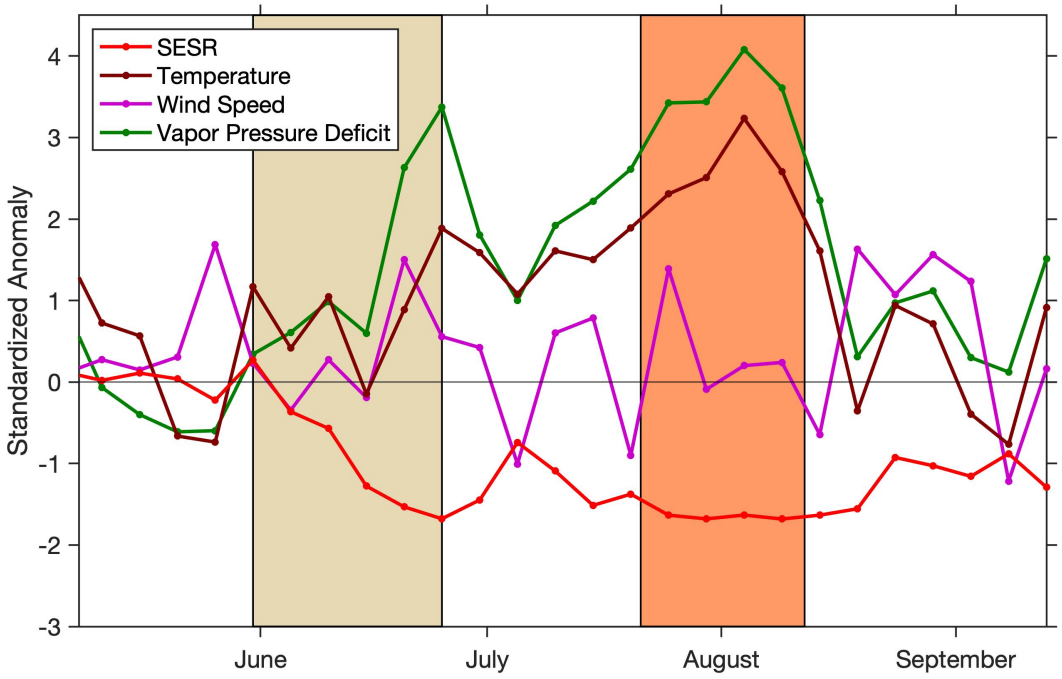

Fig. 4.8. Domain-averaged standardized anomalies of the evaporative stress ratio (SESR), 2-meter air temperature, 10-meter wind speed, and 2-meter water vapor pressure deficit for 2010 from MERRA-2. The tan color indicates the time period of rapid drought development and the orange color indicates the time period of heatwave conditions. The domain is shown in Fig. 4.2.

intensification was 25 June. During this 25-day period, SESR began slightly above normal (indicating above normal environmental moisture conditions) and then rapidly declined to a value approaching 2 standard deviations below normal. In addition to the minimal rainfall during the month of June (Figs. 4.1 and 4.7b), surface temperatures and vapor pressure deficits were above normal, with near-normal wind-speeds. Each of these components contributed to high levels of evaporative demand on the land surface and led to rapid depletion of near-surface and root zone soil moisture (Fig. 4.4). Following the flash drought event, SESR slightly recovered during the early portions of July, but then slowly declined to values near two standard deviations below normal during the rest of the summer and the concurrent heatwave event. For the purpose of relating the temporal relationship between the flash drought and heatwave, heatwave conditions were defined where surface temperature exceeded 2 standard deviations above normal (Fig. 4.8).

Temperature values reached this threshold in late July and continued until early August. Extraordinarily high vapor pressure deficits were also experienced during this period, with values that were three standard deviations above normal during the heatwave event with peak values exceeding four standard deviations.

Rainfall and reduced evaporative demand that occurred in late June and early July contributed to the temporal delay between the end of rapid drought intensification and the onset of the heatwave (Fig. 4.1). While the mean accumulated precipitation across the study domain was minimal during this time period (approximately 2 cm), the rainfall was sufficient to effectively lower the anomalous surface temperature and vapor pressure deficit for 3-4 pentads following the flash drought event (Fig. 4.8). As such, the excessive evaporative demand that occurred during the end of June (Fig. 4.9) temporarily moderated. It is important to note that the

surface temperature was rapidly increasing to heatwave conditions at the end of the flash drought event. In a two pentad change in mid- to late June, standardized temperature anomalies increased approximately 2.0 standard deviations and standardized vapor pressure deficit anomalies increased an exceptional 2.8 standard deviations. Without the rainfall and associated moderation of evaporative stress on the environment, the focus of the heatwave event may have been shifted earlier into the summer and centered in the month of July. This could have exacerbated the environmental, economic, and societal impacts compared to the original heatwave event in late July and mid-August, given that the climatological surface temperatures across the region peak

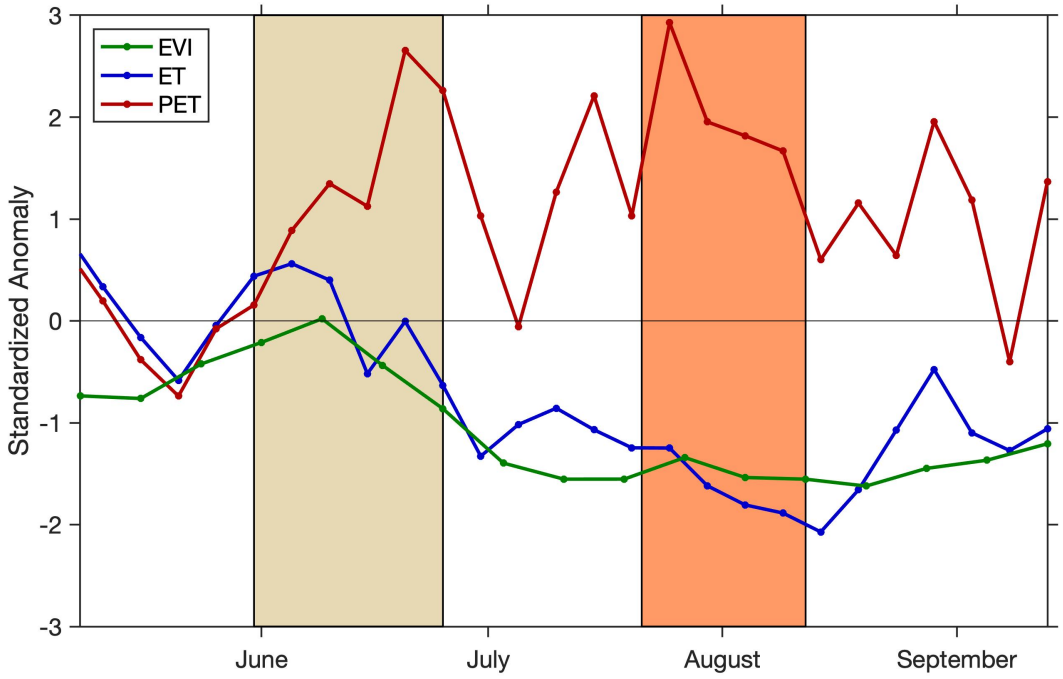

Fig. 4.9. Domain-averaged standardized anomalies of EVI from MODIS and ET and PET from MERRA-2 for 2010. The tan color indicates the time period of rapid drought development and the orange color indicates the time period of heatwave conditions. The domain is shown in Fig. 4.2.

in mid-July (Grumm 2011). Nonetheless, the temporal evolution of the flash drought event and land surface variables reveal the rapid desiccation of the environment and the associated atmospheric response. With locally-sourced boundary layer moisture (i.e. ET) significantly diminished following the flash drought (Fig. 4.9), the land-surfaced was primed for land-atmosphere temperature coupling that enhanced the development of the heatwave event (Miralles et al. 2014) in conjunction with the atmospheric conditions attributed to the quasi-stationary upper-level ridge (Barriopedro et al. 2011, Grumm 2011).

4.4 The Propagation of Land Surface Desiccation during the Flash Drought and Heatwave

The evolution and spread of land surface conditions across southwestern Russia during the flash drought and subsequent heatwave can be evaluated via changes in vegetative health conditions using the EVI. At the beginning of the rapid drought intensification period, evaporative demand increased approximately 1.2 standard deviations from near-normal to above-normal values (Fig. 4.9). During this same time period, a vegetative response was evident with increased ET and improved vegetation greenness to meet the evaporative demand of moisture at the land surface. However, as PET continued to rapidly increase into mid- and late June, plant available water was depleted due to a lack of rainfall (Figs. 4.1 and 4.4). A rapid decline of the vegetation conditions was evident during this period with an associated decrease in ET. The 1-2 pentad delayed response of vegetation to evaporative stress is similar to what has been observed in previous studies that have evaluated the lead time of evaporative stress with drought impact (Otkin et al. 2013, Chapter 2). The EVI reached its lowest values for the study domain shortly after the rapid drought intensification period, and vegetation greenness remained well below normal throughout the remainder of the summer and into the heatwave event.

Spatial analysis of EVI reveals the connection between the initial flash drought region identified in this study and the broader area associated with the heatwave event (Fig. 4.10). Peak greenness was observed approximately 5-10 days into rapid drought intensification indicated by evaporative stress (Figs. 4.8, 4.9, and 4.10a). Areas to the north of the flash drought domain,

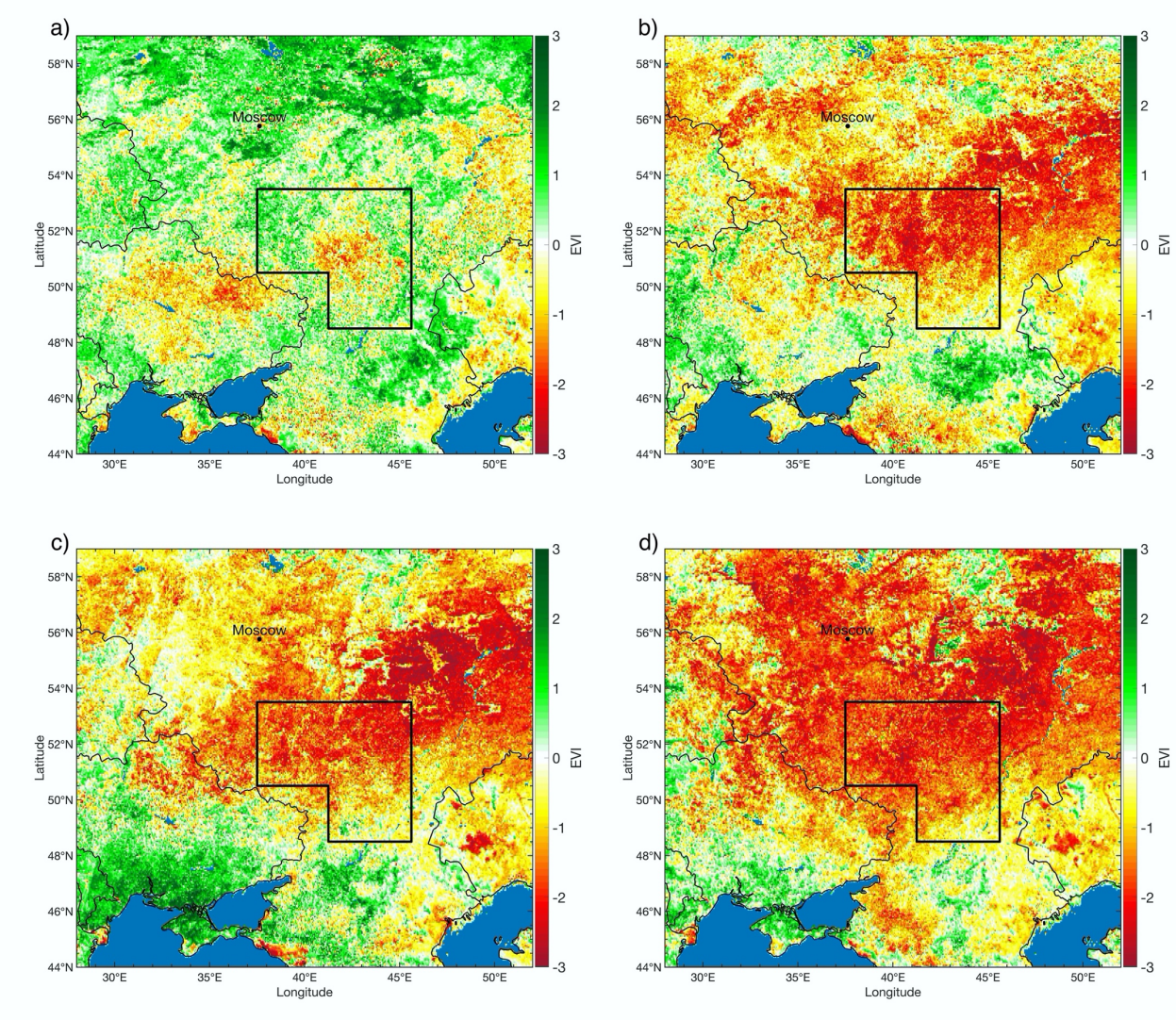

Fig. 4.10. Standardized anomalies of EVI on (a) 9 June 2010, (b) 3 July 2010, (c) 27 July 2010, and (d) 20 August 2010. The domain outlined by the black lines define the boundaries used for the temporal analysis of flash drought development.

including Moscow, also yielded EVI conditions that were well above normal during this time. However, in only 24 days after peak conditions were reached, EVI declined to well below normal across the study domain (Fig. 4.10b). The region surrounding Moscow and to the north of the study domain was also undergoing drought development, but at a slower rate than occurred within the initial flash drought region as seen by moderated EVI values. At the onset of the heatwave event, a respite in land surface degradation was visible in the flash drought region and locations north of 53.5°N (Fig. 4.10c) due to precipitation in early July (Fig. 4.1). However, the moderation in land surface conditions was temporary as the vegetation greenness decreased rapidly by the end of the heatwave throughout most of southwestern Russia (Fig. 4.10d).

An important part of this study is to reconcile the spatial differences between areas impacted by flash drought and the heatwave. The domain encompassing the region that concurrently underwent flash drought development covered an area of approximately 260,000 km^2. However, the region that had surface temperature anomalies in excess of 3 standard deviations extended farther north and west of the region characterized by rapid drought development (Twardosz and Kossowska-Cezak 2013). This mismatch between the biosphere response from flash drought and hydrometeorological extremes associated with the heatwave has been previously alluded to (Flach et al. 2018). This north/west extension of the extreme surface temperatures associated with the heatwave is linked to the advection of air parcels within the synoptic anticyclonic circulation. In the period following rapid drought development and at the beginning of heatwave conditions, the wind direction was predominately southeasterly near Moscow (Galarneau Jr et al. 2012, Witte et al. 2011). Air parcels during this time followed trajectories directly over the flash drought region in which surface temperatures and vapor pressure deficits were exceptionally high (Fig. 4.8). In addition, dry soils associated with rapid

drought development contribute to increased surface sensible heat fluxes. Strong torrents of sensible heat were advected from the flash drought region identified in this study to locations farther north (Schumacher et al. 2019), aiding in enhanced evaporative demand and desiccation of the land surface in these areas. This compounded onto the atmospheric conditions established by the upper-level ridge and the already struggling vegetation to prime the land surface for the extreme temperature anomalies associated with the heatwave event.

4.5 Summary and Discussion

The 2010 event was characterized by a series of cascading hydrometeorological and environmental factors that produced catastrophic impacts across human and natural systems (Fig. 4.11). The atmospheric conditions imposed by the quasi-stationary upper level ridge (Barriopedro et al. 2011, Grumm 2011; B11 and G11 in Fig. 4.11, respectively) inhibited rainfall (Fig. 4.1) and increased evaporative demand (Fig. 4.9) across the region for most of the summer. Flash drought development occurred across prime agricultural land in the Central, Volga, and Southern federal districts of southwestern Russia due to the coupled impacts of minimal precipitation and above-average PET (Fig. 4.2). The locality and critical phasing of the flash drought region embedded within the large-scale upper-level ridge was a result of increased ET and a rapid depletion of near-surface soil moisture as compared to a slower decrease of soil moisture in forested locations farther north (Figs. 4.3, 4.4, and 4.5). Near the terminus of the rapid drought intensification period, excessive stress on vegetation was evident across southwestern Russia and was most notable in the domain encompassing the flash drought region (Fig. 4.10b). The surface temperature was rapidly increasing to heatwave conditions (defined here as surface temperature greater than 2 standard deviations above normal) toward the end of

the rapid drought development period at the end of June (Fig. 4.8), however, rainfall across the region moderated the evaporative demand for 2-3 weeks following the flash drought event (Fig. 4.1). After this short period of reprieve, little to no rainfall (<1 cm on average across the study domain) occurred between early July and mid-August (Fig. 4.1). This lack of rainfall, in

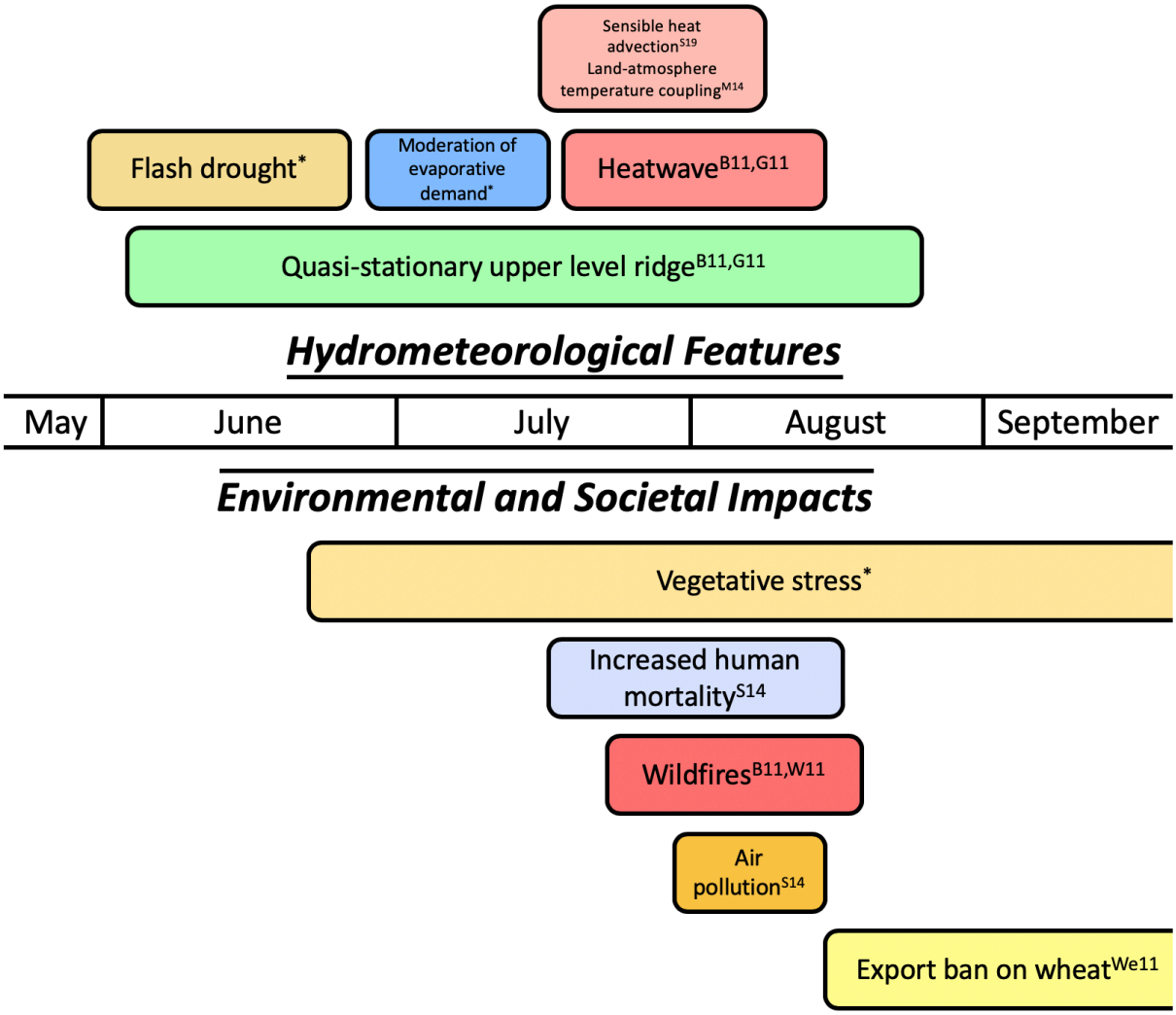

Fig. 4.11. A timeline of hydrometeorological features and cascading ecological and societal impacts associated with the precursor flash drought event and subsequent heatwave. Superscripts indicate references used to construct the timeline, while the asterisks indicate hydrometeorological features and associated impacts discussed in this study.

combination with the previously desiccated land surface and poor vegetation health associated with the precursor flash drought event, permitted a rapid increase in surface temperature and vapor pressure deficit (Fig. 4.8). This was due to a rapid depletion of near-surface soil moisture via evaporation (and transpiration from the vegetation that was remaining and capable of photosynthesis) and resulted in a decrease of evaporative fraction by mid-July (Fig. 4.4).

As exceptionally high surface temperatures began to develop in late July, human mortality increased (Shaposhnikov et al. 2014; S14 in Fig. 4.11). Further, an increased frequency of wildfires was observed (Bondur 2011, Witte et al. 2011; B11 and W11 in Fig. 4.11, respectively), contributing to widespread loss of property and heightened levels of air pollution (Shaposhnikov et al. 2014). By late July and early August, land-atmosphere temperature coupling aided in the progressive development of heat in nocturnal residual layers (Miralles et al. 2014; M14 in Fig. 4.11) and additional phasing between lower- and upper-level tropospheric circulations yielded sensible heat advection from the region that previously underwent flash drought toward locations farther to the north and west (Schumacher et al. 2019; S19 in Fig. 4.11). Air-parcel trajectories around the lower-tropospheric high (Galarneau et al. 2012, Witte et al. 2011) and along areas of previously desiccated land surfaces supplemented the magnitude and spatially expanded the heatwave conditions across much of western Russia (Twardosz and Kossowska-Cezak 2013). By the time exceptionally high surface temperatures began to decline, agricultural regions were devastated (Wegren 2011), and an export ban was placed on wheat by the Russian government 15 August (Welton 2011; We11 in Fig. 4.11).

Traditionally, flash droughts have been associated with rapid soil moisture depletion, excessive stress on vegetation and ecosystems, and agricultural yield loss. This study provides additional insight into the linkage between flash drought and the rapid desiccation of the land

surface with heatwave development by (1) priming the land-atmosphere interactions necessary to supplement excessive surface temperatures while (2) simultaneously providing a focal point for the advection of sensible heat to promote heatwave development in other locations. As a result, flash drought events can serve as the connectivity between large-scale dynamic amplification and the terrestrial-atmosphere feedbacks associated with heatwaves (Miralles et al. 2014, Schumacher et al. 2019) and can initiate cascading social, ecological, and environmental impacts.

In the context of anthropogenic climate change, heatwaves similar to severity and extent of the Russian 2010 heatwave may occur with enhanced probability over the next twenty years across Europe (Russo et al. 2015). Further, dry soils have also been shown to increase the risk for heatwaves in western Russia (Hauser et al. 2016). Given that flash droughts are associated with a rapid depletion of soil moisture and can develop even when moisture conditions do not appear conducive for rapid drought development (Chapter 3), flash droughts may be an important subseasonal phenomena to consider prior to the onset of heatwaves. This may become especially critical in a future climate where spring soil moisture levels could become independent of maximum summer temperature anomalies in western Russia during summer blocking patterns (Rasmijn et al. 2018). This would increase the likelihood for rapid drought development in the region when a combination of enhanced evaporative demand is coupled with minimal rainfall and persists for several weeks, especially in agricultural areas and climate transition zones that have an increased signal to land-atmosphere coupling (Koster et al. 2004, Seneviratne et al. 2006). As such, additional studies should investigate the role of flash drought and its associated land surface desiccation with heatwave development, especially in other locations across the globe that are susceptible to strong land-atmosphere coupling. Furthermore, future research

should examine the climatological frequency of flash droughts that are precursors to heatwave events.

Chapter 5: Global Distribution and Trends of Flash Drought Occurrence

5.1 Introduction

Flash drought is a critical subseasonal phenomenon that exhibits multifaceted challenges to agriculture, the economy, and society (Otkin et al. 2018). Given the rapid land surface desiccation associated with flash drought, agricultural sectors can be devastated and experience substantial economic damage due to lower crop yields and curtailed livestock production (Otkin et al. 2016, Otkin et al. 2018, Basara et al. 2019, Jin et al. 2020). Rapid drought intensification can severely impact ecosystems via excessive evaporative stress on the environment (Anderson et al. 2013, Otkin et al. 2013, Otkin et al. 2014, McEvoy et al. 2016, Christian et al. 2019, Nguyen et al. 2019) and contribute to compound extreme events with cascading impacts including an increased risk for wildfire development, depletion of water resources, reduction of air quality, and decreased food security (Otkin et al. 2015, Gerken et al. 2018, Otkin et al. 2019, Yuan et al. 2019, Christian et al. 2020, Hoell et al. 2020).

With a wide range of impacts associated with flash drought and challenges related to its subseasonal prediction (Pendergrass et al. 2020, DeAngelis et al. 2020), a critical goal within the scientific community is to advance knowledge of flash drought events. As such, research has been undertaken to improve the detection, evaluation, and monitoring of flash drought, including sub-surface analysis with soil moisture (Ford et al. 2015), atmospheric evaporative demand (Hobbins et al. 2016, McEvoy et al. 2016), evaporative stress via evapotranspiration (ET) and potential evapotranspiration (PET; Otkin et al. 2013, Otkin et al. 2014, Christian et al. 2019), and impact-based approaches (Chen et al. 2019). In addition, numerous case studies have explored rapid drought intensification including events across the United States (Otkin et al. 2013, Hunt et

al. 2014, Basara et al. 2019), Brazil (Anderson et al. 2016), southern Africa (Yuan et al. 2018), western Russian (Christian et al. 2020), and Australia (Nguyen et al. 2019). A critical next step that builds upon these regional studies is to quantify the global distribution of flash drought, the seasonal frequency in flash drought development, and trends in the occurrence of rapid intensification toward drought.

This study provides a global perspective of flash drought occurrence by using composite analyses from four global reanalysis datasets. The results presented here reveal (1) the regions with the strongest, reanalysis-based consensus for hotspots of flash drought development, (2) the seasonal characteristics of flash drought frequency, and (3) the trends in flash drought spatial coverage. Following the results, the implications of global flash drought hotpots are discussed, including the possible physical mechanisms that drive rapid drought intensification, the societal impacts associated with rapid drought intensification, and the ramifications of trends in flash drought spatial coverage.

5.2 Methods

5.2.1 Flash Drought Identification

Four global reanalysis datasets were used to generate the spatial and temporal composites of flash drought characteristics. These four datasets include the Modern-Era Retrospective analysis for Research and Applications (MERRA; Rienecker et al. 2011), MERRA, Version 2 (MERRA-2; Gelaro et al. 2017), ERA-Interim (Dee et al. 2011), and ERA5 (Hersbach et al. 2020). The reanalysis datasets were selected based on their global coverage of critical land surface variables used for flash drought analysis, their temporal focus on the satellite era, and their inclusion of coupled land and atmospheric models.

Daily ET and PET were obtained from each of the four global reanalysis datasets between 1980-2015. Daily PET was derived from each of the reanalysis datasets using the FAO Penman-Monteith equation (Allen et al. 1998). Daily values of the evaporative stress ratio (ESR) were calculated by taking the ratio between daily ET and PET. Mean pentad values of ESR were computed and standardized at each grid point to calculate the standardized ESR (SESR). SESR and ΔSESR are defined in equations (2) and (3), respectively. SESR and ΔSESR were both detrended prior to standardizing to accounts for changes that may have occurred in the drought threshold (SESR) or in individual pentad changes (ΔSESR) over time due to climate change. Flash drought events were identified by using the comprehensive identification methodology detailed in Chapter 2.

5.2.2 Compositing

SESR derived from each of the reanalysis datasets was used in the flash drought identification methodology to produce a climatology of flash drought occurrence (Figs. 5.1, 5.2, 5.3, and 5.4). After flash drought frequency was determined from each reanalysis, the gridded datasets were composited to combine the results from the four datasets. Because each reanalysis has a different spatial resolution (MERRA: 0.5° × 0.66°, MERRA-2: 0.5° × 0.625°, ERA-Interim: 0.75° × 0.75°, and ERA5: 0.25° × 0.25°), each flash drought frequency map was bilinearly interpolated to a new grid with a spatial resolution of 0.5° × 0.5°. The mean percentage of flash drought occurrence was then calculated between the four datasets to produce Fig. 5.5.

Time series composites were produced by selecting all grid points that were contained within the domains shown in Fig. 5.5 and averaging the associated variable. For the monthly distribution of flash drought occurrence, the starting month for rapid drought intensification was

accumulated for all grid points for each month. The percentage of flash droughts that occurred in each month (with respect to the annual total of flash drought occurrence) were then averaged between the four reanalyses. For the flash drought spatial coverage time series, all grid points that underwent flash drought for a given year were accumulated. Accumulated flash drought grid points were then converted to a percentage, representing flash drought spatial coverage with respect to the entire domain. This yearly percentage was then averaged between the four reanalyses.

Grid points that existed over locations that were too arid or cold were masked on the spatial analysis (Fig. 5.5). Arid locations were determined by calculating the aridity index as:

$$AI = \frac{P}{PET}$$

where P is the average annual precipitation and PET is the average annual potential evapotranspiration from the MERRA-2 dataset. Specifically, grid points were masked where the average annual aridity index was below 0.2 (arid and hyper-arid locations) or where average daily PET was less than 1 mm per day during the growing season for the Northern Hemisphere (March through October) and Southern Hemisphere (September through April). The aridity threshold was used to place an emphasis on rapid drought development in regions that can transition from more humid to drier environmental conditions and are more likely to experience vegetative, agricultural, or environmental effects from flash drought. In addition, the PET threshold requires regions to have enough evaporative demand throughout the growing season to allow for higher ET rates, sufficient soil moisture depletion, and increased evaporative stress to create rapid drought development.

5.3 Results and Discussion

5.3.1 Global Flash Drought Occurrence

While recent progress in flash drought research has been accomplished via case studies and regional analyses, a key scientific question remains: What global regions are the most susceptible to flash drought occurrence? To address this question, the spatial distribution of flash drought events was identified via four global reanalysis datasets for the period spanning 1980-2015. ET and PET were used from each reanalysis dataset to quantify the standardized evaporative stress ratio (SESR). SESR was then processed through a comprehensive flash drought identification methodology that incorporates multiple criteria associated with rapid intensification toward drought (the "flash" component of flash drought) and impact (the "drought" component of flash drought; Chapter 2). As a methodology for evaluating flash drought, SESR compares well with the satellite-based evaporative stress index (ESI; Anderson et al. 2007a, Anderson et al. 2007b, Chapter 2), acts as an early drought indicator, and corresponds with impacts indicated by the United States Drought Monitor (Svoboda et al. 2002, Chapter 2). Further, it provides flash drought occurrence both regionally and nationally across the United States (Chapter 2 and 3) and represents the development and evolution of flash drought case studies using different datasets across different regions around the globe (Basara et al. 2019, Chapter 4).

The regions with the highest frequency of flash drought occurrence were primarily found within the tropics and subtropics (Fig. 5.5). These locations include a large portion of Brazil, the Sahel, the Great Rift Valley, and India, with composite flash drought occurrence between 30-40% of the years within the 36-year time period of analysis. Three of these four major hotspots for flash drought occurrence had coefficients of variation below 0.3 throughout most of their

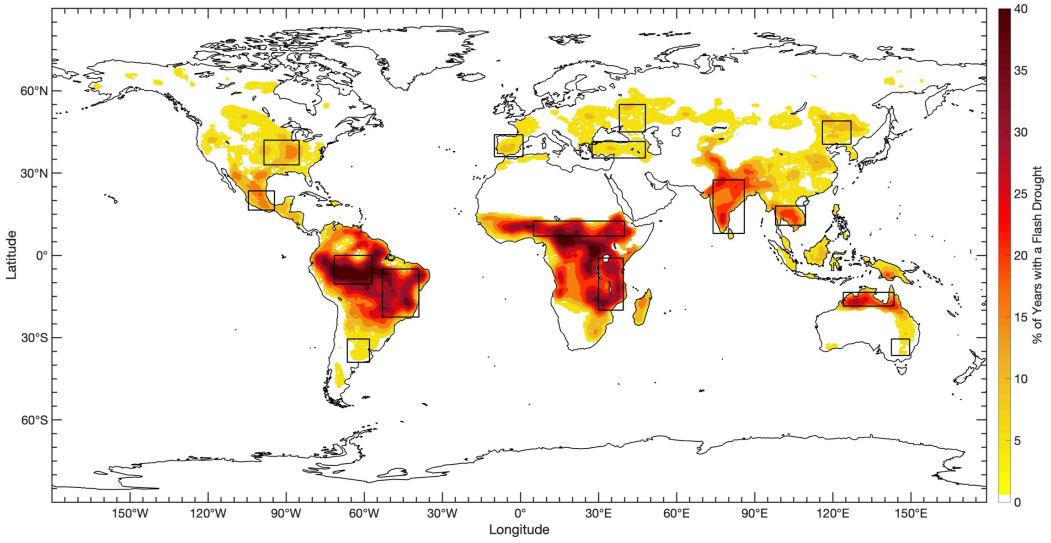

Fig. 5.1. Percent of years with a flash drought between 1980 and 2015 for the MERRA dataset. The black outlines represent domains used for the temporal analysis in Figs. 5.8, 5.9, 5.10, and 5.11.

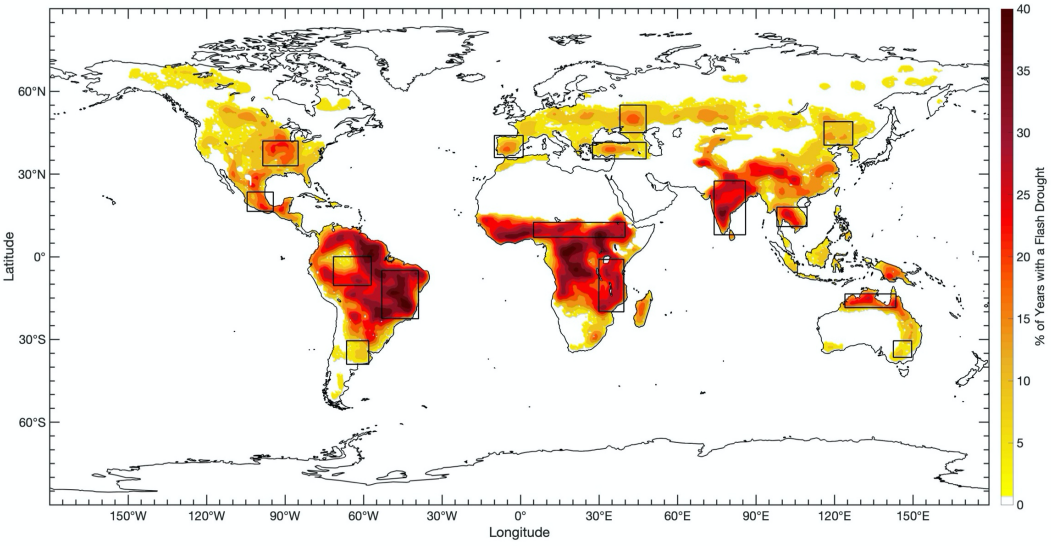

Fig. 5.2. The same as Fig. 5.1, but for the MERRA-2 dataset.

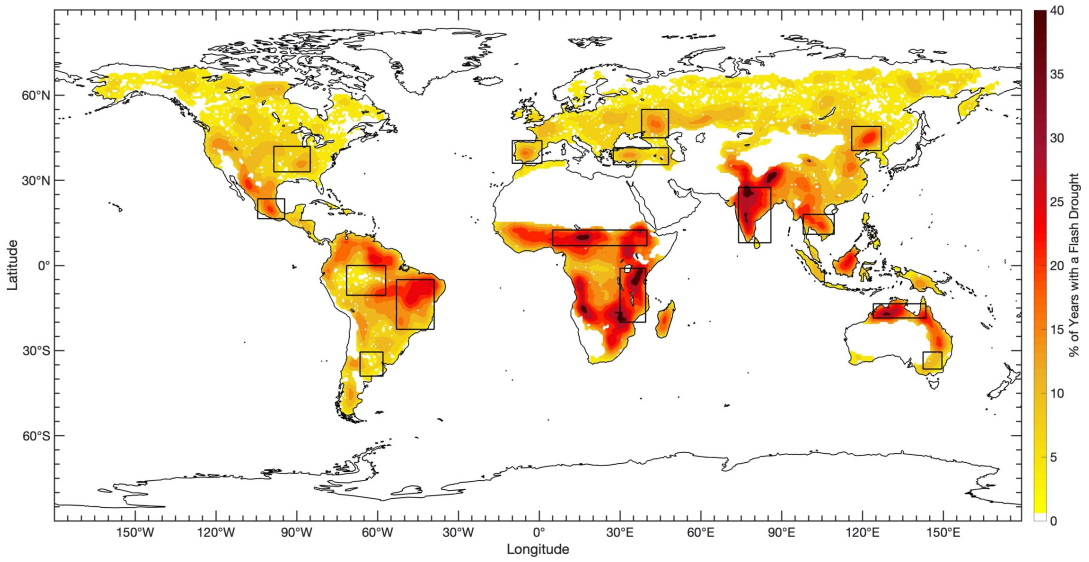

Fig. 5.3. The same as Fig. 5.1, but for the ERA-Interim dataset.

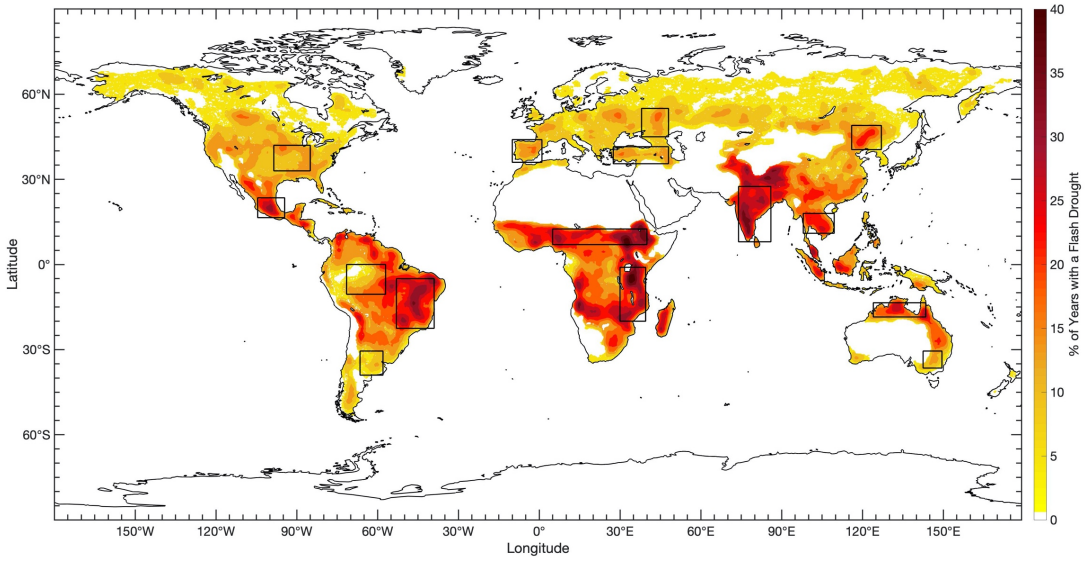

Fig. 5.4. The same as Fig. 5.1, but for the ERA5 dataset.

domains (the Sahel, the Great Rift Valley, and India), indicating strong agreement between the four reanalysis datasets (Fig. 5.6). Additional areas within the tropics that had lesser, but notable flash drought occurrence included central Mexico, the Indochinese Peninsula, and northern Australia, with flash drought occurrence between 20-30% of the years. For these regions, the Indochinese Peninsula, and northern Australia had strong agreement between datasets (coefficients of variation less than 0.3; Fig. 5.6). In the mid-latitudes, local hotspots of flash drought occurrence (10-20%) exist across the central United States, Iberian Peninsula, southwestern Russia, Asia Minor, and northeastern China. These regions exhibited larger variability between reanalyses (coefficients of variations between 0.3 and 0.6), with notable disagreement in flash drought occurrence across the central United States (Fig. 5.6).

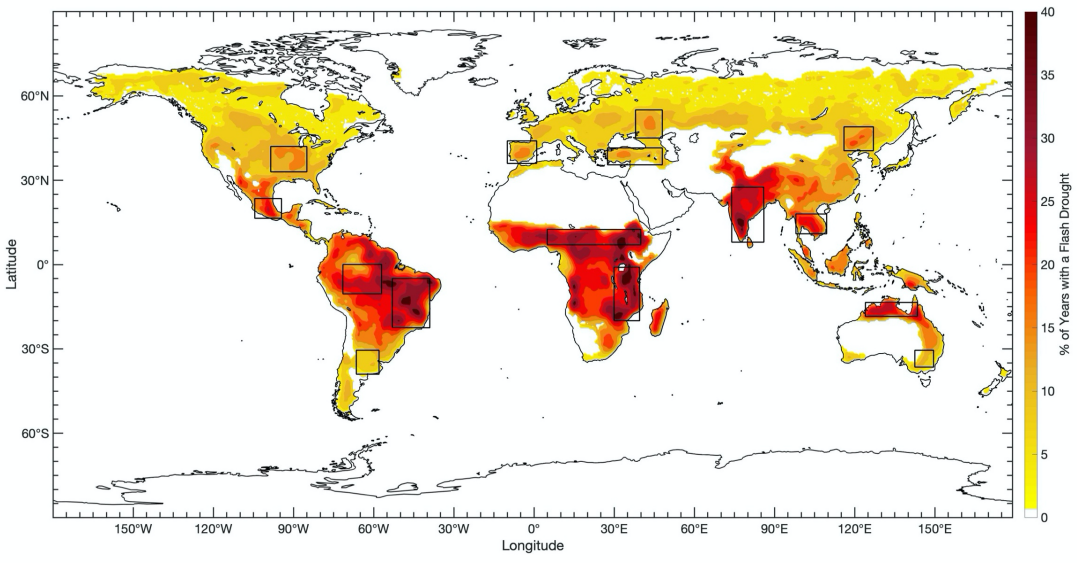

Fig. 5.5. Mean flash drought occurrence from the four reanalysis datasets. Frequency is represented as the percent of years with a flash drought between 1980 and 2015. The black outlines represent domains used for the temporal analysis in Figs. 5.8, 5.9, 5.10, and 5.11.

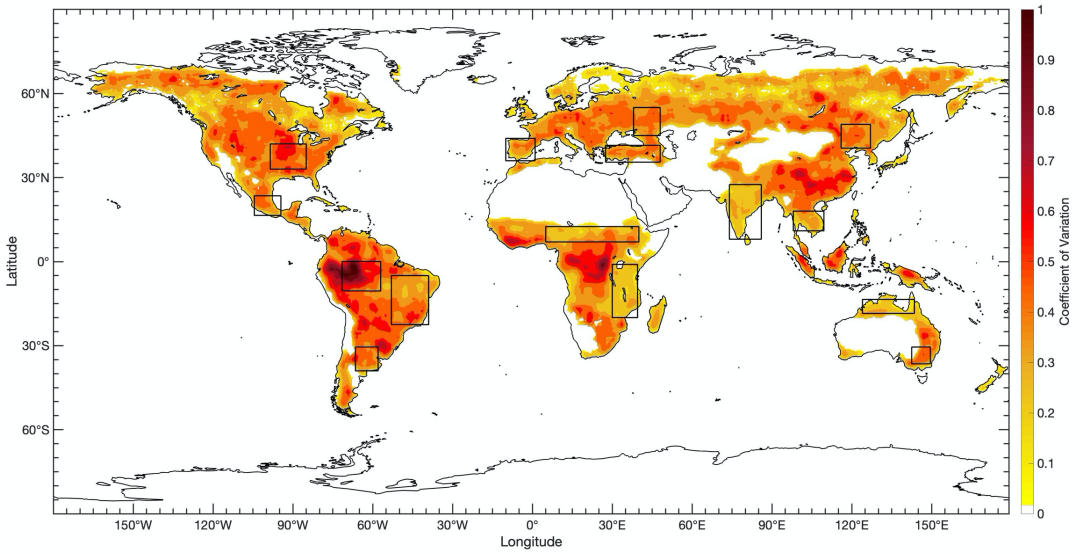

Fig. 5.6. Coefficient of variation for the percent of years with a flash drought (1980-2015) between MERRA, MERRA-2, ERA-Interim, and ERA5. The black outlines represent domains used for the temporal analysis in Figs. 5.8, 5.9, 5.10, and 5.11.

In one of the most spatially comparable studies to date, soil moisture percentiles were used to identify flash drought events across the Northern Hemisphere with two major hotspots (the Sahel and India) similar across the previous study (Koster et al. 2019) and this study (Fig. 5.5). In addition, a midlatitude band of enhanced flash drought occurrence across Europe and Asia is evident in both studies. A notable difference is located over North America, where the prior study shows a global hot spot of flash drought occurrence in the southern United States and northern Mexico (Koster et al. 2019). The results here reveal a higher frequency of flash drought occurrence in the central and Midwestern United States, with another local maximum in frequency over central Mexico (Fig. 5.5). A similar belt of enhanced flash drought risk across the central United States was shown in Chapter 2 using a regional reanalysis dataset with SESR and the same methodology (Fig. 5.5).

An important factor in the preferential occurrence of flash drought across the globe is land-atmosphere coupling (Basara et al. 2019, Gerken et al. 2018). While local land-atmosphere interactions are very complex (National Academies of Sciences, Engineering and Medicine 2016), the fundamental relationship between flash drought development and land-atmosphere coupling can be summarized with key moisture and thermal variables. As soil moisture is depleted, the evaporation and transpiration of water vapor into the atmosphere decreases. Concurrently, the effective moderation of land-surface temperatures by ET is limited, thereby further increasing evaporative demand. Reduced moisture flux from the surface contributes to a drier atmospheric column, which inhibits the generation of precipitation. This positive feedback process of drying the land surface, increasing surface temperatures, and lowering the potential for precipitation aids flash drought development. As such, it is worth noting that many of the global hotspots for flash drought identified in this study are also located over regions with an enhanced signal of land-atmosphere coupling. These regions include the central United States, the Sahel, and India (Fig. 5.5, Koster et al. 2004, Koster et al. 2006, Mei and Wang 2012, Liu et al. 2014). This overlap indicates that land-atmosphere coupling may have a critical role in rapid drought development, especially in flash drought hot spots that lie in climate transitions zones and are sensitive to coupling dynamics.

Anticyclones are also an important contributor to flash drought development. Through subsidence and the associated suppression of rainfall, upper level ridges can limit the potential for soil moisture replenishment. Concurrently, less cloud coverage and warmer surface temperatures increase evaporative demand of moisture from the land surface. As such, anticyclones have a dual impact on increasing evaporative stress by limiting moisture availability for ET and increasing PET. An increased risk for flash drought development is particularly

evident with blocking highs that persist for several weeks. Examples of this include the 2012 central US flash drought and 2010 western Russian flash drought, where a lack of rainfall and increased evaporative demand associated with a blocking high set the foundation for rapid drought development (DeAngelis et al. 2020, Chapter 4).

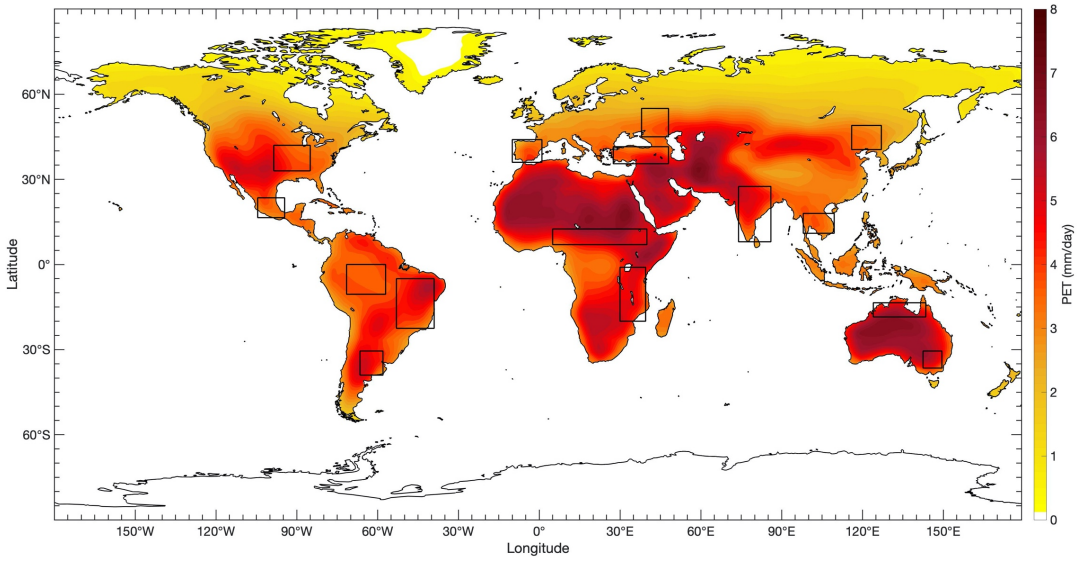

Fig. 5.7. Daily average PET in the growing season between 1980 and 2015 for the MERRA-2 dataset. The black outlines represent domains used for the temporal analysis in Figs. 5.8, 5.9, 5.10, and 5.11.

In addition to the contributions of subseasonal features on flash drought development (e.g., land-atmosphere coupling and blocking highs), climatic features can also influence the spatial distribution of flash drought events revealed from the composite analysis. An example of this is associated with average daily PET across the globe. In the tropics and subtropics, average daily PET exceeds 5 mm/day (Fig. 5.7). In contrast, a majority of land areas in the midlatitudes experience smaller daily averaged PET compared to the tropics, between 3-5 mm/day (Fig. 5.7).

Given that larger values of evaporative demand will increase the upper limit for the rate of evapotranspiration, flash drought development would most likely occur in regions with consistently high PET and result in a greater potential for rapid increases in evaporative stress on the environment. As such, the overall higher frequency of flash drought hotspots in the tropics (30-40%) as compared to the midlatitudes (15-20%) may be attributed to climatologically higher values of evaporative demand in tropics and subtropics (Fig. 5.5).

5.3.2 Temporal Flash Drought Characteristics

The onset and timing of flash drought is a critical component to agricultural impacts, as flash drought can drastically reduce crop yields and lead to severe economic losses and potentially disrupt food security. As such, the monthly distribution of flash drought occurrence was examined across (1) global flash drought hotspots and/or (2) regions with extensive crop cultivation (Fig. 5.8). Study regions were selected over global hotspots where flash drought occurred in more than 30% of the study years. These regions included Brazil, the Sahel, the Great Rift Valley, and India. Additional study regions were examined where a regional maximum in flash drought frequency exceeded 15%, including the central United States, central Mexico, the Iberian Peninsula, eastern Europe/western Russia, Asia Minor, the Indochinese Peninsula, northeastern China, and northern Australia. Three additional regions were investigated to quantify flash drought seasonality over tropical rainforest (the Amazon) and the Southern Hemisphere midlatitudes (Argentina and southeastern Australia). Of the 15 locations analyzed, ten were both a regional maximum in flash drought occurrence and regions of major agricultural production. These regions included the Corn Belt across the Midwestern United States, barley production in the Iberian Peninsula, the western Russian wheat belt, wheat

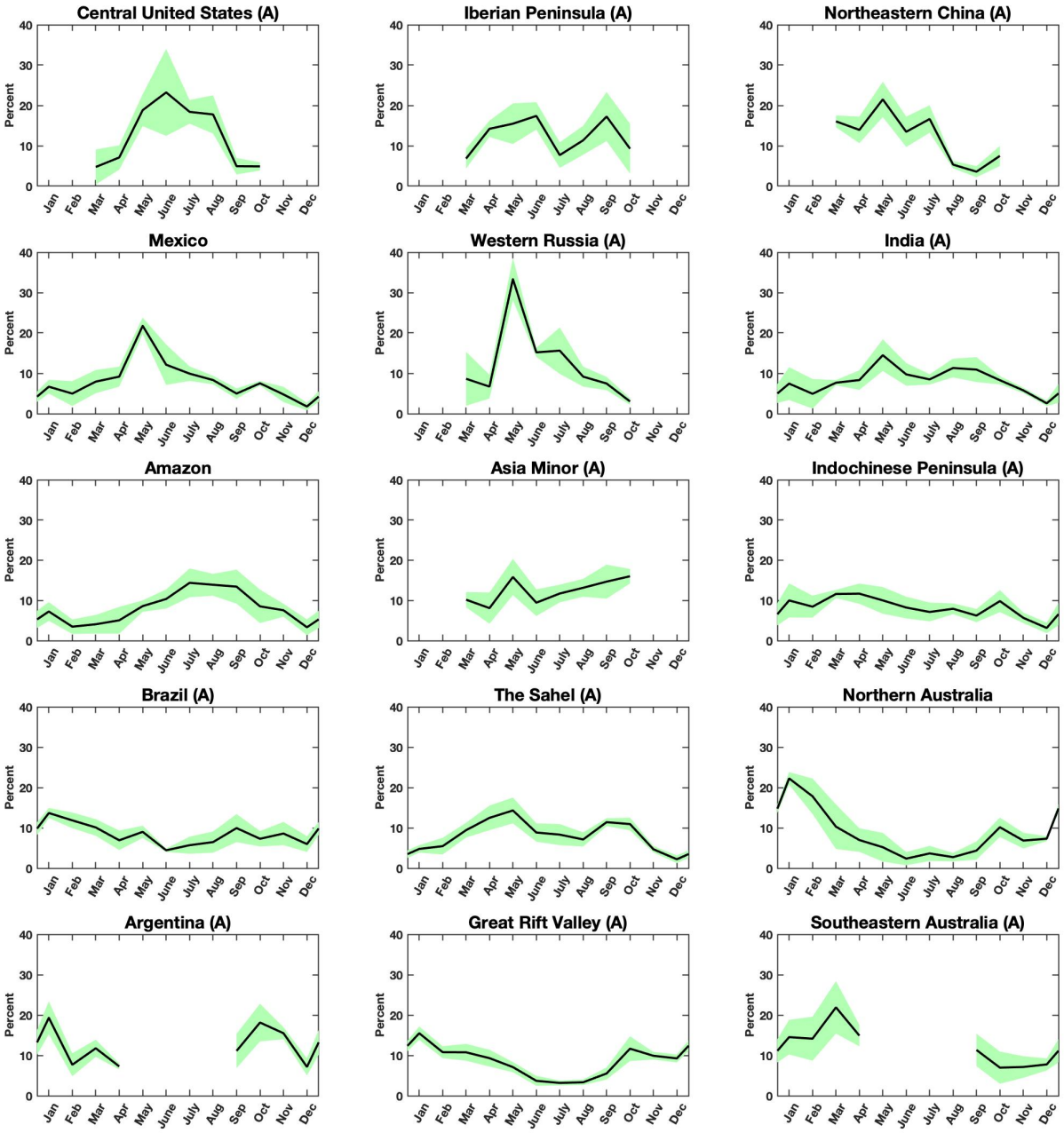

Fig. 5.8. Monthly distribution of mean flash drought occurrence from the four reanalysis datasets (black line) for each domain outlined in Fig. 5.5. The green shaded area represents the variability (standard deviation) between the four reanalyses. Regions labeled with (A) indicate locations with extensive agricultural production.

production in Asia Minor, rice producing regions in India and the Indochinese Peninsula, maize production in northeastern China, soybean production in Brazil, millet and sorghum production across the Sahel, and the maize belt along the Great Rift Valley in Africa (Leff et al. 2004). Two additional areas did not necessarily exhibit a local hotspot in flash drought occurrence, but are significant agricultural locations. These regions include maize and wheat production across the Pampas in Argentina and wheat production in southeastern Australia (Leff et al. 2004).

For each of the regions, flash drought events were partitioned by the month in which rapid drought development began. The frequency for each month was calculated as the percent of each month's contribution to the annual total of flash drought occurrence for that region. For the regions located in the tropics and subtropics (between 30°S and 30°N) flash drought occurrence was examined year-round, while regions in the mid-latitudes (between 30-60°S or N) were investigated for flash drought occurrence within their approximate growing season (i.e., March through October in the Northern Hemisphere and September through April in the Southern Hemisphere).

For a majority of regions within the mid-latitudes in the Northern Hemisphere, a seasonality in flash drought frequency is evident within the growing season with flash droughts most likely between May and July for the central United States, western Russia, and northeastern China (Fig. 5.8). An exception to this seasonality occurs in Asia Minor, where the occurrence of flash drought generally increases throughout the growing season. For the Southern Hemisphere mid-latitude regions, the monthly distribution of flash drought frequency differs from the seasonal patterns seen in the Northern Hemisphere mid-latitudes. For example, agricultural regions in Argentina display monthly variability in flash drought occurrence, while eastern

Australia exhibits a peak in flash drought occurrence near the end of the austral growing season (Fig. 5.8).

A seasonality in flash drought frequency is also evident in regions located within the tropics and subtropics, with the phase of their pattern dependent upon the hemisphere in which they reside. For example, the four regions in the Northern Hemisphere tropics and subtropics (Mexico, the Sahel, India, and the Indochinese Peninsula) generally had their highest occurrence of flash drought in the boreal growing season. Three of the four regions in the Southern Hemisphere tropics (Brazil, the Great Rift Valley, and northern Australia) exhibit peak flash drought occurrence during the austral growing season.

As previously discussed, a diverse set of meteorological and climatic drivers contribute to preferential regions for flash drought development. Similarly, various drivers will also contribute to the seasonality of flash drought occurrence. For example, the Asian-Australian monsoon provides extensive precipitation across India, eastern/southeast Asia, and northern Australia. The Asian monsoon typically begins in June and continues throughout the Northern Hemisphere summer, providing more than 57% of the total annual rainfall in these regions (Conroy and Overpeck 2011). Across India, a percentile-based methodology using soil moisture was used to identify flash droughts during the monsoon and non-monsoon seasons, with the majority of the flash drought events occurring during the monsoon season, especially across the central, northwest, and northeast regions of India (Mahto and Mishra 2020). A similar result was found using SESR over the India domain in this study, with flash droughts primarily initiating between May and September (Fig 5.8). Likewise, northern Australia receives approximately 80% of its annual mean precipitation from the monsoon during the Southern Hemisphere summer (November through April; Sharmila and Hendon 2020). From the analysis of seasonal flash

drought occurrence, these regions experience their peak frequency at the beginning of their respective monsoon seasons (Fig. 5.8). Thus, a delay, absence, or reduction of monsoon rainfall can significantly contribute to flash drought development, provided above-normal evaporative demand is also present to promote rapid land surface desiccation.

Another example of a flash drought driver can be examined in the Sahel, where the oscillation of the Inter-Tropical Convergence Zone (ITCZ) and the onset of the West African monsoon are the primary contributors to rainfall and intraseasonal rainfall variability across this region. The onset of monsoon and ITCZ induced rainfall generally begins in late June across the Sahel (Sultan and Janicot 2000, Sultan and Janicot 2003) and the timing of this onset corresponds with a peak in flash drought risk seen across the Sahel in May (Fig. 5.8). This timing indicates that flash drought development is more likely to occur in the May to June transition period associated with increasing climatological rainfall, especially if the onset of ITCZ and monsoon rainfall is delayed or significantly reduced, in combination with increased evaporative demand. The secondary peak of flash drought occurrence in September and October is likely related to the cessation of rainfall associated with the southward shift of the ITCZ (Fig. 5.8). Below average precipitation accumulation coupled with above average evaporative demand during a time frame that receives relatively small amounts of rainfall (e.g., approximately 5 cm of rainfall in September and 1-2 cm of rainfall in October on average; Sultan and Janicot 2003) will increase the likelihood of flash drought development during this time of the year.

5.3.3 Changes in Spatial Coverage of Flash Drought

To quantify the change in flash drought coverage with time, flash drought spatial coverage was calculated for each domain and year. The Mann-Kendall test was applied to each

time series to determine if statistically significant trends were evident in yearly flash drought coverage. Of the 15 regions investigated from the composite analysis in this study, six regions (the central United States, Iberian Peninsula, Asia Minor, Brazil, the Sahel, and southeastern Australia) had a statistically significant increasing trend in flash drought coverage, while three regions (India, the Great Rift Valley, and northern Australia) had a statistically significant decreasing trend at the 90% confidence level (Fig. 5.9). In addition, four of the nine regions identified as having statistically significant trends associated in the composite analysis had at least three individual reanalysis datasets produce statistically significant trends (Fig. 5.10). Overall, six of the nine regions had all four individual reanalyses indicate consistent directions of the trend (positive or negative), while two additional regions had three of the four reanalyses with consistent signs of the trend (Fig. 5.10).

Each of the regions also exhibited varying magnitudes of the trend. For example, the central United States and Iberian Peninsula had modest changes in flash drought spatial coverage associated with statistically significant trends during the study period (Fig. 5.9). In contrast, India, the Sahel, the Great Rift Valley, and northern Australia had large changes in spatial coverage, with changes during the 36-year period between 16-26%. A few regions also had minimal changes in flash drought spatial coverage with time, including Mexico, Argentina, and the Indochinese Peninsula. Each of these regions had spatial coverage changes less than 2% over the 36-year period. The overall change from the composite analysis for the Amazon revealed a decreasing trend that was not statically significant. However, large spatial areas of flash drought coverage prior to 2000 in the MERRA dataset produced large variability between the datasets (Fig. 5.10).

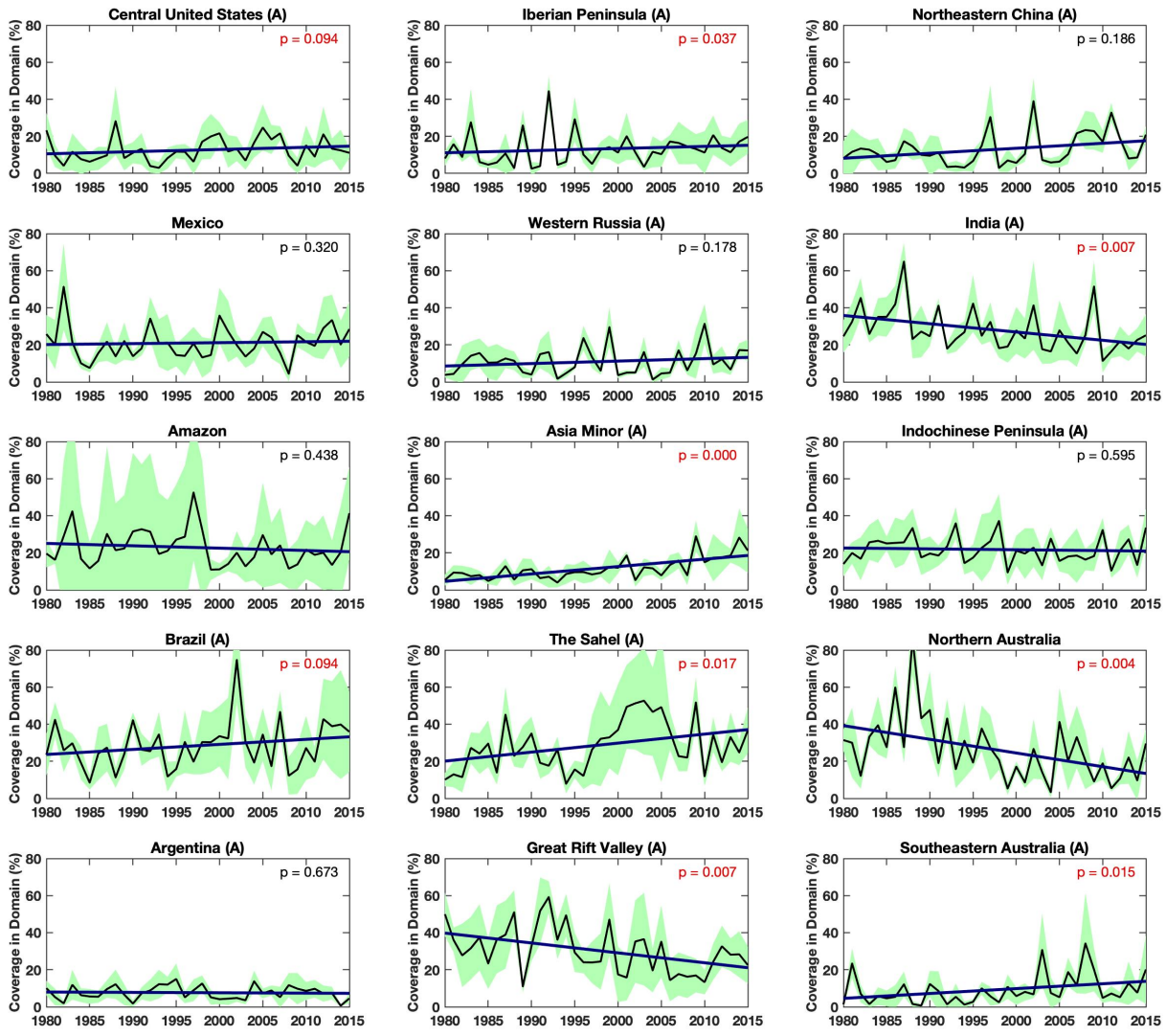

Fig. 5.9. Mean flash drought spatial coverage (percent) from the four reanalysis datasets (black line) for each of the domains shown in Fig. 5.5. The green shaded area represents the variability (standard deviation) between the four reanalyses and the thicker blue line represents the trend line for mean flash drought spatial coverage. P-values highlighted in red are statistically significant trends at the 90% confidence level using the Mann-Kendall test. Regions labeled with (A) indicate locations with extensive agricultural production.

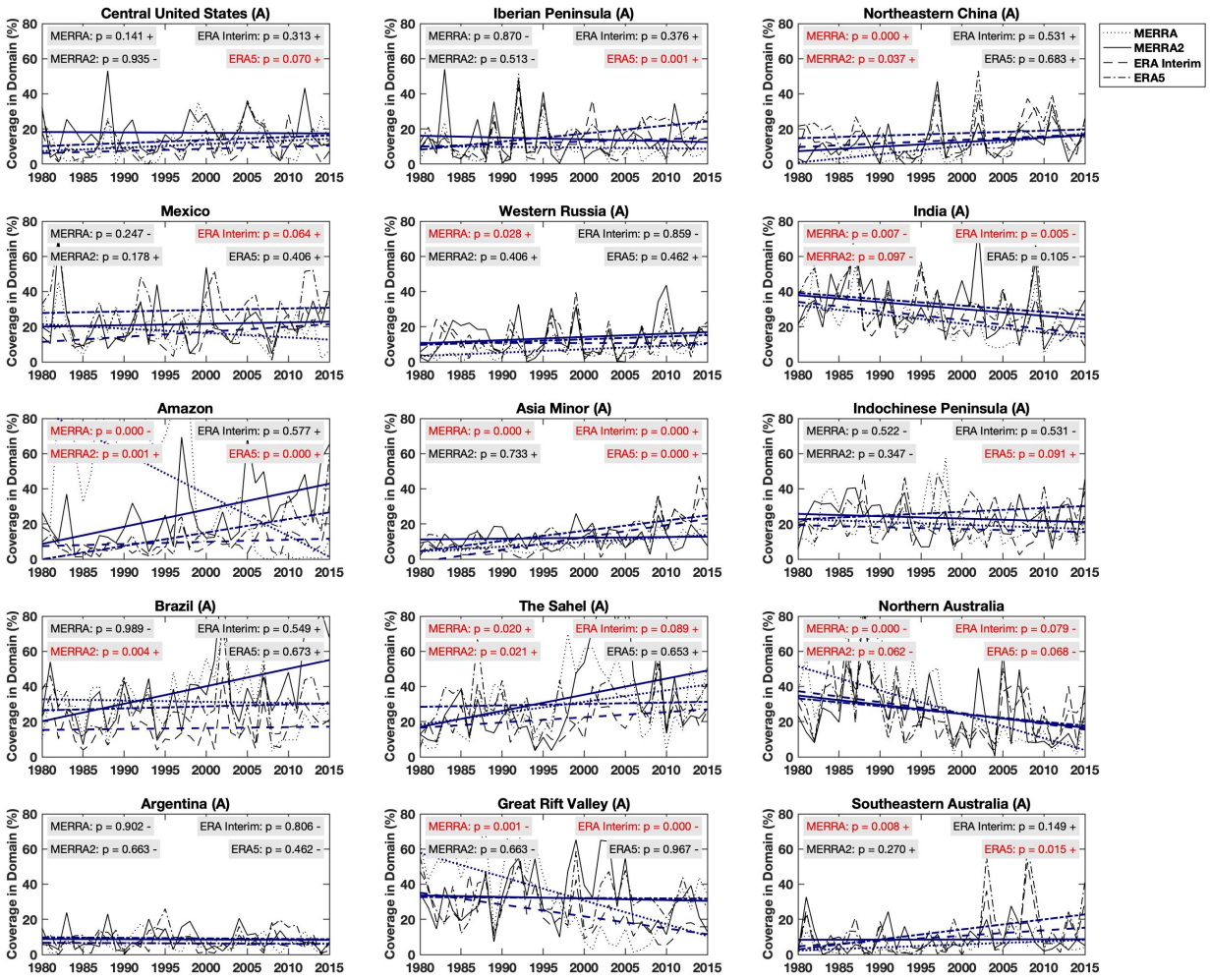

Fig. 5.10. Flash drought spatial coverage (percent) for each of the domains shown in Fig. 5.5. Each black line represents flash drought spatial coverage from each of the four reanalyses, while the thicker blue lines represent the trend line for each reanalysis. P-values highlighted in red are those that are statistically significant at the 90% confidence level using the Mann-Kendall test. Regions labeled with (A) indicate locations with extensive agricultural production.

Changes in flash drought occurrence, as a function of evaporative stress, can be examined from two perspectives: changes in ET with time or changes in evaporative demand (PET) with time. Increases in PET can be related to global climate change, with increases in surface temperature and the vapor pressure deficit (VPD) being critical factors (Hobbins et al. 2012, Scheff and Frierson 2014, Otkin et al. 2019). Locations that have increased evaporative demand will have a greater risk for flash drought development through enhanced evaporative stress. Regions that have experienced statistically significant increasing trends in flash drought spatial extent (Fig. 5.9) and statistically significant increasing trends in PET within the growing season (Fig. 5.11) include the Iberian Peninsula, Brazil, and the Sahel. The risk for flash drought development may continue to increase in certain locations due to the effect of increased evaporative demand as increases in PET are expected in a future warming climate (Cook et al. 2014). In contrast, locations with climatological increases in precipitation will have greater availability of soil moisture for ET, which will mitigate the enhanced evaporative stress and reduce opportunities for rapid drought intensification. Regions such as India and northern Australia may have decreased flash drought spatial coverage over the last several decades due to changes in the magnitude and timing of precipitation (Fig. 5.9). For example, decreases in the South Asian monsoon circulation have contributed to changes in mean precipitation and variability during the summer across India (Wang et al. 2020), while changes in the intensity of the Walker circulation may contribute to changes in precipitation over the Maritime Continent and northern Australia (Tokinaga et al. 2012, Meng et al. 2012). Climate features such as these may have a critical role in reducing the likelihood of flash drought development over time.

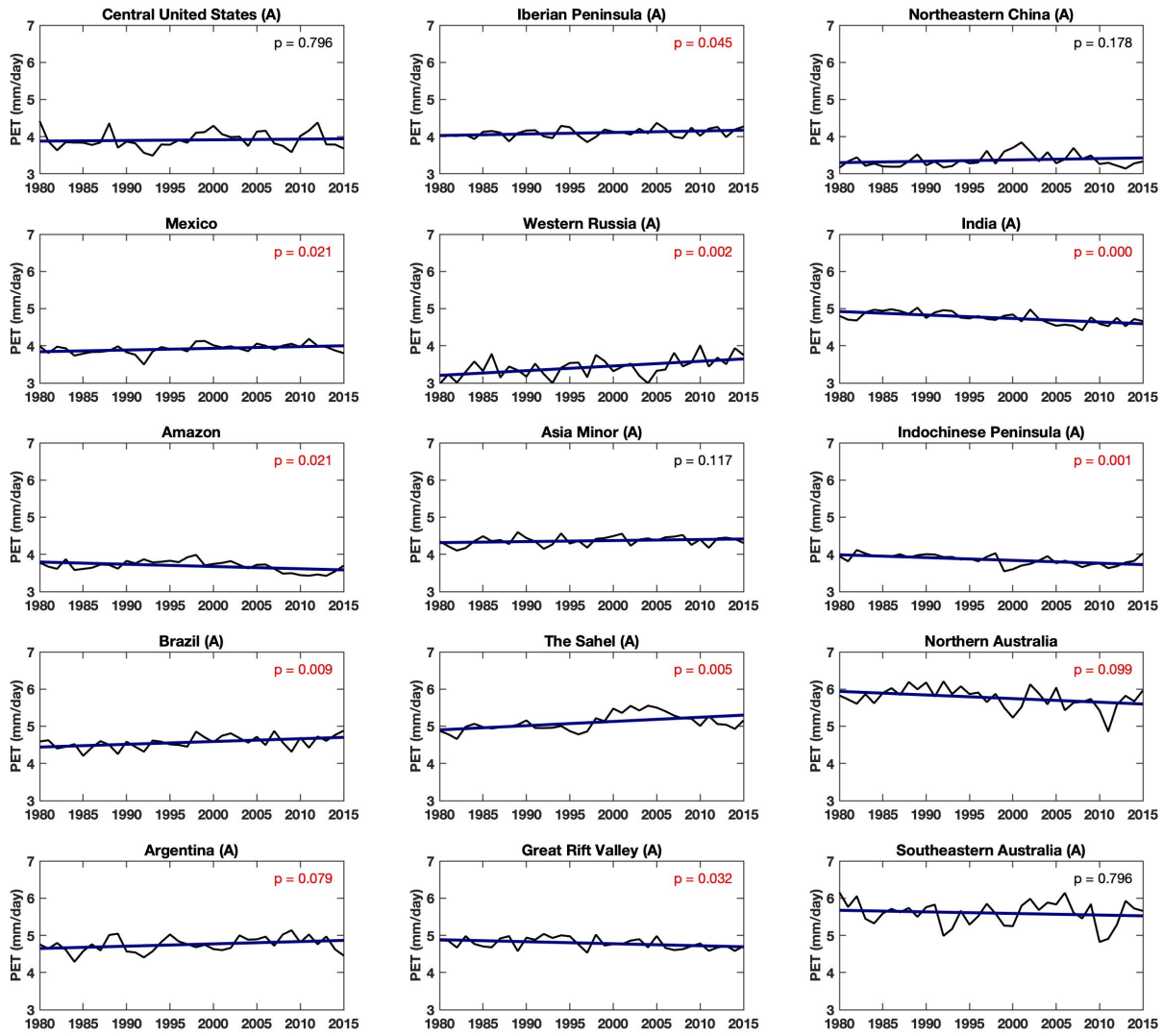

Fig. 5.11. Daily average PET in the growing season (black line) for each of the domains shown in Fig. 5.5. The thicker blue line represents the trend line for PET. P-values highlighted in red are those that are statistically significant at the 90% confidence level using the Mann-Kendall test. Regions labeled with (A) indicate locations with extensive agricultural production.

Lastly, teleconnections may also have a significant role in long-term (interannual and decadal) variability of flash drought spatial coverage. If a region's climate (e.g., temperature and precipitation) is sensitive to a particular teleconnection, the potential for flash drought development could change. For example, a teleconnection phase that promotes drier and warmer conditions for a specific region, especially during the growing season when evaporative demand is higher, may increase flash drought frequency/coverage for the time period within that phase. In contrast, wetter and colder conditions may decrease flash drought development. Periodicities associated with the El Niño-Southern Oscillation (2-7 years) may embed cyclic patterns of flash drought occurrence and spatial coverage within the climatological frequency of flash drought over time. Similarly, teleconnections with interdecadal variability (e.g., the Pacific Decadal Oscillation; Mantua and Hare 2002) may superpose a long-term cyclic signal on climatological flash drought occurrence. Thus, investigation of these signals would require a dataset that is longer than that of reanalysis data from the satellite era (1979 to present).

5.4 Conclusion

The analysis presented here reveals (1) the preferential regions for flash drought across the globe, (2) the seasonality of flash drought occurrence for selected hot spots and agricultural regions, and (3) and notable trends in flash drought spatial coverage for the examined locations. While flash drought frequency varies significantly across the globe, nearly every region experiences rapid drought development (excluding arid and cold regions). It is of critical importance that a majority of the regional hotspots of flash drought occurrence are regions with extensive agriculture production (Fig. 5.5). In addition to flash drought frequency, eight out of

the ten regions with statistically significant trends are also associated with major crop production (Fig. 5.9).

As previously discussed, a common theme associated with flash drought development is the impact on crop yields. Yield losses occur through rapid depletion of root zone soil moisture, which leads to limited moderation of surface temperatures and excessive evaporative stress on crops. Due to this direct impact, flash drought studies primarily focus on rapid drought development in the context of agricultural production (Basara et al. 2019, Otkin et al. 2016, 2018). However, results in Chapter 4 have also shown that flash droughts can initiate a set of cascading impacts, such as an increased risk for wildfires and heatwave development. In light of the results from the global climatology of flash drought occurrence and the rapid land surface desiccation attributed to rapid drought development, flash drought events have the potential to produce serious impacts beyond agricultural yield loss. Particularly in underdeveloped countries, flash drought that transitions into a long-term drought may lead to an increased risk of famine and destabilization of governments (Couttenier and Soubeyran 2014, Maystadt and Ecker 2014).

With such a diverse set of meteorological and climatological features having critical roles in the development of flash drought, multiple paths of future studies are needed to understand the drivers of rapid drought intensification across the globe. Furthermore, it is recommended that future research place an emphasis on untangling the complex interactions between flash drought and socioeconomic impacts.

Chapter 6: Summary and Key Findings

6.1 Overview

Flash droughts present many challenges across the nexus of water, weather, and climate. In evaluations of their onset and development, flash droughts form from a complex combination of thermal, moisture, and radiative flux variables. In addition to the development process of flash drought, predictability of these events remains a significant challenge, given their occurrence on subseasonal timescales. From an agricultural perspective, flash droughts can devastate crop yields and lead to heavy economic loss. As such, the purpose of this research was to propel the flash drought science forward to help unravel some of these challenges by pursuing three key goals: 1) to develop an objective methodology for flash drought identification, 2) to explore the role of flash drought in socio-economic impacts, and 3) to create a global climatology of flash drought occurrence. These goals were used to address the overarching hypothesis that if a comprehensive methodology for flash drought identification was created, then the timing, intensity, and associated impacts of rapid drought intensification could be effectively evaluated from local to global scales.

6.2 Key Findings

Following the guidelines presented in Otkin et al. (2018), a methodology for identifying flash drought events was created and is outlined in Chapter 2. The methodology was aimed towards satisfying two fundamental characteristics of flash drought: longevity and impact. Two criteria emphasized the rapid rate of intensification toward drought, while the other two criteria focused on vegetative impact resulting from flash drought. After evaluating SESR and the

methodology with the ESI and USDM, a climatology of flash drought occurrence was produced for the United States. Overall, it was shown that a hotspot of flash drought frequency exists across the Great Plains and Midwest regions of the United States. Further, the most intense flash drought events also occurred most often across the central United States.

Using the directory of flash drought events that were compiled from the analysis in Chapter 2, regional characteristics of flash drought across the United States were explored in Chapter 3. It was found that regional differences exist in the timing and intensity of flash drought within the growing season. For example, flash drought development is more frequent in the beginning of the growing season for the western United States, but has a higher occurrence in the latter portion of the growing season for a majority of the eastern United States. While flash drought intensity was found to have a climatological peak in the middle of the growing season for all climate regions, the Midwest regions contained flash drought events with the most rapid rate of intensification. In addition to timing and intensity, antecedent dry conditions were found to increase flash drought risk and less than half of all flash drought events persisted to hydrological drought in all climate regions.

To explore the utility of SESR and the flash drought identification methodology presented in Chapter 2, a flash drought event that occurred across southwestern Russia in the summer of 2010 was investigated. It was found that rapid drought intensification occurred prior to an intense heatwave that occurred in late July and early August and primed the land-atmosphere interactions necessary to supplement excessive surface temperatures experienced during the heatwave. The region that underwent flash drought also acted as a focal point for the advection of warm, dry air and promoted the development of heatwave conditions downwind of

the flash drought location. Ultimately, the flash drought event in southwestern Russia initiated a set of cascading impacts that severely affected ecosystems, agriculture, and human health.

After the development of a flash drought identification methodology, applying it to a regional climatology, and evaluating its use in case study analysis, a culmination of the findings presented in Chapters 2, 3, and 4 were applied in Chapter 5 to explore the distribution and trends of flash drought occurrence across the globe. Global hotspots were found to exist over Brazil, the Sahel, the Great Rift Valley, and India, with several local hotspots also evident across the midlatitudes in the Northern Hemisphere. In the temporal analysis, a majority of the regions investigated had their highest flash drought occurrence in the late spring and early summer. Lastly, 9 of the 15 study regions were shown to have either a statistically significant increase or decrease in flash drought spatial coverage over time.

6.3 Future Work

The study in Chapter 2 completed two important tasks. First, the methodology that was created can be applied to many different datasets, given that ET and PET are available to calculate SESR and a sufficient period of record is available for percentiles (e.g., 20-30 years). For example, the methodology was originally applied to the NARR (Chapter 2 and 3), but was also used with different reanalysis datasets (e.g., MERRA-2, ERA5; Chapter 4 and 5). The methodology may also be used with other gridded datasets, such as the Global Forecast System (GFS), for subseasonal forecasting of flash drought. In addition, data from individual monitoring stations (e.g., the Oklahoma Mesonet) can be used to identify flash droughts as long as the necessary data is available. The second result from Chapter 2 revealed fundamental knowledge of flash drought occurrence across the United States via climatological analysis. This result

provides a focal point for drought monitoring applications (e.g., the USDM) when monitoring regions for rapid drought development and lays a foundation for improving subseasonal predictability.

The insights provided from Chapter 3 can be summed into one main result: not all flash droughts are the same. The regionality of flash drought across the United States applies not only to the seasonal timing and intensity of rapid drought intensification, but also to the environmental conditions that precede flash drought development and follow flash drought events. As such, the findings from this study may benefit flash drought monitoring and predictability. For example, flash droughts were found to occur most often during the middle of the summer across the Midwest. Therefore, these months would particularly be closely monitored for rapid drought intensification across this region during the growing season. From the perspective of predictability, it was shown that moisture conditions preceding flash drought development in the Southeast were typically much drier than climatological moisture conditions. This indicates that antecedent moisture conditions (e.g. soil moisture) may serve as a first order method of predictably for rapid drought intensification in this region.

In addition to monitoring and predictability, the results from Chapter 3 strongly suggest that different surface and atmospheric drivers are associated with flash drought development. As such, several pathways of research are needed to investigate how various atmospheric features across different regions contribute to the overall development of flash drought and how environmental conditions and land surface type play a role in rapid drought intensification.

The case study of flash drought development across southwestern Russia in Chapter 4 revealed essential insights on the relationship between flash drought and its associated impacts. While flash drought impacts in the scientific literature have primarily focused on agricultural

yield loss, the flash drought event in Russia was found to play a critical role in the development of heatwave conditions and contributed to a sequence of societal impacts across the region. Overall, the results from this study necessitate future research in two subjects. First, further research is needed to explore the relationship between flash drought and heatwaves. This includes the investigation of additional case studies of flash drought development that can prime the land surface for heatwave development (as shown in Chapter 4), and the converse with the role of heatwaves in flash drought development. The second pathway of research involves unraveling the relationship between flash drought and socioeconomic impacts. Chapter 4 showed how flash drought sparked a set of cascading impacts, including vegetative stress, wildfires, air pollution, and increased human mortality. Future research should also explore how flash drought contributes to a sequence of environmental and societal impacts that may lead to famine and civil unrest, especially in underdeveloped countries.

In Chapter 5, the role of meteorological and climatological drivers of flash drought were discussed with respect to several global hotspots of flash drought occurrence. As land-atmosphere interactions, upper level ridging, monsoons, and teleconnections play a role in flash drought development for different regions around the globe, multiple pathways of research are needed to investigate the regional drivers of flash drought. Furthermore, many flash drought hotspots were found to overlap with regions with extensive agricultural production. This increases the importance of understanding flash drought and its relationship to food security, especially with underdeveloped countries.

While the results in this dissertation have provided several new insights on the characteristics of flash drought, it is important to place these results in the context of flash drought research within the broader scientific community. For example, the primary sources of

data used for the studies presented here are derived from regional and global reanalysis datasets. ET is a fundamental variable in the calculation of SESR used for flash drought identification, but each reanalysis dataset uses a different land surface model to estimate ET rates. This simplified approach of estimating ET over coarse grid resolutions can lead to a high amount of uncertainty in ET, the associated SESR calculation, and the resulting identification of flash drought events. As such, the robustness of a reanalysis-based approach can be supported by using different datasets and variables for flash drought identification. The ESI (Otkin et al. 2013, Otkin et al. 2014), a satellite-derived variant of SESR, could be used to compare flash drought identification with the same type of variable (evaporative stress), but with a different data source (ESI being satellite-based and SESR being reanalysis-based). In addition, climatological flash drought development should be compared with different variables, such as soil moisture (Hunt et al. 2014, Ford et al. 2015) or evaporative demand (Hobbins et al. 2016, McEvoy et al. 2016).

Different approaches and identification methodologies should also be considered when exploring climatological aspects of flash drought. While the methodology presented in Chapter 2 uses a pentad-to-pentad approach for flash drought identification, prescribed temporal windows for flash drought analysis have also be utilized. An example of this includes the 40^{th} to 20^{th} percentile decline in soil moisture in 4 pentads or less presented from Ford and Labosier (2017) and the application of this methodology to the Northern Hemisphere in Koster et al. (2019). Further, the methodology in Chapter 2 focuses on rapid drought intensification that also reaches drought conditions, while the methodology presented in Yuan et al. (2019) emphasizes the inclusion of persistent drought conditions in the identification of flash drought. Comparison of flash drought methodologies will further refine the identification of climatological flash drought hotspots regionally and across the globe.

As we enter a new frontier of flash drought research, several topics associated with rapid drought intensification need to be explored. These focal points include the improvement of subseasonal forecasting of flash drought events, modeling future changes in flash drought occurrence and intensity in a changing climate, refining flash drought identification metrics, and enhancing techniques for monitoring rapid drought intensification. While the research presented in this dissertation provides a fundamental step forward in many of these categories, continued work in flash drought research is essential. The ever-growing knowledge of flash drought will improve our understanding of the role of rapid drought intensification in the land-atmosphere Earth system and unravel the complex, cascading impacts associated with flash drought.

References

Allen, R. G., L. S. Pereira, D. Raes, and M. Smith, 1998: Crop evapotranspiration-Guidelines for computing crop water requirements-FAO Irrigation and drainage paper 56. *FAO*.

Anderson, M. C., J. M. Norman, J. R. Mecikalski, J. A. Otkin, and W. P. Kustas, 2007a: A climatological study of evapotranspiration and moisture stress across the continental United States based on thermal remote sensing: 1. Model formulation. *J. Geophys. Res.*, **112**, D10117, https://doi.org/10.1029/2006JD007506.

Anderson, M. C., J. M. Norman, J. R. Mecikalski, J. A. Otkin, and W. P. Kustas, 2007b: A climatological study of evapotranspiration and moisture stress across the continental United States based on thermal remote sensing: 2. Surface moisture climatology. *J. Geophys. Res.*, **112**, D11112, https://doi.org/10.1029/2006JD007507.

Anderson, M. C., C. R. Hain, B. Wardlow, J. R. Mecikalski, and W. P. Kustas, 2011: Evaluation of drought indices based on thermal remote sensing of evapotranspiration over the continental United States. *J. Climate*, **24**, 2025-2044, https://doi.org/ 10.1175/2010JCLI3812.1.

Anderson, M. C., C. Hain, J. Otkin, X. Zhan, K. Mo, M. Svoboda, B. Wardlow, and A. Pimstein, 2013: An Intercomparison of Drought Indicators Based on Thermal Remote Sensing and NLDAS-2 Simulations with U.S. Drought Monitor Classifications. *J. Hydrometeor.,* **14**, 1035–1056, https://doi.org/10.1175/JHM-D-12-0140.1.

Anderson, M. C., C. A. Zolin, C. R. Hain, K. Semmens, M. Tugrul Yilmaz, and F. Gao, 2015: Comparison of satellite-derived LAI and precipitation anomalies over Brazil with a thermal

infrared-based Evaporative Stress Index for 2003–2013. *J. Hydrol.*, **526**, 287–302, https://doi.org/10.1016/j.jhydrol.2015.01.005.

Anderson, M. C., and Coauthors, 2016a: The Evaporative Stress Index as an indicator of agricultural drought in Brazil: An assessment based on crop yield impacts. *Remote Sens. Environ.*, **174**, 82–99, https://doi.org/10.1016/j.rse.2015.11.034.

Anderson, M. C., C. R. Hain, F. Jurecka, M. Trnka, P. Hlavinka, W. Dulaney, J. A. Otkin, D. Johnson, and F. Gao, 2016b: Relationships between the Evaporative Stress Index and winter wheat and spring barley yield anomalies in the Czech Republic. *Climate Res.*, **70**, 215-230, https://doi.org/10.3354/cr01411.

Bajgain, R., X. Xiao, P. Wagle, J. Basara, and Y. Zhou, 2015: Sensitivity analysis of vegetation indices to drought over two tallgrass prairie sites. *ISPRS J. Photogramm. Remote Sens.*, **108**, 151–160, doi:10.1016/j.isprsjprs.2015.07.004.

Barriopedro, D., E. M. Fischer, J. Luterbacher, R. M. Trigo, and R. García-Herrera, 2011: The Hot Summer of 2010: Redrawing the Temperature Record Map of Europe. *Sci.*, **332**, 220–224, doi:10.1126/science.1201224.

Basara, J. B., J. N. Maybourn, C. M. Peirano, J. E. Tate, P. J. Brown, J. D. Hoey, and B. R. Smith, 2013: Drought and Associated Impacts in the Great Plains of the United States—A Review. *Int. J. Geosci.*, **4**, 72–81, http://doi.org/10.4236/ijg.2013.46A2009.

Basara, J. B., and J. I. Christian, 2018: Seasonal and interannual variability of land-atmosphere coupling across the Southern Great Plains of North America using the North American regional reanalysis. *Int. J. Climatol.*, **38**, 964–978, https://doi.org/10.1002/joc.5223.

Basara, J. B., J. I. Christian, R. A. Wakefield, J. A. Otkin, E. H. Hunt, and D. P. Brown, 2019: The evolution, propagation, and spread of flash drought in the Central United States during 2012. *Environ. Res. Lett*, **14**, 084025, doi:10.1088/1748-9326/ab2cc0.

Bondur, V. G., 2012: Satellite monitoring of wildfires during the anomalous heat wave of 2010 in Russia. *Izv. Atmos. Ocean. Phys.*, **47**, 1039–1048, doi:10.1134/S0001433811090040.

Boyer, J. S., and Coauthors, 2013: The U.S. drought of 2012 in perspective: A call to action. *Global Food Secur.*, **2**, 139-143, doi:10.1016/j.gfs.2013.08.002.

Brun, J., and A. P. Barros, 2014: Mapping the role of tropical cyclones on the hydroclimate of the southeast United States: 2002–2011, *Int. J. Climatol.*, 34, 494-517, doi:10.1002/joc.3703.

Chang, F.-C., and J. M. Wallace, 1987: Meteorological Conditions during Heat Waves and Droughts in the United States Great Plains. *Mon. Wea. Rev.*, **115**, 1253–1269, https://doi.org/10.1175/1520-0493(1987)115<1253:MCDHWA>2.0.CO;2.

Chen, L. G., J. Gottschalck, A. Hartman, D. Miskus, R. Tinker, and A. Artusa, 2019: Flash Drought Characteristics Based on U.S. Drought Monitor. *Atmos.*, **10**, 498, doi:10.3390/atmos10090498.

Christian, J. I., J. B. Basara, J. A. Otkin, E. D. Hunt, R. A. Wakefield, P. X. Flanagan, and X. Xiao, 2019a: A Methodology for Flash Drought Identification: Application of Flash Drought Frequency across the United States. *J. Hydrometeor.*, **20**, 833–846, doi:10.1175/JHM-D-18-0198.1.

Christian, J. I., J. B. Basara, J. A. Otkin, and E. D. Hunt, 2019b: Regional characteristics of flash droughts across the United States. *Environ. Res. Commun.*, **1**, 125004, doi:10.1088/2515-7620/ab50ca.

Christian, J. I., J. B. Basara, E. D. Hunt, J. A. Otkin, and X. Xiao, 2020: Flash drought development and cascading impacts associated with the 2010 Russian heatwave. *Environ. Res. Lett.*, **15**, 094078, doi:10.1088/1748-9326/ab9faf.

Cook, B. I., J. E. Smerdon, R. Seager, and S. Coats, 2014: Global warming and 21st century drying. *Clim. Dyn.*, **43**, 2607–2627, doi:10.1007/s00382-014-2075-y.

Conroy, J. L., and J. T. Overpeck, 2011: Regionalization of Present-Day Precipitation in the Greater Monsoon Region of Asia*. *J. Climate*, **24**, 4073–4095, doi:10.1175/2011JCLI4033.1.

Couttenier, M., and R. Soubeyran, 2014: Drought and Civil War In Sub-Saharan Africa. *Econ. J.*, **124**, 201–244, doi:10.1111/ecoj.12042.

DeAngelis, A. M., H. Wang, R. D. Koster, S. D. Schubert, Y. Chang, and J. Marshak, 2020: Prediction Skill of the 2012 U.S. Great Plains Flash Drought in Subseasonal Experiment (SubX) Models. *J. Climate*, **33**, 6229–6253, doi:10.1175/JCLI-D-19-0863.1.

Dee, D. P., and Coauthors, 2011: The ERA-Interim reanalysis: configuration and performance of the data assimilation system. *Quart. J. Roy. Meteor. Soc.*, **137**, 553–597, doi:10.1002/qj.828.

Diaz, H. F., 1983: Drought in the United States. *J. Climate Appl. Meteor.*, **22**, 3–16, https://doi.org/10.1175/1520-0450(1983)022<0003:DITUS>2.0.CO;2.

Dirmeyer, P. A., 2006: The Hydrologic Feedback Pathway for Land–Climate Coupling. *J. Hydrometeor.*, **7**, 857–867, https://doi.org/10.1175/JHM526.1.

Dirmeyer, P. A., 2011: The terrestrial segment of soil moisture-climate coupling. *Geophys. Res. Lett.*, **38**, L16702, doi:10.1029/2011GL048268.

Dominguez, F., and P. Kumar, 2008: Precipitation Recycling Variability and Ecoclimatological Stability—A Study Using NARR Data. Part I: Central U.S. Plains Ecoregion. *J. Climate*, **21**, 5165–5186, https://doi.org/10.1175/2008JCLI1756.1.

Findell, K. L., and E. A. B. Eltahir, 2003a: Atmospheric Controls on Soil Moisture–Boundary Layer Interactions. Part I: Framework Development. *J. Hydrometeor.*, **4,** 552–569, https://doi.org/10.1175/1525-7541(2003)004<0552:ACOSML>2.0.CO;2.

Findell, K. L., and E. A. B. Eltahir, 2003b: Atmospheric Controls on Soil Moisture–Boundary Layer Interactions. Part II: Feedbacks within the Continental United States. *J. Hydrometeor.*, **4**, 570–583, https://doi.org/10.1175/1525-7541(2003)004<0570:ACOSML>2.0.CO;2.

Flach, M., S. Sippel, F. Gans, A. Bastos, A. Brenning, M. Reichstein, and M. D. Mahecha, 2018: Contrasting biosphere responses to hydrometeorological extremes: revisiting the 2010 western Russian Heatwave. *Biogeosciences*, **16**, 6067–6085, doi:10.5194/bg-2018-130.

Ford, T. W., D. B. McRoberts, S. M. Quiring, and R. E. Hall, 2015: On the utility of in situ soil moisture observations for flash drought early warning in Oklahoma, USA. *Geophys. Res. Lett.*, **42**, 9790–9798, doi:10.1002/2015GL066600.

Ford, T. W., and C. F. Labosier, 2017: Meteorological conditions associated with the onset of flash drought in the Eastern United States. *Agric. For. Meteor.*, **247**, 414–423, https://doi:10.1016/j.agrformet.2017.08.031.

Galarneau, T. J., Jr., T. M. Hamill, R. M. Dole, and J. Perlwitz, 2012: A Multiscale Analysis of the Extreme Weather Events over Western Russia and Northern Pakistan during July 2010. *Mon. Wea. Rev.*, **140**, 1639–1664, doi:10.1175/MWR-D-11-00191.1.

Gelaro, R., and Coauthors, 2017: The Modern-Era Retrospective Analysis for Research and Applications, Version 2 (MERRA-2). *J. Climate*, **30**, 5419–5454, https://doi.org/10.1175/JCLI-D-16-0758.1.

Gerken, T., G. T. Bromley, B. L. Ruddell, S. Williams, and P. C. Stoy, 2018: Convective suppression before and during the United States Northern Great Plains flash drought of 2017. *Hydrol. Earth Syst. Sci.*, **22**, 4155–4163, doi:10.5194/hess-22-4155-2018.

Griffin, D., and K. J. Anchukaitis, 2014: How unusual is the 2012-2014 California drought? *Geophys. Res. Lett.*, **41**, 9017–9023, https://doi.org/10.1002/2014GL062433.

Grumm, R. H., 2011: The central European and Russian heat event of July–August 2010. *Bull. Amer. Meteor. Soc.*, **92**, 1285-1296, https://doi.org/10.1175/2011BAMS3174.1.

Guo, Z., and Coauthors, 2006: GLACE: The Global Land–Atmosphere Coupling Experiment. Part II: Analysis. *J. Hydrometeor.*, **7**, 611–625, https://doi.org/10.1175/JHM511.1.

Hauser, M., R. Orth, and S. I. Seneviratne, 2016: Role of soil moisture versus recent climate change for the 2010 heat wave in western Russia. *Geophys. Res. Lett.*, **43**, 2819–2826, doi:10.1002/2016GL068036.

Hersbach, H., and Coauthors, 2020: The ERA5 global reanalysis. *Quart. J. Roy. Meteor. Soc.*, **146**, 1999–2049, doi:10.1002/qj.3803.

Higgins, R. W., and W. Shi, 2000: Dominant Factors Responsible for Interannual Variability of the Summer Monsoon in the Southwestern United States, *J. Climate*, **13**, 759-776, doi:10.1175/1520-0442(2000)013<0759:DFRFIV>2.0.CO;2.

Hobbins, M., A. Wood, D. Streubel, K. Werner, 2012: What Drives the Variability of Evaporative Demand across the Conterminous United States? *J. Hydrometeor.*, **13**, 1195–1214, doi:10.1175/JHM-D-11-0101.1.

Hobbins, M. T., A. Wood, D. J. McEvoy, J. L. Huntington, C. Morton, M. Anderson, and C. Hain, 2016: The Evaporative Demand Drought Index. Part I: Linking Drought Evolution to Variations in Evaporative Demand. *J. Hydrometeor.*, **17**, 1745–1761, https://doi.org/10.1175/JHM-D-15-0121.1.

Hoell, A., and Coauthors, 2020: Lessons Learned from the 2017 Flash Drought Across the U.S. Northern Great Plains and Canadian Prairies. *Bull. Amer. Meteor. Soc.*, 1–46, doi:10.1175/BAMS-D-19-0272.1.

Huete, A., K. Didan, T. Miura, E. P. Rodriguez, X. Gao, and L. G. Ferreira, 2002: Overview of the radiometric and biophysical performance of the MODIS vegetation indices. *Remote Sens. Environ.*, **83**, 195–213, doi:10.1016/S0034-4257(02)00096-2.

Hunt, E. D., M. Svoboda, B. Wardlow, K. Hubbard, M. Hayes, and T. Arkebauer, 2014: Monitoring the effects of rapid onset of drought on non-irrigated maize with agronomic data and climate-based drought indices. *Agric. For. Meteor.*, **191**, 1–11, doi:10.1016/j.agrformet.2014.02.001.

Kennedy, A. D., X. Dong, B. Xi, S. Xie, Y. Zhang, and J. Chen, 2011: A Comparison of MERRA and NARR Reanalyses with the DOE ARM SGP Data. *J. Climate*, **24**, 4541–4557, https://doi.org/10.1175/2011JCLI3978.1.

Koster, R. D., and Coauthors, 2004: Regions of Strong Coupling Between Soil Moisture and Precipitation. *Sci.*, **305**, 1138–1140, doi:10.1126/science.1100217.

Koster, R. D., and Coauthors, 2006: GLACE: The Global Land–Atmosphere Coupling Experiment. Part I: Overview. *J. Hydrometeor.*, **7**, 590–610, doi:10.1175/JHM510.1.

Koster, R. D., H. Wang, S. P. Mahanama, A. M. DeAngelis, S. D. Schubert, S. P. Mahanama, and A. M. DeAngelis, 2019: Flash Drought as Captured by Reanalysis Data: Disentangling the

Contributions of Precipitation Deficit and Excess Evapotranspiration. *J. Hydrometeor.*, **20**, 1241–1258, doi:10.1175/JHM-D-18-0242.1.

Krishnan, P., T. A. Black, N. J. Grant, A. G. Barr, E. T. H. Hogg, R. S. Jassal, and K. Morgenstern, 2006: Impact of changing soil moisture distribution on net ecosystem productivity of a boreal aspen forest during and following drought. *Agric. For. Meteor.*, **139**, 208–223, https://doi.org/10.1016/j.agrformet.2006.07.002.

Jin, C., X. Luo, X. Xiao, J. Dong, X. Li, J. Yang, and D. Zhao, 2019: The 2012 Flash Drought Threatened US Midwest Agroecosystems. *Chin. Geogr. Sci.*, **29**, 768–783, doi:10.1007/s11769-019-1066-7.

Leff, B., N. Ramankutty, and J. A. Foley, 2004: Geographic distribution of major crops across the world. *Global Biogeochem. Cycles*, **18**, 320–339, doi:10.1029/2003GB002108.

Liu, D., G. Wang, R. Mei, Z. Yu, and H. Gu, 2014: Diagnosing the Strength of Land–Atmosphere Coupling at Subseasonal to Seasonal Time Scales in Asia. *J. Hydrometeor.*, **15**, 320–339, doi:10.1175/JHM-D-13-0104.1.

Mahrt, L., and M. Ek, 1984: The Influence of Atmospheric Stability on Potential Evaporation. *J. Climate Appl. Meteor.*, **23**, 222–234, https://doi.org/10.1175/1520-0450(1984)023<0222:TIOASO>2.0.CO;2.

Mahto, S. S., and V. Mishra, 2020: Dominance of summer monsoon flash droughts in India. *Environ. Res. Lett.*

Mantua, N. J., and S. R. Hare, 2002: The Pacific Decadal Oscillation. *J. Oceanogr.*, **58**, 35–44, doi:10.1023/A:1015820616384.

Manuel, J., 2008: Drought in the Southeast: Lessons for Water Management. *Environ. Health Perspect.*, **116**, A168–A171.

Maystadt, J.-F., and O. Ecker, 2014: Extreme Weather and Civil War: Does Drought Fuel Conflict in Somalia through Livestock Price Shocks? *Amer. J. Agric. Econ.*, **96**, 1157–1182, doi:10.1093/ajae/aau010.

Maxwell, J. T., J. T. Ortegren, P. A. Knapp, and P. T. Soulé, 2013: Tropical cyclones and drought amelioration in the Gulf and southeastern coastal United States. *J. Climate*, **26**, 8440-8452, doi:10.1175/JCLI-D-12-00824.1.

McCabe, G. J., J. L. Betancourt, S. T. Gray, M. A. Palecki, and H. G. Hidalgo, 2008: Associations of multi-decadal sea-surface temperature variability with US drought. *Quat. Int.*, **188**, 31–40, https://doi.org/10.1016/j.quaint.2007.07.001.

McEvoy, D. J., J. L. Huntington, M. T. Hobbins, A. Wood, C. Morton, M. Anderson, and C. Hain, 2016: The Evaporative Demand Drought Index. Part II: CONUS-Wide Assessment against Common Drought Indicators. *J. Hydrometeor.*, **17**, 1763–1779, https://doi.org/10.1175/JHM-D-15-0122.1.

Mei, R., and G. Wang, 2012: Summer Land–Atmosphere Coupling Strength in the United States: Comparison among Observations, Reanalysis Data, and Numerical Models. *J. Hydrometeor.*, **13**, 1010–1022, doi:10.1175/JHM-D-11-075.1.

Meng, Q., M. Latif, W. Park, N. S. Keenlyside, V. A. Semenov, and T. Martin, 2012: Twentieth century Walker circulation change: Data analysis and model experiments. *Climate Dyn.*, **38**, 1757-1773.

Mesinger, F., and Coauthors, 2006: North American Regional Reanalysis. *Bull. Amer. Meteor. Soc.*, **87**, 343–360, https://doi.org/10.1175/BAMS-87-3-343.

Miguez-Macho, G., H. Li, and Y. Fan, 2008: Simulated Water Table and Soil Moisture Climatology Over North America. *Bull. Amer. Meteor. Soc.*, **89**, 663–672, https://doi.org/10.1175/BAMS-89-5-663.

Miralles, D. G., A. J. Teuling, C. C. van Heerwaarden, and J. V.-G. de Arellano, 2014: Mega-heatwave temperatures due to combined soil desiccation and atmospheric heat accumulation. *Nat. Geosci.*, **7**, 345–349, doi:10.1038/ngeo2141.

Mo, K. C., and D. P. Lettenmaier, 2015: Heat wave flash droughts in decline. *Geophys. Res. Lett.*, **42**, 2823–2829, https://doi.org/10.1002/2015GL064018.

Mo, K. C., and D. P. Lettenmaier, 2016: Precipitation Deficit Flash Droughts over the United States. *J. Hydrometeor.*, **17**, 1169–1184, https://doi:10.1175/jhm-d-15-0158.1.

Mundhenk, B. D., E. A. Barnes, and E. D. Maloney, 2016: All-Season Climatology and Variability of Atmospheric Rivers Frequencies over the North Pacific, *J. Climate*, **29**, 4885-4903, doi:10.1175/JCLI-D-15-0655.1.

National Academies of Sciences, Engineering and Medicine, 2016: Next Generation Earth System Prediction: Strategies for Subseasonal to Seasonal Forecasts, The National Academies Press, Washington, DC.

National Centers for Environmental Information, 2019: Billion-dollar weather and climate disasters: Overview, NOAA NCEI, https://ncdc.noaa.gov/billions/.

National Drought Mitigation Center, 2019: United States Drought Monitor, Accessed 28 March 2019, https://droughtmonitor.unl.edu.

Nguyen, H., M. C. Wheeler, J. A. Otkin, T. Cowan, A. Frost, and R. Stone, 2019: Using the evaporative stress index to monitor flash drought in Australia. *Environ. Res. Lett.*, **14**, 064016, doi:10.1088/1748-9326/ab2103.

Otkin, J. A., M. C. Anderson, C. Hain, I. E. Mladenova, J. B. Basara, and M. Svoboda, 2013: Examining Rapid Onset Drought Development Using the Thermal Infrared–Based Evaporative Stress Index. *J. Hydrometeor.*, **14**, 1057–1074, https://doi.org/10.1175/JHM-D-12-0144.1.

Otkin, J. A., M. C. Anderson, C. Hain, and M. Svoboda, 2014: Examining the Relationship between Drought Development and Rapid Changes in the Evaporative Stress Index. *J. Hydrometeor.*, **15**, 938–956, https://doi.org/10.1175/JHM-D-13-0110.1.

Otkin, J. A., M. Shafer, M. Svoboda, B. Wardlow, M. C. Anderson, C. Hain, and J. Basara, 2015: Facilitating the Use of Drought Early Warning Information through Interactions with Agricultural Stakeholders. *Bull. Amer. Meteor. Soc.*, **96**, 1073–1078, doi:10.1175/BAMS-D-14-00219.1.

Otkin, J. A., and Coauthors, 2016: Assessing the evolution of soil moisture and vegetation conditions during the 2012 United States flash drought. *Agric. For. Meteor.*, **218-219**, 230–242, https://doi.org/10.1016/j.agrformet.2015.12.065.

Otkin, J. A., M. Svoboda, E. D. Hunt, T. W. Ford, M. C. Anderson, C. Hain, and J. B. Basara, 2018a: Flash Droughts: A Review and Assessment of the Challenges Imposed by Rapid-Onset Droughts in the United States. *Bull. Amer. Meteor. Soc.*, **99**, 911–919, https://doi.org/10.1175/BAMS-D-17-0149.1.

Otkin, J. A., T. Haigh, A. Mucia, M. C. Anderson, and C. Hain, 2018b: Comparison of Agricultural Stakeholder Survey Results and Drought Monitoring Datasets during the 2016 U.S. Northern Plains Flash Drought. *Wea. Climate Soc.*, **10**, 867–883, doi:10.1175/WCAS-D-18-0051.1.

Otkin, J. A., Y. Zhong, E. D. Hunt, J. Basara, M. Svoboda, M. C. Anderson, and C. R. Hain, 2019: Assessing the evolution of soil moisture and vegetation conditions during a flash drought - flash recovery sequence over the south-central U.S. *J. Hydrometeor.*, https://doi.org/10.1175/JHM-D-18-0171.1

Pendergrass, A. G., and Coauthors, 2020: Flash droughts present a new challenge for subseasonal-to-seasonal prediction. *Nat. Climate Change*, **10**, 191–199, doi:10.1038/s41558-020-0709-0.

Pielke, R. A., Sr., 2001: Influence of the spatial distribution of vegetation and soils on the prediction of cumulus Convective rainfall. *Rev. Geophys.*, **39**, 151–177, https://doi.org/10.1029/1999RG000072.

Rasmijn, L. M., G. Van der Schrier, R. Bintanja, J. Barkmeijer, A. Sterl, and W. Hazeleger, 2018: Future equivalent of 2010 Russian heatwave intensified by weakening soil moisture constraints. *Nat. Clim. Change*, **8**, 381–385, doi:10.1038/s41558-018-0114-0.

Rienecker, M. M., and Coauthors, 2011: MERRA: NASA's Modern-Era Retrospective Analysis for Research and Applications. *J. Climate*, **24**, 3624–3648, doi:10.1175/JCLI-D-11-00015.1.

Russo, S., J. Sillmann, and E. M. Fischer, 2015: Top ten European heatwaves since 1950 and their occurrence in the coming decades. *Environ. Res. Lett.*, **10**, 124003, doi:10.1088/1748-9326/10/12/124003.

Rutz, J. J., W. J. Steenburgh, and F. M. Ralph, 2014: Climatological Characteristics of Atmospheric Rivers and Their Inland Penetration over the Western United States, *Mon. Wea. Rev.*, **142**, 905-921, doi:10.1175/MWR-D-13-00168.1.

Santanello, J. A., Jr., J. Roundy, and P. A. Dirmeyer, 2015: Quantifying the Land–Atmosphere Coupling Behavior in Modern Reanalysis Products over the U.S. Southern Great Plains. *J. Climate*, **28**, 5813–5829, https://doi.org/10.1175/JCLI-D-14-00680.1.

Scheff, J., and D. M. W. Frierson, 2014: Scaling Potential Evapotranspiration with Greenhouse Warming. *J. Climate*, **27**, 1539–1558, doi:10.1175/JCLI-D-13-00233.1.

Schumacher, D. L., J. Keune, C. C. van Heerwaarden, J. V.-G. de Arellano, A. J. Teuling, and D. G. Miralles, 2019: Amplification of mega-heatwaves through heat torrents fueled by upwind drought. *Nat. Geosci*, **12**, 712–717, doi:10.1038/s41561-019-0431-6.

Seneviratne, S. I., D. Lüthi, M. Litschi, and C. Schär, 2006: Land–atmosphere coupling and climate change in Europe. *Nat.*, **443**, 205–209, doi:10.1038/nature05095.

Shaposhnikov, D., and Coauthors, 2014: Mortality Related to Air Pollution with the Moscow Heat Wave and Wildfire of 2010. *Epidemiol.*, **25**, 359–364, doi:10.1097/EDE.0000000000000090.

Sharmila, S., and H. H. Hendon, 2020: Mechanisms of multiyear variations of Northern Australia wet-season rainfall. *Sci. Rep.*, **10**, 1–11, doi:10.1038/s41598-020-61482-5.

Sheppard, P. R., A. C. Comrie, G. D. Packin, K. Angersbach, and M. K. Hughes, 2002: The climate of the US Southwest, *Climate Res.*, **21**, 219-238, doi:10.3354/cr021219.

Sultan, B., and S. Janicot, 2000: Abrupt shift of the ITCZ over West Africa and intra-seasonal variability. *Geophys. Res. Lett.*, **27**, 3353–3356, doi:10.1029/1999GL011285.

Sultan, B., and S. Janicot, 2003: The West African Monsoon Dynamics. Part II: The “Preonset” and “Onset” of the Summer Monsoon. *J. Climate*, **16**, 3407–3427, doi:10.1175/1520-0442(2003)016<3407:TWAMDP>2.0.CO;2.

Svoboda, M., and Coauthors, 2002: The Drought Monitor. *Bull. Amer. Meteor. Soc.*, **83**, 1181–1190, https://doi.org/10.1175/1520-0477-83.8.1181.

Thacker, M. T. F., R. Lee, R. I. Sabogal, and A. Henderson, 2008: Overview of deaths associated with natural events, United States, 1979–2004. Disasters, **32**, 303–315, https://doi:10.1111/j.1467-7717.2008.01041.x.

Tokinaga, H., S.-P. Xie, C. Deser, Y. Kosaka, and Y. M. Okumura, 2012: Slowdown of the Walker circulation driven by tropical Indo-Pacific warming. *Nat.*, **491**, 439–443, doi:10.1038/nature11576.

Twardosz, R., and U. Kossowska-Cezak, 2012: Exceptionally hot summers in Central and Eastern Europe (1951–2010). *Theor. Appl. Climatol.*, **112**, 617–628, doi:10.1007/s00704-012-0757-0.

Wagle, P., and Coauthors, 2014: Sensitivity of vegetation indices and gross primary production of tallgrass prairie to severe drought. *Remote Sens. Environ.*, **152**, 1–14, doi:10.1016/j.rse.2014.05.010.

Wang, K., R. E. Dickinson, and S. Liang, 2012: Global Atmospheric Evaporative Demand over Land from 1973 to 2008. *J. Climate*, **25**, 8353–8361, doi:10.1175/JCLI-D-11-00492.1.

Wang, L., X. Yuan, Z. Xie, P. Wu, and Y. Li, 2016: Increasing flash droughts over China during the recent global warming hiatus. *Sci. Rep.*, **6**, https://doi.org/10.1038/srep30571.

Wang, B., and Coauthors, 2020: Monsoons Climate Change Assessment. *Bull. Amer. Meteor. Soc.*, doi:10.1175/BAMS-D-19-0335.1.

Wegren, S. K., 2013: Food Security and Russia's 2010 Drought. *Eurasian Geogr. Econ.*, **52**, 140–156, doi:10.2747/1539-7216.52.1.140.

Wei, J., and P. A. Dirmeyer, 2012: Dissecting soil moisture-precipitation coupling. *Geophys. Res. Lett.*, **39**, L19711, https://doi.org/10.1029/2012GL053038.

Welton, G., 2011: The Impact of Russia's 2010 Grain Export Ban. Oxfam Res. Rep., 1-32.

Westerling, A. L., and T. W. Swetnam, 2003: Interannual to decadal drought and wildfire in the western United States. Eos, *Trans. Amer. Geophys. Union*, **84**, 545–555, https://doi.org/10.1029/2003EO490001.

Wilhite, D. A., and M. H. Glantz, 1985: Understanding: the Drought Phenomenon: The Role of Definitions. *Water Int.*, **10**, 111–120, https://doi.org/10.1080/02508068508686328.

Wilhite, D. A., 2000: Chapter 1 Drought as a Natural Hazard: Concepts and Definitions. Drought Mitigation Center Faculty Publications. **69**.

Wilhite, D. A., M. D. Svoboda, and M. J. Hayes, 2007: Understanding the complex impacts of drought: A key to enhancing drought mitigation and preparedness. *Water Resour. Manage.*, **21**, 763–774, https://doi.org/10.1007/s11269-006-9076-5.

Witte, J. C., A. R. Douglass, A. DaSilva, O. Torres, R. Levy, and B. N. Duncan, 2011: NASA A-Train and Terra Observations of the 2010 Russian Wildfires. *Atmos. Chem. Phys.*, **11**, 9287-9301, https://doi.org/10.5194/acp-11-9287-2011.

Xia, Y., and Coauthors, 2012: Continental-scale water and energy flux analysis and validation for the North American Land Data Assimilation System project phase 2 (NLDAS-2): 1. Intercomparison and application of model products. *J. Geophys. Res.*, **117**, D03109, https://doi:10.1029/2011JD016048.

Yuan, X., L. Wang, and E. F. Wood, 2018: Anthropogenic Intensification of Southern African Flash Droughts as Exemplified by the 2015/16 Season. *Bull. Amer. Meteor. Soc.*, **99**, S86–S90, https://doi:10.1175/BAMS-D-17-0077.1.

Yuan, X., L. Wang, P. Wu, P. Ji, J. Sheffield, and M. Zhang, 2019: Anthropogenic shift towards higher risk of flash drought over China. *Nat. Commun.*, **10**, 1-8, https://doi.org/10.1038/s41467-019-12692-7.

Zhang, Y., Q. You, C. Chen, and X. Li, 2017: Flash droughts in a typical humid and subtropical basin: A case study in the Gan River Basin, China. *J. Hydrol.*, **551**, 162–176, https://doi.org/10.1016/j.jhydrol.2017.05.044.

Zou, Z., X. Xiao, J. Dong, Y. Qin, R. B. Doughty, M. A. Menarguez, G. Zhang, and J. Wang, 2018: Divergent trends of open-surface water body area in the contiguous United States from 1984 to 2016. *Proc. Natl. Acad. Sci. U.S.A.*, **115**, https://doi.org/10.1073/pnas.1719275115.